The Institution of Engineers, Malaysia
PRIME MOVERS of
NATION BUILDING

IEM JOURNAL

THE JOURNAL OF THE INSTITUTION OF ENGINEERS, MALAYSIA

KDN PP5476/10/2009 (022607)
ISSN 0126-513X

Vol. 71, No.2
June 2009

THE INSTITUTION OF ENGINEERS, MALAYSIA
Bangunan Ingenieur, Lots 60 & 62, Jalan 52/4, P.O.Box 223, (Jalan Sultan) 46720 Petaling Jaya, Selangor.
Tel: 03-7968 4001/4002   Fax: 03-7957 7678   E-mail: sec@iem.org,my   Homepage: http://www.iem.org.my

Vol. 71, No.2, June 2009
KDN PP5476/10/2009 (022607) ISSN 0126-513X

THE INSTITUTION OF ENGINEERS, MALAYSIA
Bangunan Ingenieur, Lots 60 & 62, Jalan 52/4, P.O.Box 223 (Jalan Sultan), 46720 Petaling Jaya, Selangor Darul Ehsan.
Tel: 03-7968 4001/4002 Fax: 03-7957 7678
E-mail: sec@iem.org.my Homepage: http://www.iem.org.my

Printed by: SETIAKAWAN PRINTERS SDN. BHD. (42662U)
NO. 5 & 7, Jalan Industri PBP 11,Taman Industri Pusat Bandar Puchong, 47100 Selangor Darul Ehsan.
Tel: 603-5891 7363 Fax: 603-5891 7232/33 E-mail: skpsb@tm.net.my

CONTENTS

1 **IEM Presidential Address: Building the Past, Engineering the Present, Educating the Future**
Y.Bhg. Dato' Engr. Prof. Dr. Chuah Hean Teik

5 **Use of Suitable Equation of State for the Conversion of Volumetric to Mass Flowrates in NGV Refueling Measurement**
by Mahidzal Dahari and Ibrahim Abdul Mutalib

13 **Analysis of Potential Flow Around Two-Dimensional Hydrofoil by Source Based Lower and Higher Order Panel Methods**
by Md. Shahjada Tarafder, Gazi Md. Khalil and Muhammad Rabiul Islam

22 **Design and Analysis Multi-Cavity Traditional and H-Branching Runners for Plastic Injection Mold**
by Mohd. Rizwan Hamsin, Azuddin Mamat and Aznijar Ahmad-Yazid

36 **Essential Quality Practices in Indonesian Manufacturing SMEs**
by Mohd. Nizam Ab. Rahman, Hernadewita, Baba Md. Deros and Ahmad Rasdan Ismail

44 **Investigation of Transient Perfomance of Capacitor Voltage Transfomer (CTV)**
by S. Mekhilef, C. H. Lim and A. H. A. Bakar

51 **A CFD Analysis on the Effect of Vortex Finder and Cylindrical Length on Cyclone Hydrodynamics and Centrifugal Forces**
by T. G. Chuah, Jolius Gimbun, Thomas S. Y. Choong and A. Fakhru'l-Razi

59 **Rheological Properties of SS316L MIM Feedstock Prepared with Different Particle Sizes and Powder Loadings**
by Sri Yulis M. Amin, Khairur Rijal Jamaludin and Norhamidi Muhamad

INTERNATIONAL ADVISORY PANELS

IEM BRANCHES

HEADQUARTERS	**THE INSTITUTION OF ENGINEERS, MALAYSIA** Bangunan Ingenieur, Lot 60/62, Jalan 52/4, P.O.Box 223, (Jalan Sultan), 46720 Petaling Jaya, Selangor	Tel: 03-7968 4001 / 4002 Fax: 03-7957 7678 sec@iem.org.my www.iem.org.my
NORTHERN (Penang)	**IEM PENANG BRANCH SECRETARIAT** Level 5, 5-A Northam Venture, 37, Jalan Sultan Ahmad Shah, 10050 Penang	Tel: 04-818 2045 / 04-818 2046 Fax: 04-226 4490 iempenangbranch@gmail.com
SOUTHERN (Johor Bahru)	**IEM SOUTHERN BRANCH SECRETARIAT** No. 24-B, Jalan Abiad, Taman Tebrau Jaya, 80400 Johor Bahru, Johor	Tel: 07-331 9705 Fax: 07-331 9710 iemsouthern@gmail.com www.iemsb.org.my
PERAK	**IEM PENANG BRANCH SECRETARIAT** No. 8-10, Jalan Tokong, 31650 Ipoh, Perak	Tel: 05-254 5962 Fax: 05-253 4362 meiyu@streamyx.com
EASTERN (Kelantan)	**IEM EASTERN BRANCH SECRETARIAT** KMS Ingenieur Sdn Bhd, Unit 1-11 & 1-12, Wisma Ingenieur, Jalan Raja Perempuan Zainab II, 16150 Kubang Kerian, Kota Bahru, Kelantan	Tel: 09-764 3791 Fax: 09-765 1058 ayahmin@gmail.com kmsingenieur@gmail.com
TERENGGANU	**C/O THE CHIEF EXECUTIVE OFFICER** Syarikat Air Terengganu Berhad (SATU), Jalan Sultan Ismail, 20200 Kuala Terengganu, Terengganu	Tel: 09-620 1103 Fax: 09-620 1104 juliana@satuwater.com.my
NEGERI SEMBILAN	**ENGR. MOHD. NOR** C/O Prodesign Engineers S/B, No. 28-1, Jalan Durian Emas 4, Betaria Business Centre, Off Jalan Dato' Siamang Gagap, 70100 Seremban, Negeri Sembilan	Tel: 06-767 7333 Fax: 06-767 7000 prodesignsb@gmail.com
MELAKA	**IEM MELAKA BRANCH SECRETARIAT** C/O Sri Perunding Consulting Engineers, 2, Jalan Malinja 2, Taman Malinja, Bukit Baru, 75150 Melaka	Tel: 06-284 8028 Fax: 06-283 8919 spcesb@gmail.com
SARAWAK	**IEM SARAWAK BRANCH SECRETARIAT** Ultimate Professional Centre, No.16, 2nd Floor, Jalan Bukit Mata Kuching, 93100 Kuching, Sarawak	Tel: 082-428 506 Fax: 082-243 718 iemsarawak@gmail.com
SABAH	**IEM SABAH BRANCH SECRETARIAT** Lot 25, 3rd Floor, Block C, Damai Pointcommercial Centre, Lorong Damai Point, Off Jalan Damai, 88100 Kota Kinabalu, Sabah	Tel: 088-259 122 Fax: 088-236 749 iemsabah@sabah.org.my
MIRI	**IEM MIRI BRANCH SECRETARIAT** Lot 2935, 2nd Floor, Faradale Commercial Centre, Jalan Bulan Sabit, 98000 Miri, Sarawak.	Tel: 085-423 718 Fax:085-424 718 iem-miri@org.my
KEDAH/PERLIS	**IEM KEDAH/PERLIS BRANCH SECRETARIAT** 135-C, Tingkat 2, Kompleks Alor Setar, Lebuhraya Darul Aman, 05100 Alor Setar, Kedah	Tel: 04-734 3420 Fax:04-733 3962 ijmcxp@yahoo.my

BUILDING THE PAST, ENGINEERING THE PRESENT, EDUCATING THE FUTURE

Y.Bhg. Dato' Engr. Prof. Dr Chuah Hean Teik

President
The Institution of Engineers, Malaysia
Session 2009/2010

The Immediate Past President, Past Presidents, Deputy President, Vice-Presidents, Members of Council, and my fellow engineers.

1.0 BUILDING THE PAST – A TRIBUTE TO OUR PAST ENGINEERING LEADERS

Year 2009 marks a significant milestone in the history of the Institution of Engineers Malaysia (IEM) as it crosses the half-century mark of its formation. It has been 50 years since its birth on 1 May 1959 when IEM began its journey through uncharted territory, as the first professional institution dedicated to promote and advance professional engineering in all disciplines and to facilitate the exchange of information and ideas relating to engineering.

Let us refresh our memory on the history of formation of professional engineering organisations in our country. In 1932, an engineering association was founded in Kuala Lumpur. However, it did not last long. It was only after a few other unsuccessful efforts that a glimpse of achievement was attained with the formation of the Technical Association of Malaya (TAM) in April 1946. TAM was set up for all those in engineering, architectural and surveying disciplines. A joint group of the United Kingdom-based Institutions of Civil, Mechanical and Electrical Engineers was established in 1949 to service these professions. Arising to the increasing number of local engineers, the need to have a professional organisation dedicated to advance our profession was inevitable. Under the stewardship of our founding president the late Tan Sri Ir. Haji Yusoff bin Ibrahim and his team, the Institution of Engineers Malaya was formed on 1 May 1959 and later renamed The Institution of Engineers, Malaysia.

Born exactly 20 months after Merdeka, IEM has been a constant force to post-independence nation building as Malaysian economy rose from an agriculture-based to a dynamic manufacturing- and services-based economy today. I am proud to say that engineering is the backbone of our country's economic growth. When Malaysia first gained our independence, we did not have much of an economy. Over the years, we have witnessed tremendous development in the infrastructure, manufacturing, telecommunications, information technology, construction, marine and automobile industries, and so on. Inevitably, engineering plays an integral role in creating the platform that stimulates and sustains our economy. Indeed, engineers have played an invaluable role in our nation building in the past 50 years and will continue to play a powerful role in bringing us closer to an environmentally sustainable and economically viable future.

Today, IEM, with a proud tradition of *50 years*, has grown from infancy to become one of the largest learned civil society organisations in our country. While there are still many areas for improvement, IEM can be proud of what have been achieved thus far. Starting with our humble beginnings of a small number of members, IEM is currently serving more than 24,500 members. With the membership base and the pool of engineering expertise available, IEM can claim recognition as the voice of engineers in

Malaysia that plays a pivotal role in upholding our professional status and image at national, regional and international levels.

The history of IEM could not have been written without the bold vision and foresight of our founding fathers and predecessors who have brought us to this milestone in our journey. On this historic occasion to commemorate our commendable legacy, I would like to specially pay tribute to our founding fathers, the Past Presidents and Council Members for nurturing this institution to what it is today. We are all indeed thankful to them and we salute their selfless dedication and tireless efforts in serving the institution. I would also like to thank all of you for your confidence in supporting me in assuming the office as IEM President for the year 2009/10 session. I will certainly need the advice and guidance from each and every one of you here, as we collectively take IEM to greater heights in leading the way ahead of the engineering profession.

2.0 ENGINEERING THE PRESENT: THREE ICS

The Year of 2008 was full of events. The petrol price went on a roller coaster last year. The world is now facing global economic uncertainties, triggered very much by the US subprime crisis. There is no exception back home. Malaysia's economy is also facing significant challenges and undergoing some restructuring. In a world full of changes, the only thing that does not change is the change and the only way to survive is to direct the changes to the right destination. As in the words of Charles Darwin, "it is not the strongest of the species that survive, nor the most intelligent, but the one most responsive to change". Indeed, as engineers, our ability to respond to change is the key to our survival. Therefore, we must engineer our own profession. We must be pro-active and creative. We must come up with new or alternative and yet cost effective engineering solutions. We must again be the prime movers for economic revival. You will be happy to note that at IEM we have seized all opportunities possible to serve our members and our nation better. For example, due to the collective efforts of IEM HQ and IEM branches approaching the relevant Government agencies, Ministries and state governments, engineers are now appointed to local councils and various advisory committees at state and national levels.

In the 21st century, globalization is a powerful driver of relentless change. The turn of the millennium witnessed a change in the world economy from the Atlantic Rim to the Pacific Rim. Asia currently comprises some of the world's most exciting economies. China and India, with their large population base and vast talent pool, are surging ahead as competing economies. In order to thrive in this fast advancing global market, all of us need to carry three ICs in our minds, in addition to our national IC. The first IC is Integrity and Competency; the second IC is Integration and Communication and the third IC is Internationalisation and Cooperation. Let me share with you some of my thoughts on these guiding principles for our future strategic direction.

INTEGRITY AND COMPETENCY

Integrity is consistency between one's actions, values, methods, measures and principles. The value of a person is defined by the knowledge in the mind, the worth of the character and the principles upon which we build our life. Handling ethical dilemmas and making ethical decisions are important parts of being a professional. Engineering is a profession that has specialised knowledge, the privilege of self-regulation, and a responsibility to the public. As engineers, it is important that we maintain a high ethical standard as the decisions we make will have a direct effect on the society. It is the awareness of these heavy responsibilities and obligations that lies at the heart of the professional code of conduct and ethics that govern the engineering profession. In the practice of the profession, engineers must adhere to high principles of ethical conduct on behalf of the public, clients, employers, and the profession.

Ethical misconduct seems to be the topics of everyday headlines and news. We are bombarded with stories about the moral failings of our political leaders and corporate leaders. Engineers are also not spared from public scrutiny. Whenever there is an engineering failure, the first reaction from the public is to pin-point engineers, sometimes even before any thorough investigation. Engineering ethics is attracting increasing interest in the nation as a result of the attention that the media has given to cases such as MMR2 cracks, NKVE bridge collapse, Matrade Building, the Bukit Antarabangsa Landslide, and the frequent floods. The voice of engineers, without fear or favour, be it from individual experts or from established institutions such as IEM, need to be heard among policy making bodies. Professional engineering organisations should initiate and conduct thorough studies and open discussions on the problems from the technical perspective. Engineers can share their ideas, offer solutions and engage in meaningful public discussion. It is timely for engineers to further promote a new culture of transparency and openness in-line with ethics and professionalism that we hold on to in order to protect the honour, dignity and integrity of the profession. It is my sincere hope that IEM continues to strive to be the profession's most respected voice on the practice of ethical engineering.

Clearly, in order to protect the safety, health and welfare of the public, engineers must be competent to provide professional service and advice. In a field as technically complex as engineering, new discoveries and changes in practice occur frequently. Engineers need to equip ourselves with everything we need to thrive in a very competitive world. Engineers will have to be equipped with the highest standards of R&D skills, keep abreast with global technological trends, be strategic thinkers and planners and develop market driven services and high-tech products/systems.

In order to stay current, engineers should continue their professional and ethical development throughout their careers to further enhance a greater level of professionalism and professional expertise. Engineers must take steps that go beyond their job, such as participating in professional societies, attending continuing education courses, gaining new skills and competencies in both technical and non-technical aspects through Continuous Professional Development (CPD) programmes, reading professional publications and developing a network of fellow professionals. The adoption of lifelong learning is imperative and has become a benchmark in responding to new challenges and demands posed by a highly competitive global market.

INTEGRATION AND COMMUNICATION

The world is becoming increasingly integrated by information systems, economic markets and political social issues. These pose challenges that are growing in complexity and transcend specific disciplines and are driving the emergence of multidisciplinary and interdisciplinary thinking.

Innovations and technological breakthroughs are the product of convergence of multidisciplines. New multidisciplinary fields such as nanotechnology combine a host of related subjects from biochemistry, pharmacology, and medicine to mathematics, computer science, and of course, basic engineering principles. Biotechnology, another field of great potential, merges engineering, physics, chemistry, biology, other life sciences and medicine. These, and other disciplines of the future, require engineers to master an overwhelming array of technical knowledge.

As we move towards a more knowledge-based and innovation-driven economy, engineers too will move beyond being technically equipped, towards obtaining an even wider range of expertise, such as in research and development, consulting, regulatory knowledge, leadership, management *etc*. Thus, inter- and multidisciplinary approaches are becoming more prevalent in engineering.

To operate successfully in a multidisciplinary environment, it requires a broad intellectual perspective. Equally important is the ability to manipulate information into knowledge as well as understand and communicate across disciplines. Similarly, engineers are tackling multifaceted problems that require solutions beyond the reach of any single discipline. Much of the work will involve teams of people, other engineers and people in disciplines such as science, marketing, finance, and information technology. In some cases, team members will work in other locations around the world. Thus, engineers must be able to collaborate and work in multidisciplinary and multicultural teams as well as communicate well in order to be effective in engineering itself.

The ability to communicate, both in writing and orally, will determine the chances of being successful as an engineer and advancing our career. As engineers we are required to write specifications and technical descriptions, prepare written status or progress reports to management, present design concepts to senior engineering management at design reviews, communicate technical information to staff members that have no technical training, prepare product brochures and marketing materials as well as prepare bids or other kinds of funding proposals. Therefore, our technical expertise, creativity and work ethics will not be enough if we are not able to communicate useful information to our colleagues, supervisors and clients.

INTERNATIONALISATION AND COOPERATION

Globalisation, characterised by the increase in international trade, mobility of labour and capital, as well as borderless communications, presents new opportunities and challenges for engineering sector. The WTO (World Trade Organisation), the APEC (Asia Pacific Economic Cooperation) and the AFTA (ASEAN Free Trade Area) are developments of the concept of a borderless world. This borderless world will give participating economies the capacity for boundless prosperity. Trends such as the increasing transfer of technology, global mobility of engineers and trade liberalization have given rise to many issues that require co-operation and co-ordination. Our engineers should aim at achieving engineering excellence not only in our home country, but also contribute to the development of the region and the world. We can fly further and soar higher if we leverage on one another's strengths and broaden our intellectual and business networking.

In the regional landscape, engineering is one of the active service sectors in the ASEAN economic integration. The signing of the Mutual Recognition Arrangement (MRA) on Engineering Services in December 2005 by the ASEAN Economic Ministers reflected a shared interest between the governments and the engineering community in ASEAN to improve and enhance the competitiveness of engineering services quality as well as facilitating the free flow of engineering professionals within the region. The momentum towards economic integration in ASEAN is further driven by the progress of ASEAN engagement in Free Trade Area (FTA) negotiations with an increasing number of its Dialogue Partners. These FTA's will encompass all aspects of the economy, including goods, services, and investment and thus will provide greater opportunities for ASEAN engineers.

In the last 20 years there has been a growing interest in multilateral agreements for engineering graduates, criteria for working independently and for the recognition of experienced engineers. Similarly, there are several initiatives undertook by IEM to enhance the professional mobility of engineers within the globalization setup. Among these are the Engineers Mobility Forum (EMF), Asia Pacific Economic Cooperation (APEC) and ASEAN Engineers Register (AER).

The AER being a trade register for professionals within ASEAN is set up by ASEAN Federation of Engineering Organisations (AFEO) in which IEM is a founding member. The APEC register provides mobility for engineers between the signatory economies from Asia Pacific Rim. The EMF agreement is a multi-national agreement between engineering organizations of member countries providing the framework for the establishment of an international standard of competence for professional engineering. It empowers member organizations to establish a section of the International Professional Engineers Register. The standard of competence applied to the EMF is similar to that of the APEC Engineers agreement. These regional benchmarks should be maintained so that a regional level of confidence can be assured when clients utilise services of the professionals in these registers.

In addition, IEM is the permanent Secretariat of the Federation of Engineering Institutions of Asia and the Pacific (FEIAP). The task at hand is to work on the establishment of an Engineering Education Accreditation Procedure/System which will act as a platform for mutual recognition of engineering degrees across the region. Besides FEIAP, IEM is also an affiliated member of the World Federation of Engineering Organisations (WFEO). To provide opportunities for our engineers to share knowledge and expertise with their international counterpart, IEM has established Memoranda of Understanding with similar organisations in the US, UK, Australia and many others.

With the globalisation of professional services, local professional engineers should look beyond national boundaries and create winning partnership with foreign professionals and high technology industry leaders abroad. Moving forward, IEM would look into creating various business forums and platforms for members to network, exchange ideas explore business opportunities and promote their expertise overseas.

This era of globalisation has opened up boundless opportunities in the mobility of technical expertise within the region and the global community which will certainly contribute to the overall economic development of the region. In this regard, IEM shall continue its commitment in bringing the engineering profession to greater heights and to extend and strengthen our achievements and esteem around the globe, in the interests of our members and the profession.

3.0 EDUCATING THE FUTURE

I believe that addressing the fast paced, competitive, global environment of the 21st century requires redefinition of the role of universities in preparing tomorrow's engineers to face these challenges. Universities have to be responsive to all these changes and realign themselves to produce graduates who are adept in working with the new paradigms. Engineering qualifications with emphasis on risk management, ethical practice and sustainable outcomes have become highly regarded by worldwide employers.

Engineering is a dynamic profession with the next generation of engineering career paths embracing complex systems issues. Examples include the issue of sustainable development such as conserving our Mother Nature, managing the increasing demand for energy resources and mitigating the effects of climate change; infrastructure systems renewal; nano systems and mega systems; living systems engineering which is a dimension beyond bioengineering; smart systems and creative enterprise transformation generally. The future challenge for the engineering profession will be the increasing diversity of the disciplines which are grouped under the umbrella of engineering.

Universities need to provide their students with greater experiential breadth of preparation in a variety of non-technical areas and simultaneously developing in them the foundation they need in a complex evolving discipline. There is a pressing need for broad-based engineers who have the ability to think logically and analytically, and be able to make wise decisions based on fundamental principles of engineering. Engineering students also need effective communication skills, grounding in social science, introduction to the principles of leadership and teamwork, entrepreneurial skills to translate their discoveries to practical use, solid foundation in ethics to discern the way their discoveries impact human societies, and a deeper appreciation for cultures. In other words, universities need to create inter- and multidisciplinary experiences for engineering students to parallel what they will experience in real life technological situations.

Professional bodies such as IEM should work hand in hand with institutions of higher learning to nurture competent engineers with critical thinking and analytical minds coupled with uncompromising integrity and ethical values. Policy maker, industry, society and universities should take greater steps towards establishing quality interaction and seamless working relationship.

Besides promoting the good work of the engineering profession, IEM, together with the tertiary institutions, should instil the right values in engineering education, and provide the necessary continuing education for the engineering profession. IEM may work with universities to establish engineering degree programmes that are of relevance in today's context. For example, there is a need to couple engineering programmes with business and law to train engineers who are both technically competent and ready to become entrepreneurs who are able to bring technological innovations from the laboratory to the market place. On top of that, the engineering discipline needs to attract its graduates to pursue postgraduate qualifications and raise the engineering skills to boost local innovation capability and research and development.

Moving ahead, as Malaysia develops into a knowledge-based and innovation-driven economy, we will have to continue to strengthen our engineering education and stimulate the growth of engineering population. Recognizing the importance of developing our nation's engineering manpower, IEM should place great emphasis on encouraging young and talented Malaysians to study engineering and ultimately build a career in engineering. On this note, IEM will initiate high quality outreach programmes to schools such as school adoption and back-to-school programmes to get more students from lower secondary onwards to be interested in mathematics, science and technology and of course, to promote engineering as an exciting profession. This is also in tandem with our government's effort to produce suitably equipped human capital especially in science and technology for nation-building to further enhance our economic competitiveness and transform Malaysia into a vibrant global nation.

4.0 MOVING FORWARD

Ahead of us, it will be a challenging job, especially when we are on the brink of re-engineering our institution to ensure IEM is well positioned to meet the needs and expectations of an evolving engineering society.

What is the role of IEM as a membership driven society? As we all know, membership is the lifeblood of our institution. Without our members, IEM does not exist. Therefore, recruiting, servicing and retaining our members is the cornerstone of our survival. In order to achieve membership satisfaction and loyalty, IEM needs to understand the needs and expectations of the diverse segment of our members. Next, we need to analyse and assess whether our positioning of membership offer and services match those needs and expectations. We should also bear in mind that these needs and expectations will change with time.

For IEM to remain relevant and appealing to the engineers, it has to evolve to enhance the value of IEM membership. To inject professional and intellectual values to IEM membership, IEM will provide a myriad of avenue for members to improve themselves. Professional training will be increased to provide more opportunities for members to gain CPD hours nation wide. We want to make IEM as the lead body for all engineers. As part of our membership drive, we would like to attract more professionals from the industry especially the manufacturing and service sectors into IEM fold.

Besides continuing the on-going efforts to raise fund for our newly acquired building, we will have to move into high gear to steer ourselves to focus on other initiatives that have been stated earlier such as establishing seamless relationship and collaboration with institutions of higher learning, policy makers and industries; stimulating the growth of engineering graduates within our population; improving IEM's responsiveness to current issues; providing opportunities for business networking and maintaining the highest standards of the profession through international and global alliances. The world is changing rapidly and we, as professionals, must keep pace and work at re-engineering process with ultra speed in order to remain the premier professional organisation in the country.

5.0 CONCLUSION

Today, we have the baton in our hands. Let us embrace the esprit de corps as we, the engineers, continue the marathon with courage and determination to rise to the challenges that lie ahead of us. For this, I seek your strong support as well as enthusiasm as we pledge our sincere commitment to the betterment of the Institution, our profession and above all, our nation. May the vision and drive of our Founding Members live on. ■

REFERENCES

[1] "Engineers in Nation Building", Board of Engineers Malaysia 30th Anniversary Commemorative Book, 2002

USE OF SUITABLE EQUATION OF STATE FOR THE CONVERSION OF VOLUMETRIC TO MASS FLOWRATE IN NGV REFUELING MEASUREMENT

(Date received: 19.6.2006)

Mahidzal Dahari[1], Nor Azizah Hisam[2], Raihana Ramlan[3] and Mohamed Ibrahim Abdul Mutalib[4]
[1, 2, 3, 4] *Universiti Techology of PETRONAS, Bandar Sri Iskandar,*
31750 UTP, Tronon, Perak
Email: [1]mahidzal@gmail.com/ [2]azizah@hotmail.com

ABSTRACT

Natural Gas Vehicle (NGV) is not new in the industry; however, it is becoming an uprising issue owing to the multitude advantages natural gas posses compared to the conventional fuel. The challenges, on the other hand, are putting in place an NGV refueling facility and keeping the cost of natural gas operated vehicles competitive with conventional vehicles. One of the identified cause for the dearly NGV refueling station installation cost is the mass measurement device, Coriolis flow meter, used in each station. This research is aimed at finding and implementing a cost effective alternative to the Coriolis flow meter. A typical volumetric flow meter i.e., turbine, orifice and vortex is much lower in price but does not produce measurement in the natural gas trading unit. To compensate for this, a conversion tool based on an Equation of State (EOS) is developed. In this method, mass flowrate of natural gas is calculated using the volumetric flowrate measured by volumetric flow meter, whilst temperature and pressure of the flowing gas are fed into the conversion tool. Based on results, it is found that the developed conversion tool is able to compute the mass flowrate of natural gas with reasonably average error which is 2.66% compared to the actual measurement using Coriolis flowmeter.

Keywords: *Coriolis Flow Meter, Equation Of State, NGV Refueling Station*

1.0 INTRODUCTION

Automotive industry is one of the fastest growing industries in the world. In 2005, Daud [1] reported that in Malaysia for the past ten years, the average vehicle population growth is about 7% per annum. The fast growing industry enables people to travel faster than before and a vehicle has become an essential tool for mankind. However, the increasing number of vehicles also resulted in severe environmental problems. Emissions from millions of cars and light-duty trucks, almost exclusively operating on gasoline and diesel fuel, are major contributors to this problem. In addition, heavy-duty trucks and buses using diesel fuel are major sources of particulates (small unburned particles of hydrocarbons and sulfur) and *nitrogen oxide* (NO_x) emissions in urban areas. Particulates are a special concern because the public is frequently exposed to them and a research conducted by Bechtold in 1997 [2] suggested that particulates have cancer-causing potential and it could cause significant respiratory problems.

Alternative vehicle fuels such as natural gas have long been proposed as a way to provide significant air quality benefits over liquid petroleum fuels. Significant advances have been made in the past few years that have highlighted the efficiency and emissions potential of *NGV* [3-7]. In transportation sector, natural gas is becoming more important. *NGV* has many overwhelming advantages in comparison with traditional means of transportation using gasoline and diesel. It is more environmentally friendly [3-5], safer and lower fuel cost compared to gasoline powered vehicle. Nylund and Erkkila [6] reported that *NGV* was found to give NO_x emission of about 75% less, compared to gasoline powered vehicle. This is further supported by an emission study conducted at Argonne National Laboratory [7] that showed natural gas with CO_2 emissions of 140gm CO_2 eq/km, gasoline at 176gm CO_2 eq/km, and diesel at 147gm CO_2 eq/km.

To date, there are only 40 *NGV* refueling stations to cater for 15,600 *NGVs* in Malaysia [1]. To encourage public transport operators to use natural gas, more *NGV* stations would have to be built. Lack of refueling facility is the major obstacles to the growth of *NGV* usage. The problem is not only faced by Malaysia but also other countries in the world. High cost of its metering system is believed to be one of the main constraints to the growth of *NGV* refueling facility. The high cost of the metering system is mainly due to very expensive flow meter used in the metering system that is the Coriolis flow meter. Current technology used in *NGV* refueling equipment's metering system is by using Coriolis mass flow meter [8]. This meter uses the Coriolis Effect to measure the amount of mass moving through the element. The substance to be measured runs through a U-shaped tube as shown by Figure 1 which vibrates in a perpendicular direction to the flow. Fluid forces running through the tube interact with the vibration, causing it to twist. The greater the angle of the twist, the greater is the flow based on momentum change that is related to mass.

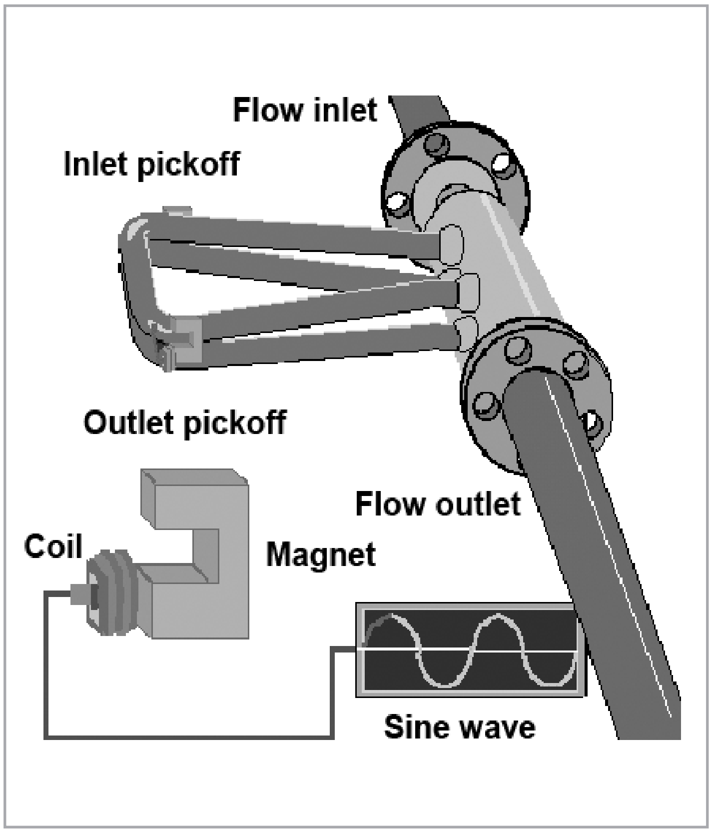

Figure 1: Coriolis Principle

Being the only flow meter that gives readings in mass per unit time for gas application, Coriolis Flow Meter is a very expensive flow meter compare to other flow meter such as volumetric flow meter, which are widely available in the market. Compare to other flow meters, the difference on the unit price is very significant. Therefore, the objective of the present research is to develop an alternative, cheap and efficient metering system to eliminate dependency on Coriolis flow meter.

2.0 MATERIALS AND METHOD

As an alternative flow meter to replace Coriolis, volumetric flow meter was found to be very attractive because of its lower price. However, volumetric flow meter gives reading in volume/time and this unit does not comply with the natural gas custody transfer regulations. To compensate for this, a conversion tool based on an *equation of state* (EOS) was developed to calculate mass flowrate of natural gas using volumetric flow meter, temperature and pressure data.

2.1 Equation of State (EOS)

An *equation of state* (EOS) [9] is a formula describing the interrelation between various macroscopically measurable properties of a system. For physical states of matter, equation of state usually relates the thermodynamic variables of pressure, temperature, volume and number of moles of material. The simplest *EOS* is the ideal gas law, which is given by

$$P\ V = n\ R\ T \tag{1}$$

where P is pressure, V is volume, n is number of moles, R is the universal gas constant and T is temperature. All substances behave according to this simple equation at sufficiently high specific volume (low density). This is because, at extremely low density, the individual molecules are essentially "point particles", occupying zero volume and never colliding with one another [10].

2.2 Development of the Conversion Model

In engineering applications, which are most often at atmospheric pressure or higher, no fluid is truly an ideal gas. However in many cases the assumption is within a few percent to be exact. Real gas laws try to predict the true behavior of a gas better than the ideal gas law by putting in terms to represent attractions and repulsions between molecules. These laws have been determined empirically, based on a conceptual model of molecular interactions or derived from statistical mechanics. The *Soave-Redlich-Kwong* (SRK) equation by Soave [11] was the first modification of the simple *Redlich-Kwong* (RK) equation where the parameter *a*, was made temperature dependent in such a way that the vapour pressure curve could be reproduced well.

The *Peng-Robinson* (PR) equation [12] is the most widely used equation in chemical engineering thermodynamics and modified by several researchers. Stryjek *et al*. [13] had proposed new alpha functions by introducing a new temperature dependence of the parameter $a(T)$ known as *Peng-Robinson-Stryjek-Vera* (PRSV) equation. It is known to give slightly better predications of liquid densities than the *SRK*. The *Lee-Kesler-Plocker* (LKP) equation is an accurate general method for non-polar substances and mixtures. Plocker *et al*. [14] applied the *Lee-Kesler* (LK) equation to mixtures, which itself was modified from the *Benedict-Webb-Rubin* (BWR) equation.

The *Zudkevitch Joffee* (ZJ) model [15] is a modification of the *RK* equation. This model has been enhanced for better prediction of vapour liquid equilibrium for hydrocarbon systems, and systems containing H_2. The major advantage of this model over the previous version of the *RK* equation is the improved capability of predicting pure component equilibrium, and the simplification of the method for determining the required coefficients for the equation. The *Kabadi-Danner model* (KD) [16] is a modification of the original *SRK* equation, enhanced to improve the vapour-liquid-liquid equilibrium calculations for H_2O-hydrocarbon systems, particularly in the dilute regions. The model is an improvement over previous attempts that were limited in the region of validity. The modification is based on an asymmetric mixing rule, whereby the interaction in the water phase (with its strong H_2 bonding) is calculated based on both the interaction between the hydrocarbons and the H_2O, and on the perturbation by hydrocarbon on the H_2O-H_2O interaction (due to its structure). In the following section, Table 1 summarizes the applicability of all models.

Table 1: Applicability of model

Model	Origins of model	Applicability of model
Soave-Redlich-Kwong	Redlich-Kwong	- Vapour pressure curve could be reproduced well
Peng-Robinson	-	- widely used in engineering thermodynamics
Peng-Robinson-Stryjek-Vera	Peng-Robinson	- Give better predications of liquid densities
Lee-Kesler-Plocker	Benedict-Webb-Rubin	- accurate method for non-polar substances and mixtures
Zudkevitch Joffee	Redlich-Kwong	- better prediction of vapour liquid equilibrium
Kabadi-Danner	Soave-Redlich-Kwong	- improve vapour-liquid-liquid equilibrium calculations

2.3 Application of EOS in Mass Flowrate Determination

EOS can be used to predict properties of mixtures ranging from well-defined light hydrocarbon systems to complex oil mixtures and highly non-ideal (non-electrolyte) chemical systems. Enhanced *EOS* such as *PR* and *PRSV* can be used for rigorous treatment of hydrocarbon systems; semi empirical and vapour pressure models for the heavier hydrocarbon systems; steam correlations for accurate steam property predictions; and activity coefficient models for chemical systems. In the following section, Table 2 lists some typical systems and recommended correlations.

Table 2: Recommended EOS for various applications

Type of System	Recommended Equations	Reference
Sour Gas	*PR*	Li and Guo [18]
Hydrocarbon with Hydrogen Sulfide and Carbon Dioxide	*SRK* *BWR*	Huron *et al*. [19] Evelein and Moore [20] Orye [21]
Carbon Dioxide and Chlorodiflouromethane Mixtures	*PR*	Lee *et al*. [22]
Non-aqueous Binary Mixtures	*SRK, PR, PRSV*	Lee and Lee [23]
Pure Alkanes, Ethers and Their Mixtures	*GCEOS*	Hofman *et al*. [24]
Oil Extraction Process	*ZJ, SRK*	Boss *et al*. [25]

From the table, it is shown that *EOS* is widely used in hydrocarbon system including natural gas. Radhakrishnan *et al*. [17] has conducted a study to compare all the *EOS* equations for measuring mass flowrate of natural gas using *NGV* refueling test rig located at *Universiti Teknologi Petronas* (UTP). By comparing results with Coriolis measurement, it was found that Peng Robinson was the most accurate equation and had been identified to be the *EOS* that could represent for high-pressure natural gas system. Thus, Peng Robinson was selected as *EOS* equation for the conversion purpose whilst the same test rig is used in this research.

2.4 Experimental Procedure

Two distinctive methods are used in determining the mass flowrate of natural gas passing through the measurement device: Dynamic Mass Flowrate Method and Dynamic Density Flowrate Method. Data such as volumetric flowrate, pressure and temperature obtained from the test rig are used together with pre-identified *EOS i.e.*, Peng-Robinson and will be assessed using both methods in order to identify which method will be most reliable to be used.

Three dynamic experiments were also conducted. The difference between experiments is owed to the pre-determined experimental conditions such as the initial pressure of storage tanks and the initial pressure of vehicle or receiver tank to be refueled. For all experiments, three banks of storage tanks containing natural gas at same pressure *i.e.*, 3600 psig are used to provide the source of gas for refueling the vehicle tank up to a pressure of 3000 psig. The purpose of using three different banks is to enable for refueling to take place from one bank to another thus avoiding equal deterioration of pressure in all the storage tanks. It is essential to do so in order to ensure sufficient pressure drive is available from the storage tanks to continue refueling the natural gas to the vehicle tank up to the 3000 psig requirement. An automatic switching mechanism was installed to control the subsequent switch over from one bank to another. Dynamic experiment in this project is defined as experiment that is conducted continuously, meaning natural gas is dispensed continuously into the vehicle tank and experimental data are collected for every single second during the refueling. Data obtained from each set of experiment is analyzed using the two alternative measurement methods as described earlier in the paper. Results of analysis are presented in the following section.

In the Dynamic Mass Flowrate Method, the density of natural gas is assumed to be constant and the v variable in the *EOS* represents the molar volume of natural gas. Using this method, the algorithm will straight away provide the dynamic mass flowrate of natural gas dispensed using the experimental volumetric flowrate, temperature and pressure data. The first step in Dynamic Mass Density Method is to manipulate the original Peng-Robinson *EOS* to include mass term in the equation. The equations below are used in introducing the mass term;

$$v = \frac{V}{n} \tag{2}$$

$$n = \frac{m}{MW} \tag{3}$$

where,

v = molar volume (m^3/mol)
V = volume of tank (m^3)
n = number of mol of natural gas inside the vehicle tank (kmol)
m = mass of natural gas inside vehicle tank (kg)
MW = molecular weight of natural gas (kg/kmol)

With the substitution, the following equation is obtained;

$$\mathrm{P} = \frac{RT}{\frac{V\,(MW)}{m} - b} - \frac{a\alpha}{\left(\frac{V\,(MW)}{m}\right)^2 + 2b\left(\frac{V\,(MW)}{m}\right) - b^2} \tag{4}$$

Since the concern is to obtain the mass flowrate instead of mass of natural gas inside the vehicle tank, the volumetric and mass flowrate terms is introduced to substitute the volume of tank and the mass of natural gas inside the tank and this is shown in the following equation;

$$\mathrm{P} = \frac{RT}{\frac{\dot{V}\,(MW)}{\dot{m}} - \mathrm{b}} - \frac{a\alpha}{\left(\frac{\dot{V}\,(MW)}{\dot{m}}\right)^2 + 2b\left(\frac{\dot{V}\,(MW)}{\dot{m}}\right)} \tag{5}$$

where,
$\dot{V}$ = volumetric flowrate (m^3/min)
$\dot{m}$ = mass flowrate (kg/min)

The equation is then arranged into a polynomial form below so that the root of the equation will represent the mass flowrate of natural gas.

$$(Pb^3 + RTb^2 - ab\alpha)\dot{m}^3 - (a\alpha - 3Pb^2 - 2RTb)\dot{V}(MW))\dot{m}^2 + (Pb - RT)\,(\dot{V}(MW))^2\dot{m} - P(\dot{V}(MW))^3 = 0 \tag{6}$$

The next step is the computation of the mass flowrate of natural gas. Since it is impossible to obtain the mass flowrate by means of manual calculation, the MATLAB software is employed and utilising the root function, the mass flowrate of natural gas could be obtained.

In the Dynamic Density Flowrate Method, the v variable in the *EOS* represents the specific volume of natural gas hence the specific gas constant is used rather than the universal gas constant. Using this approach, the algorithm is arranged in such a way that it will provide the dynamic density of natural gas flowing through the measurement device and the mass flowrate of natural gas will be the product of the density and the volumetric flowrate given by the measurement device. The original *EOS* is manipulated to include density term in the equation. The equation below is used in introducing the density term;

$$v = \frac{1}{\rho} \tag{7}$$

where,
v = specific volume (m^3/kg)
ρ = density of natural gas (kg/m^3)

Thus, the following equation will be obtained;

$$\rho = \frac{RT}{v - b} - \frac{a\alpha}{v^2 + 2bv - b^2} \tag{8}$$

The equation is then arranged into a polynomial form below so that the root of the equation will represent the density of natural gas.

$$(Pb^3 + b^2RT - ab\alpha)\,\rho^3 + (3Pb^2 + 2bRT - a\alpha)\rho^2 + (Pb - RT)\rho + P = 0 \tag{9}$$

The MATLAB program is once again employed to solve for the root of the above equation, which represents the density of natural gas. The mass flowrate of natural gas dispensed into vehicle tank is the product of the dynamic density computed using the *EOS* and the volumetric flowrate measured by the alternative flow meter. For both methods, profiles of calculated mass flowrates using Peng Robinson equation and volumetric data are compared with actual mass flowrate directly measured by Coriolis flow meter to identify the deviation extent between them.

3.0 RESULTS AND DISCUSSIONS

Experiment 1 was conducted under automatic sequencing mode with initial storage pressure of 3600 psig for all three banks and refueling was done to a receiver tank with initial storage pressure less than 20 psig. The analysis using the Dynamic Mass Flowrate Method and Dynamic Density Flowrate Method had produced mass flowrate result that was presented in Figures 2 and 3 respectively. Each of the figures represents calculated mass flowrate obtained from both EOS conversions respectively which was also compared with mass flowrate data obtained from actual Coriolis meter (*please refer graph legend*). From Figures 2 and 3 again, it was observed that the calculated mass flowrate followed the trend of actual Coriolis flowmeter. For experiment 1, the average error for Dynamic Mass Flowrate Method and Dynamic Density Flowrate Method compared to Coriolis were 6.755% and 4.973%, respectively. Average error was defined as error of mass flowrate between the developed method and Coriolis measurement starting from initial pressure until receiver pressure reaches about 3000 psig.

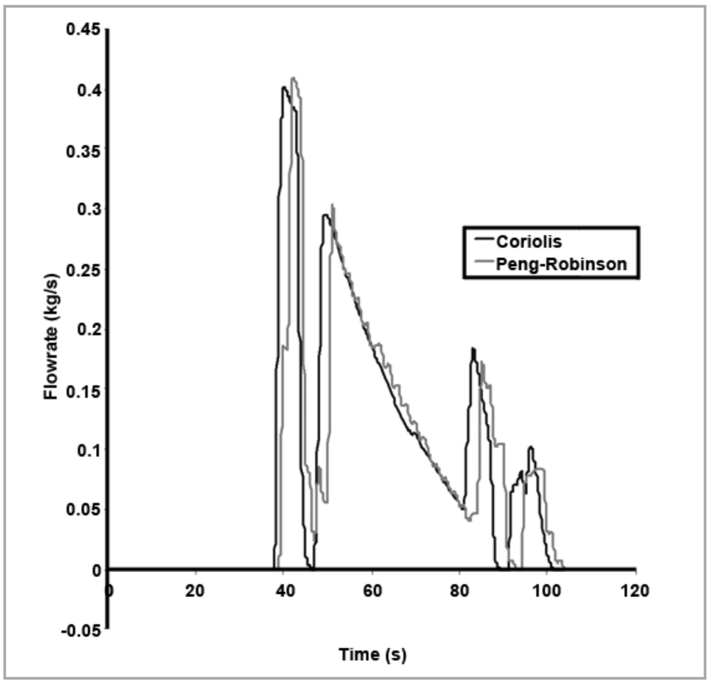

Figure 2: Mass flowrate for experiment 1 using dynamic mass flowrate method

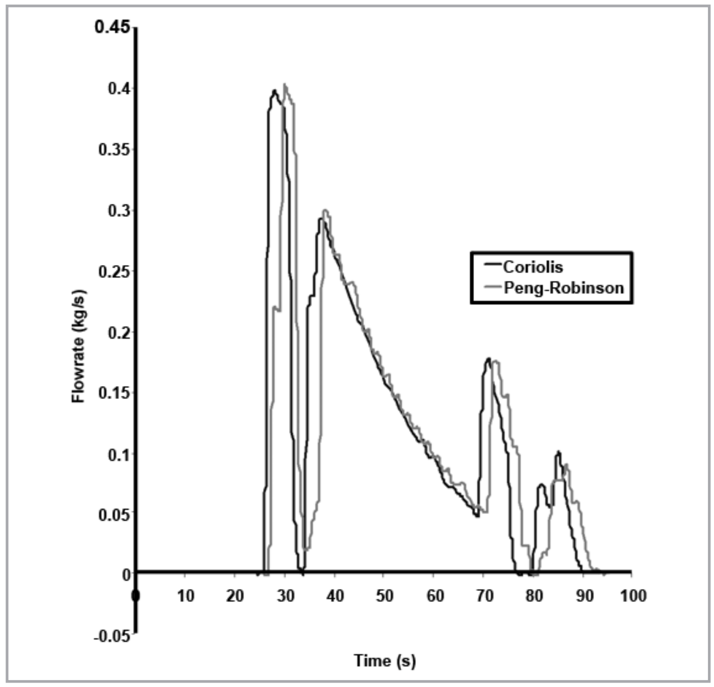

Figure 3: Mass flowrate for experiment 1 using dynamic density flowrate method

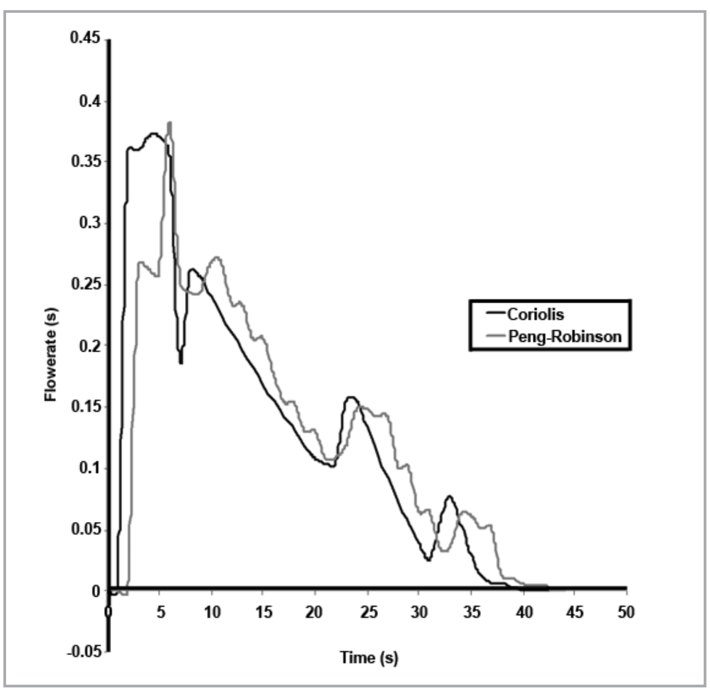

Figure 4: Mass flowrate for experiment 2 using dynamic mass flowrate method

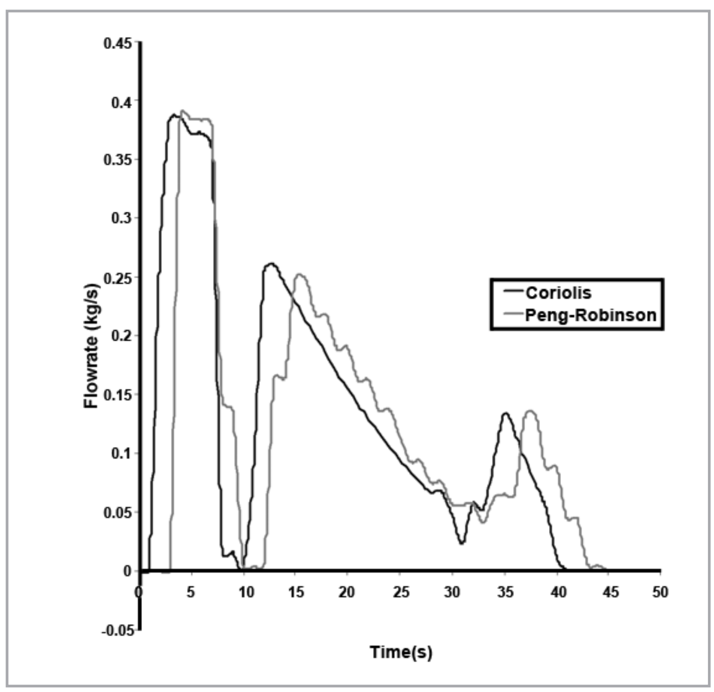

Figure 5: Mass flowrate for experiment 2 using dynamic density flowrate method

Experiment 2 was conducted with initial storage pressure of 3600 psig for all the 3 banks and receiver's initial pressure was about 1000 psig. The result of mass flowrates obtained using the Dynamic Mass Flowrate Method and Dynamic Density Flowrate Method was shown in Figures 4 and 5, respectively. From Figures 4 and 5 again, it was observed that the mass flowrate obtained using the *EOS* conversion measurement followed the trend of the Coriolis plot. However, there was still a reasonably big deviation from the reference. For experiment 2, the average error for Dynamic Mass Flowrate Method and Dynamic Density Flowrate Method compared to Coriolis were 5.889% and 0.791%, respectively.

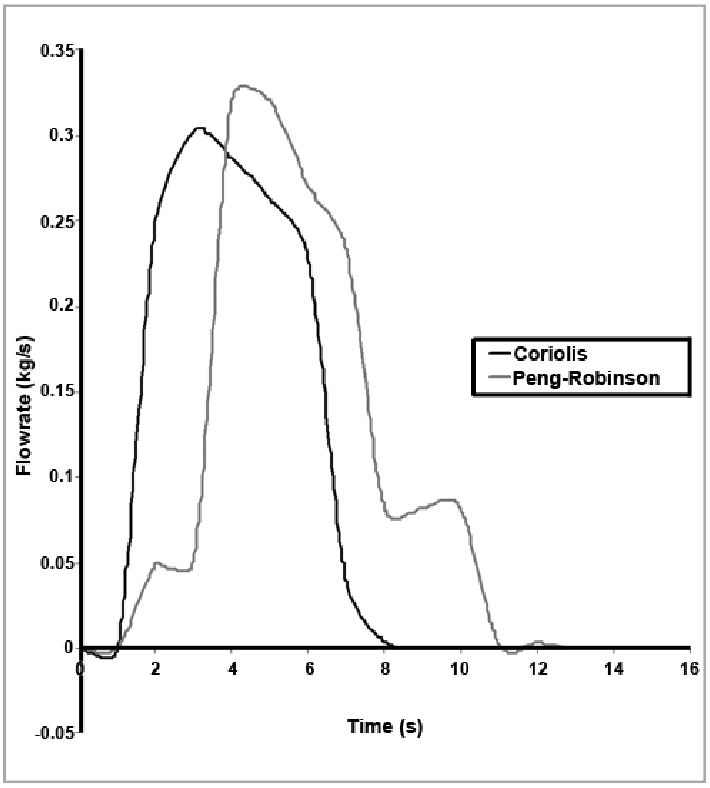

Figure 6: Mass flowrate for experiment 3 using dynamic mass flowrate method

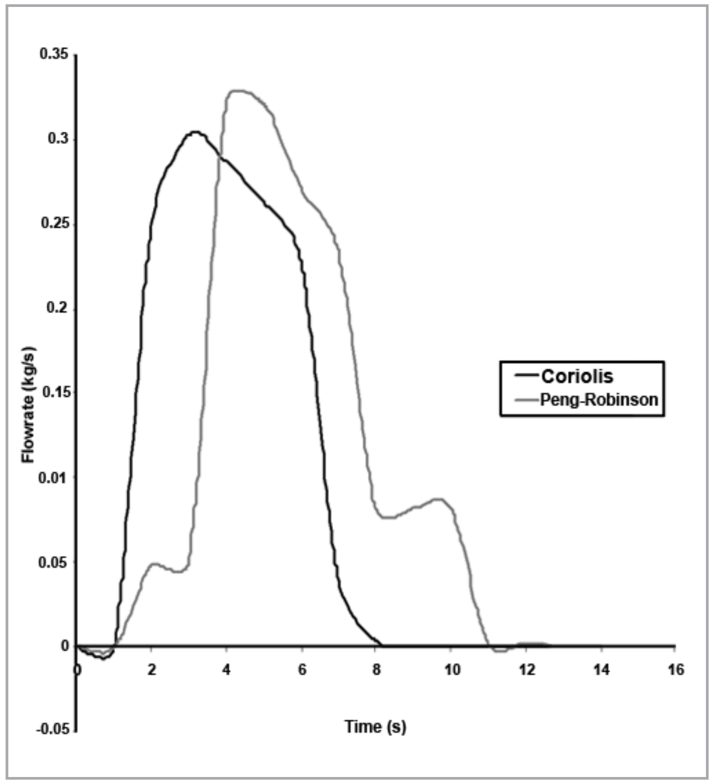

Figure 7: Mass flowrate for experiment 3 using dynamic density flowrate method

Experiment 3 was conducted with initial storage pressure of 3600 psig for all the 3 banks and receiver's initial pressure was about 2000 psig. The results obtained using the Dynamic Mass Flowrate Method and Dynamic Density Flowrate Method was shown in Figures 6 and 7, respectively. From Figures 6 and 7 again, it was observed that the mass flowrates obtained using the developed *EOS* metering system followed the trend of the Coriolis plot. For experiment 3, the average error for Dynamic Mass Flowrate Method and Dynamic Density Flowrate Method compared to Coriolis were 8.995% and 2.533% respectively.

Even though the natural gas was transferred from only three storage banks, it was clearly observed that there were four maximum peaks in all graphs. The first peak was the turn out of the initialisation of flow as stated in the process description, while the subsequent three peaks were due to the sudden flow increase of natural gas as a result of switching from one bank to another. An error analysis was done to detect which methods produced minimal error compared to Coriolis. Tables 3 and 4 show the result of error analysis.

Table 3: Error analysis for dynamic mass flowrate method

Experiment	Method	Coriolis (kg)	EOS (kg)	Error (%)
1	Mass	8.734	8.144	6.755
2	Mass	5.791	5.450	5.889
3	Mass	1.373	1.496	8.995
Average Error				7.213

Table 4: Error analysis for dynamic density flowrate method

Experiment	Method	Coriolis (kg)	EOS (kg)	Error (%)
1	Density	8.760	8.324	4.973
2	Density	5.700	5.655	0.791
3	Density	1.411	1.446	2.533
Average Error				2.766

From the error analysis, it was found that Dynamic Density Flowrate Method had produced smaller average error compared to Dynamic Mass Flowrate Method which was 2.766% compared to 7.213% respectively.

5.0 CONCLUSIONS

In this research, two distinctive methods were presented to be used as conversion tool in determining the mass flowrate of natural gas: Dynamic Mass Flowrate Method and Dynamic Density Flowrate Method. However, when both methods were compared with actual measurement using Coriolis flowmeter, it was found that Dynamic Density Flowrate Method had produced minimal average error compared to Dynamic Mass Flowrate Method. From the results obtained and analysis performed, it was found that the average error between Dynamic Density Flowrate Method and data measured by Coriolis flow meter was about 2.766%. Thus, Dynamic Density Flowrate Method was verified as the suitable conversion tool to be used as *EOS* metering system for converting volumetric to mass flowrate of natural gas. From here, it could be said that the research objective to develop an alternative metering system which offer an efficient and lower cost method for measuring mass flowrate in *NGV* refueling measurement has been successfully achieved. ■

REFERENCES

[1] Daud. M.G., "Experiences and Challenges in the Implementation of NGV/ CNG as a Clean Fuel of Choice for Malaysian Transportation Sector", ANGVA 2005 Conference, Kuala Lumpur, July, 2005.

[2] Bechtold R.L., "Alternative Fuels for Vehicle Fleet Demonstration Program" (Volume 1), March, 1997.

[3] Harris G., A.Lawson, "Are NGV's Better At Reducing Emissions Than Alternatives?", IANGVA Conf, Buenos Aires, Oct, 2004.

[4] Aberant M., N. Checklick, B. Elmendorf, "Greenhouse Gas Reduction Projects and Natural Gas Vehicles", IANGVA Conf, Buenos Aires, Oct, 2004.

[5] Lawson A., "Natural Gas Buses Can Meet EPA 2010 Standards Toda", IANGVA Conf, Buenos Aires, Oct, 2004.

[6] Nylund N., K. Erkkila, "Transit Bus Emission Study-Comparison of Emission from Diesel to Natural Gas Buse", IANGVA Conf, Buenos Aires, Oct, 2004.

[7] "Well to Wheel Energy Use and Greenhouse Gas Emissions of Fuel/ Vehicle Systems-Executive Summary Report", General Motors Corporation, Argonne National Laboratory, BP, ExxonMobile, Shell, June, 2001.

[8] Schuker M., "Experiences and Challenges in CNG Measurement – The Case for Coriolis Flow Meter", ANGVA 2005, Kuala Lumpur, July, 2005.

[9] Daubert T.E., Chemical Engineering Thermodynamics, McGraw Hill, 1985.

[10] Winnick J., Chemical Engineering Thermodynamics, John Wiley and Sons, Inc, 1997.

[11] Soave G., "Equilibrium Constants from a Modified Redlich–Kwong Equation of State", Journal of Chemical Engineering Science, Volume 27, No. 6, 1197-1203, 1972.

[12] Peng, D. Y., Robinson, D. B., "A Two Constant Equation of State", I.E.C. Fundamentals, 15, 59-64, 1976.

[13] Stryjek R., J.H. Vera, "PRSV: An Improved Peng Robinson Equation of State with New Mixing Rules For Strongly Non-ideal Mixtures", Canadian Journal of Chemical Engineering, Volume 64, 334-340, (1986).

[14] Plocker U., H. Knapp, J. Prausnitz "Calculation of High-pressure Vapor-Liquid Equilibria from a Corresponding-States Correlation with Emphasis on Asymmetric Mixtures" Ind. Eng. Chem. Process Des. Dev., Vol. 17, No. 3, (1978).

[15] Zudkevitch, D., Joffee, J. "Correlation and Prediction of Vapor-Liquid Equilibria with the Redlich-Kwong Equation of State", AIChE Journal, Volume 16, No. 1, 112-119, (1970).

[16] Kabadi, V.N., Danner R.P. "A Modified Soave-Redlich-Kwong Equation of State for Water-Hydrocarbon Phase Equilibria", Ind. Eng. Chem. Process Des. Dev., Volume 24, No. 3, 537-54, 1985.

[17] Radhakrishnan V.R., N.A. Hisam, M.I.A. Mutalib, M.Dahari, N.B Mellon, M.A. Abdullah, J. Mengat, "Calculation of Mass of Gas Using Equation of State for NGV Refueling Equipment" ANGVA 2005 Conf, Kuala Lumpur, July, 2005.

[18] Li Q., T.M. Guo, "A Study on the Super Compressibility and Compressibility Factors of Natural Gas Mixtures" Journal of Petroleum Science and Engineering, Volume 6, 235–247, 1991.

[19] Huron M.J., G.N. Dufour, J. Vidal, "Vapour-liquid Equilibrium and Critical Locus Curve Calculations with the Soave Equation for Hydrocarbon Systems with Carbon Dioxide and Hydrogen Sulphide", Journal of Fluid Phase Equilibria 1 247–252, 1978.

[20] Evelein K.A, G.R. Moore, "Prediction of Phase Equilibria in Sour Natural Gas System Using the Soave-Redlich-Kwong Equation of State", Journal of Industrial Engineering Chemical Process Design Dev.18, Volume 10 No. 4, 1979.

[21] Orye R.V. "Prediction and Correlation of Phase Equilibria and Thermal Properties with the BWR Equation of State" Ind. Eng. Chem. Res. Vol. 8 No. 4, Oct, 1969.

[22] Lee J.M., B.C. Lee, C.H. Cho, "Measurement of Bubble Point Pressures and Critical Points of Carbon Dioxide and Chlorodifluoromethane Mixtures Using the Variable-Volume View Cell Apparatus" Korean J. Chem. Eng., Volume 17, No.5, 510-515, 2000.

[23] Lee L. S., Y. S. Lee, "The Application of the Equations of State Incorporated with Mixing Rules for Viscosity Estimations of Binary Mixtures" Fluid Phase Equilibria 181 47–58, 2001.

[24] Hofman T., J. Gonzalez, C. Casanova "Properties of Pure Alkanes, Ethers and Their Mixtures by a Hole Model Group-Contribution Equation of State" Fluid Phase Equilibria 156, 3–20, 1999.

[25] Boss E. A., M.M. Santos, R.M. Filho "Plant Performance Analysis of Conventional and Supercritical oil Extraction Processes", Brazilian Congress of Phase Equilibrium and Fluid Properties for Chemical Process Design.

PROFILES

MAHIDZAL DAHARI

Mahidzal Dahari is the Research Officer at University Technology of PETRONAS. Currently, he is working for his PhD in Electrical and Electronic Engineering and his research focus is Natural Gas Refueling Technology.

AP. DR MOHAMED IBRAHIM ABDUL MUTALIB

AP. Dr Mohamed Ibrahim Abdul Mutalib is the Project Leader for NGV Refueling Facilities and Equipment at University Teknologi Petronas, an intensified research project granted by Ministry of Science, Technology and Innovation (MOSTI), Malaysia.

ANALYSIS OF POTENTIAL FLOW AROUND TWO-DIMENSIONAL HYDROFOIL BY SOURCE BASED LOWER AND HIGHER ORDER PANEL METHODS

(Date received: 21.5.2008)

Md. Shahjada Tarafder[1], Gazi Md. Khalil[2] and Muhammad Rabiul Islam[3]
[1,2,3]Department of Naval Architecture and Marine Engineering
Bangladesh University of Engineering and Technology
Dhaka-1000, Bangladesh
E-mail: shahjada68@yahoo.com.[1]

ABSTRACT

This paper deals with the computation of potential flow problem around the two-dimensional hydrofoil without considering the effect of free surface by the source based lower and higher order panel methods. Using Green's second identity the Laplace equation is transformed into an integral equation in terms of a distribution of singular solutions, such as sources on the boundaries. After satisfying the boundary conditions the integral equation can be written into a matrix form and the matrix is solved by Gaussian Elimination procedure. The validity of the computer scheme is examined by comparing the numerical results with the analytical as well as experimental results of van de Vooren and NACA 0012 hydrofoils. In comparison to the higher order method, the use of the lower order method results in fewer numerical manipulations and hence less computational time. Each method has the problem near the trailing edge of the hydrofoil.

Keywords: *Kutta Condition, Lower and Higher Order Panel Method, Potential Flow, NACA 0012 Hydrofoils and van de Vooren*

1.0 INTRODUCTION

Hydrofoil is a winglike structure attached to the hull of a boat that raises all or part of the hull out of the water when the boat is moving forward, reducing drag. The practical importance of hydrodynamic analysis of hydrofoils moving under a free surface is very well-known. Thin-foil approximation and the Neumann boundary condition were generally used. Giesing and Smith [1] distributed the Kelvin wave source on the hydrofoil surface, which satisfies the linearised free surface condition, and they obtained an integral equation for the source strength by applying the kinematic Neumann body boundary condition. This integral equation was solved numerically.

Hough and Moran [2] studied thin-foil approximation with linearised free surface condition. They examined the flow around flat-plate and cambered-arc hydrofoils. Salvesen and Von Kerczek [3,4] first computed steady nonlinear free-surface waves due to a two-dimensional hydrofoil and a point vortex under the free surface by a finite-difference iterative technique. Bai [5] applied the localised finite element numerical technique using Galerkin's method. In this method, an integral equation on the hydrofoil surface is replaced by a system of equations, over a much larger fluid domain but having a much simpler kernel. Yeung and Bouger [6] used a hybrid integral equation method based on Green's theorem. They satisfied the linearised free surface condition and the exact body boundary condition.

Kennell and Plotkin [7] addressed the potential flow about a thin two-dimensional hydrofoil moving with constant velocity at a fixed depth beneath a free surface. The thickness-to-chord ratio of the hydrofoil and disturbances to the free stream were assumed to be small. These small perturbation assumptions were used to produce first-and second-order sub problems structured to provide consistent approximations to boundary conditions on the body and the free surface.

Forbes [8] presented a method for computing two-dimensional potential flow about a wing with a cusped trailing edge immersed beneath the free surface of a running stream of infinite depth. The full non-linear boundary conditions were retained at the free surface of the fluid and the conditions on the hydrofoil were also stated exactly. The problem was solved numerically using integral-equation technique combined with Newton's method. Bai and Han [9] applied the localised finite element method to solve the nonlinear problem. Wu and Eatock Taylor [10] compared the finite element method with the boundary element method for the nonlinear time stepping solution of 2-D hydrofoils.

Bal [11] described a potential-based panel method for the hydrodynamic analysis of 2-D hydrofoils moving under a free surface with constant speed without consideration of the cavitation phenomenon. By applying Green's theorem and choosing the value of internal potential as equal to the incoming flow potential, an integral equation for the total potential was obtained under the potential flow theory. The free surface condition was linearised and the Dirichlet boundary condition was used instead of the Neumann boundary condition. The 2-D hydrofoil was approximated by line panels on which there were only constant doublet distributions. The method of image was used for satisfying the linearised free surface condition and all the terms in the fundamental solution of total potential were integrated over a line panel.

Bal [12] addressed steady cavitating flows around swept and *V*-type hydrofoils under a free surface by using an iterative numerical method. The iterative nonlinear numerical method based on Green's theorem allowed separating cavitating hydrofoil problem and free surface problem. These two problems were solved separately with the effect of one on the other being accounted for in an iterative manner. Cavitating hydrofoil surface and the free surface were modeled numerically with constant strength doublet and constant strength source panel. The source strength on the free surface was expressed in terms of perturbation potential by applying the free surface condition. No radiation condition was enforced for the downstream and transverse boundary on the free surface.

Tarafder *et. al*. [13] presented the Rankine source panel for the potential flow around the two-dimensional body moving under a free surface. The method of image is used to satisfy the linearised free surface condition. In addition, an iterative panel method has been applied for surface piercing hydrofoils without cavitation in Hsin and Chou [14]. Kim [15] and Ragab [16] solved the submerged high speed hydrofoil problem without cavitation.

The aim of this paper is to present the basic mathematical theory behind the lower and higher order source based panel methods and draw a comparison in order to find the suitable method for the analysis of the potential flow around the hydrofoils without considering the effect of free surface.

2.0 MATHEMATICAL MODELLING OF THE PROBLEM

Consider a hydrofoil fixed in a stream of uniform flow with a velocity Q_∞ as shown in Figure 1. The depth of water from the mean line of the hydrofoil is *h*. A Cartesian co-ordinate system is placed on the free surface and the components of the free stream velocity Q_∞ in the *x*-*z* frame of reference are U_∞ and W_∞ respectively. The angle of attack α is defined as the angle between the free stream velocity and the *x*-axis

$$\alpha = tan^{-1}\frac{W_\infty}{U_\infty}$$

It is assumed that the fluid is inviscid, incompressible and the flow irrotational. The perturbation velocity potential ϕ is defined by $\Phi = \phi + \Phi_\infty$

where, $\Phi_\infty = U_\infty x + W_\infty z = x\, Q_\infty \cos\alpha + z\, Q_\infty \sin\alpha$

The total velocity potential Φ_∞ satisfies the Laplace equation

$$\nabla^2\Phi = 0 \qquad (1)$$

in the fluid domain Ω. The domain Ω is bounded by the body surface S_B, wake surface S_W and an outer control surface S_∞ surrounding the body and the wake surface. Now the problem for the hydrofoil can be constructed by specifying the boundary conditions as follows:

(a) The velocity component normal to the solid boundaries of the hydrofoil must be zero and in a frame of reference:

$$\nabla\Phi \cdot n = 0 \qquad (2)$$

where *n* is a unit normal vector directed outward from the fluid domain Ω.

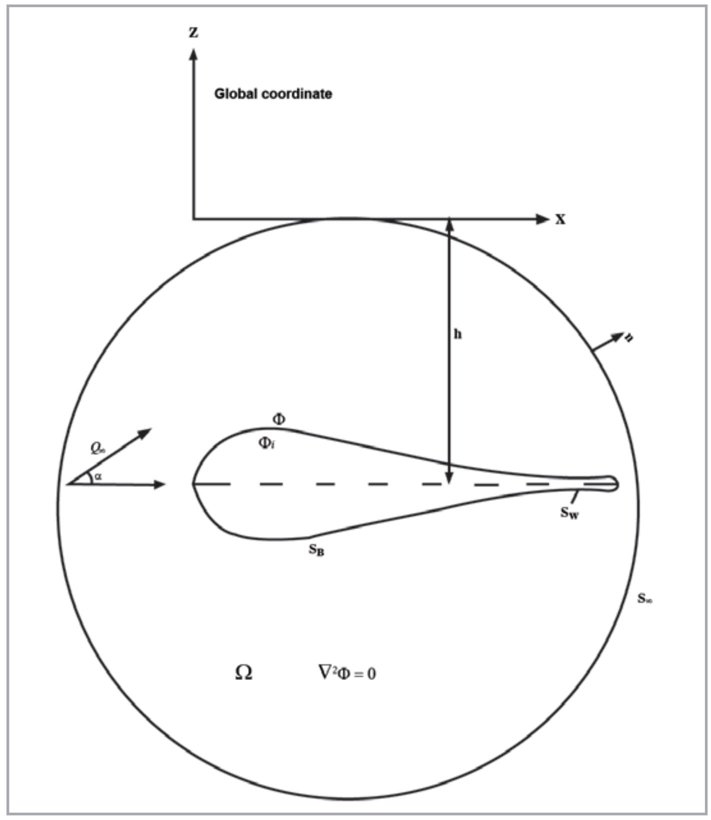

Figure 1 : Potential flows over a closed body

(b) The disturbance induced by the hydrofoil will decay far from the body

$$\lim_{r\to\infty}\nabla\Phi = Q_\infty \qquad (3)$$

which is automatically fulfilled by the singular solutions such as for the source, doublet or the vortex elements.

(c) A proper solution for the doublet distribution will have to fulfil the Kutta condition at the trailing edge of the lifting body such that the potential jump across the wake surface S_W is the same as the circulation and is constant in the streamwise direction on S_W. If the velocity potential inside the body surface S_B is defined by Φ_i then,

$$[\Delta\Phi]_{on\, S_W} = \Phi - \Phi_i = \Gamma = \text{Constant}$$
$$= \Delta\Phi_{\text{T.E.}} \qquad (4)$$

3.0 THE GENERAL SOLUTION BASED ON GREEN'S IDENTITY

Applying Green's Second identity the Laplace equation can be transformed into an integral equation as:

$$\Phi(P) = -\frac{1}{2\pi}\int_S (1\text{n}\, r\nabla\Phi - \Phi\nabla\, 1\text{n}\, r).n\, dS$$

in which the boundary *S* is composed of S_B, S_W and S_∞. If the point of singularity lies inside the domain Ω, the velocity potential can be expressed as

$$\Phi(P) = -\frac{1}{2\pi}\int_{S_B} (1\text{n}\, r\, \nabla(\Phi - \Phi_i) - (\Phi - \Phi_i)\,\nabla\, 1\text{n}\, r)\,.\, n\, dS$$

$$+\frac{1}{2\pi}\int_{S_W}\Phi\, n\,.\,\nabla\, 1\text{n}\, r\, dS+\Phi_\infty(p) \tag{5}$$

If the difference between the external and internal potentials or the difference between the normal derivative of the external and internal potentials by

$$-\mu=\Phi-\Phi_i \tag{6}$$

$$-\sigma=\frac{\partial\Phi}{\partial \text{n}}-\frac{\partial\Phi_i}{\partial \text{n}} \tag{7}$$

the integral equation (5) can be written as

$$\Phi(P)=\frac{1}{2\pi}\int_{S_B}\left[\sigma\, 1\text{n}\, r-\mu\frac{\partial}{\partial n}(1\text{n}\, r)\right] dS$$

$$-\frac{1}{2\pi}\int_{S_W}\left[\mu\frac{\partial}{\partial n}(1\text{n}\, r)\right] dS+\Phi_\infty(P) \tag{8}$$

The elements μ and σ in Equations (6) and (7) are called the strength of the doublet and source respectively and the minus sign is a result of the normal vector n pointing into S_B. To satisfy the Neumann boundary condition of Equation (2) directly, the velocity field due to the singularity distribution of Equation (8): is used

$$\nabla\Phi(x,y)=\frac{1}{2\pi}\int_{S_B}\sigma\nabla(1\text{n}\, r)\, dS$$

$$-\frac{1}{2\pi}\int_{S_B+S_W}\mu\nabla\left[\frac{\partial}{\partial \text{n}}(1\text{n}\, r)\right] dS+\nabla\Phi_\infty \tag{9}$$

If the singularity distribution strengths σ and μ are known, then Equation (9) describes the velocity field everywhere (of course special treatment is needed when the velocity is evaluated on the surface S_B). Substitution of Equation (9) into the boundary condition in Equation (2) results in

$$\left\{\frac{1}{2\pi}\int_{S_B}\sigma\nabla(1\text{n}\, r)dS\right.$$

$$\left.-\frac{1}{2\pi}\int_{S_B+S_W}\mu\nabla\left[\frac{\partial}{\partial \text{n}}(1\text{n}\, r)\right] dS+\nabla\Phi_\infty\right\}.n=0 \tag{10}$$

This equation is the basis for many numerical solutions and should hold for every point on the surface S_B. To construct a numerical solution the surface S is divided into N panels and the integration is performed for each panel such that

$$\frac{1}{2\pi}\sum_{j=1}^{N}\int_{S_B}\sigma\nabla(1\text{n}\, r)dS\,.\,n$$

$$-\frac{1}{2\pi}\sum_{j=1}^{N}\int_{S_B}\mu\nabla\left[\frac{\partial}{\partial n}(1\text{n}\, r)\right] dS\,.\,n$$

$$-\frac{1}{2\pi}\sum_{j=1}^{N}\int_{S_W}\mu\nabla\left[\frac{\partial}{\partial n}(1\text{n}\, r)\right] dS\,.\,n+\nabla\Phi_\infty\,.\,n=0 \tag{11}$$

3.1 LOWER ORDER PANEL METHOD

An even simpler lower order panel method (constant strength source method) can be derived by setting the doublet strength μ to zero in Equation (11). Thus

$$\frac{1}{2\pi}\sum_{j=1}^{N}\int_{S_B}\sigma\nabla(1\text{n}\, r)dS\,.\,n+\nabla\Phi_\infty\,.\,n=0 \tag{12}$$

Now the above equation can be written as

$$\sum_{\substack{j=1\\i=1}}^{N}a_{ij}\sigma_j+\sum_{i=1}^{N}\nabla\Phi_\infty\,.\,n=0 \tag{13}$$

where,

$$\frac{1}{2\pi}\int\nabla(1\text{n}\, r)dS\,.\,n_i=(u,w)_{ij}\,.\,n_i=a_{ij} \tag{14}$$

The influence co-efficient a_{ij} is defined as the velocity component normal to the surface. The velocity induced by the panel $(u, w)_{ij}$ will be calculated by using Equations (A10) and (A11) of Appendix. Writing the term Φ_∞ in terms of velocity component, Equation (13) can be written as

$$\sum_{\substack{j=1\\i=1}}^{N}a_{ij}\sigma_j+\sum(U_\infty, W_\infty)\,.\,n_i=0 \tag{15}$$

where $(U_\infty, W_\infty) = -Q_\infty\,(cos\ \alpha, sin\ \alpha)$ and $n_i = (\sin\alpha_i, \cos\alpha_i)$. For the case of symmetric hydrofoil $W_\infty = 0$ and the free stream normal velocity component is transferred to the right hand side and the following equation can be written as:

$$RHS_i=-U_\infty\, sin\ \alpha_i \tag{16}$$

At each collocation point the influences of the singularity elements (a_{ij}) are calculated and then specifying the boundary condition for each ($i = 1\rightarrow N$)of the collocation points results in a set of algebraic equations with the unknown σj ($j = 1\rightarrow N$). A combination of Equations (15) and (16) will have the form

$$\begin{pmatrix} a_{11} & a_{12} & \cdots & a_{1N} & \sigma_1\\ a_{21} & a_{22} & \cdots & a_{2N} & \sigma_2\\ a_{31} & a_{32} & \cdots & a_{3N} & \sigma_3\\ \cdot & \cdot & \cdots & \cdot & \cdot\\ \cdot & \cdot & \cdots & \cdot & \cdot\\ \cdot & \cdot & \cdots & \cdot & \cdot\\ \cdot & \cdot & \cdots & \cdot & \cdot\\ a_{N1} & a_{N2} & \cdots & a_{NN} & \sigma_N \end{pmatrix}=\begin{pmatrix} RHS_1\\ RHS_2\\ RHS_3\\ \cdot\\ \cdot\\ \cdot\\ \cdot\\ RHS_N \end{pmatrix} \tag{17}$$

The above set of algebraic equations has a well-defined diagonal and can be solved for σ_j by using Gaussian elimination method.

3.1.1. Calculations of Pressures and Loads

Once the strengths of the sources σ_j is known, the total tangential velocity Q_t at each collocation point can be calculated as

$$Q_{ti}=\left[\sum_{\substack{j=1\\i=1}}^{N}(u,w)_{ij}+(U_\infty,W_\infty)\right].\ t_i \tag{18}$$

where, $t_i = (cos\ \alpha_i, -sin\ \alpha_i)$. Now the pressure coefficient then becomes

$$C_p=1-\frac{Q_t^2}{Q_\infty^2} \tag{19}$$

Note that this method is derived here for non-lifting shapes and the Kutta condition is not used. Consequently, the circulation of the hydrofoil will be zero and hence no lift and drag will be produced.

3.2 HIGHER ORDER PANEL METHOD

The formulation for the higher order panel method (linear strength source method) can be derived by setting the doublet strength μ to zero in Equation (11)

$$\frac{1}{2\pi}\sum_{j=1}^{N}\int \sigma\nabla(\ln r)dS.\, n + \nabla\Phi_{\infty}\,.\, n = 0 \qquad (20)$$

Now the above equation can be written as

$$\sum_{\substack{j=1\\ i=1}}^{N} a_{ij}\sigma_j + \sum_{j=1}^{N}\nabla\Phi_{\infty}\,.\, n_i = 0 \qquad (21)$$

where,

$$\frac{1}{2\pi}\int\nabla(\ln r)dS\,.\, n_i = a_{ij} \qquad (22)$$

The source-only based method will be applicable only to non-lifting configurations and is considered to be a more refined model than the one based on constant-strength source elements. The influence co-efficient a_{ij} will be calculated as follows:

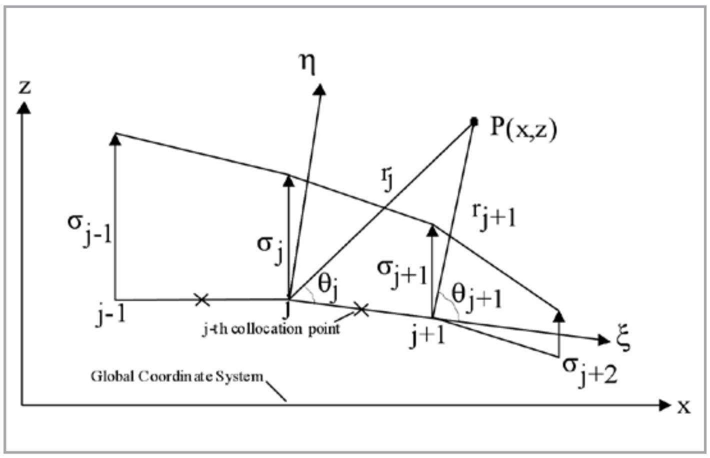

Figure 2 : Nomenclature for a linear-strength surface singularity element

A segment of the discretised singularity distribution on a solid surface is shown in Figure 2. To establish a normal-velocity boundary condition based method, the induced-velocity formulas of a constant and a linear-strength source distribution are combined by Equations (A7), (A20), (A8) and (A21) of Appendix. The parameters r and θ are shown in Figure 2 and the velocity (u, w) measured in the panel local coordinate system $p(\xi, \eta)$ has components

$$u_p = \frac{\sigma_0}{4\pi}\ln\frac{r_1^2}{r_2^2} + \frac{\sigma_1}{2\pi}\left[\frac{x-\xi_1}{2}\ln\frac{r_1^2}{r_2^2} + (\xi_1-\xi_2) + z(\theta_2-\theta_1)\right] = \left[\frac{\sigma_0}{2\pi} + \frac{\sigma_1}{2\pi}(x-\xi_1)\right]\ln\frac{r_1}{r_2} + \frac{\sigma_1}{2\pi}\left[(\xi_1-\xi_2) + z(\theta_2-\theta_1)\right] \qquad (23)$$

$$W_p = \frac{\sigma_0}{2\pi}(\theta_2-\theta_1) + \frac{\sigma_1}{4\pi}\left[z\ln\frac{r_2^2}{r_1^2} + 2(x-\xi_1)(\theta_2-\theta_1)\right]$$

$$= \frac{\sigma_1}{2\pi} z\ln\frac{r_2}{r_1} + \frac{\sigma_0}{2\pi}(\theta_2-\theta_1) + \frac{\sigma_1}{2\pi}(x-\xi_1)(\theta_2-\theta_1) \qquad (24)$$

where the subscripts 1 and 2 refer to the panel edges j and $j+1$ respectively. In these Equations σ_0 and σ_1 are the source strength values, as shown in Figure 3. If the strength of σ at the beginning of each panel is set equal to the strength of the source at the end point of the previous panel (as shown in Figure 2), a continuous source distribution is obtained.

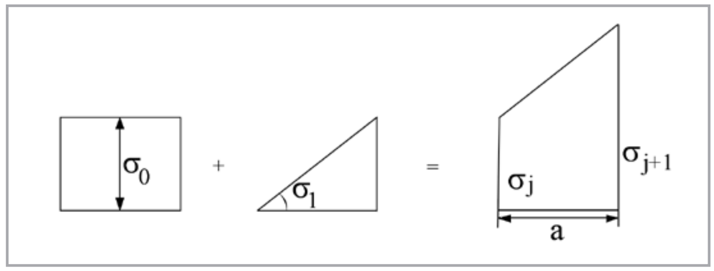

Figure 3 : Decomposition of a generic linear-strength singularity element.

Now, if the unknowns are the panel edge values of the source distribution (σ_j, $\sigma_j + {}_1$, ······· as in Figure 2) then for N surface panels on a closed body the number of unknowns is N+1. The relation between the source strengths of the elements shown in Figure 3 and the panel edge values is

$$\sigma_j = \sigma_0 \qquad (25a)$$

$$\sigma_{j+1} = \sigma_0 + \sigma_1 a \qquad (25b)$$

where a is the panel length, and for convenience the induced-velocity equations are rearranged in terms of the panel-edge surface strengths σ_j and σ_{j+1} (and the subscripts 1 and 2 are replaced with the j and j+1 subscripts respectively):

$$u_p = \frac{\sigma_j(\xi_{j+1}-\xi_j) + (\sigma_{j+1}-\sigma_j)(x-\xi_j)}{2\pi(\xi_{j+1}-\xi_j)}\ln\frac{r_j}{r_{j+1}} - \frac{z}{2\pi}\frac{(\sigma_{j+1}-\sigma_j)}{(\xi_{j+1}-\xi_j)}\frac{(\xi_{j+1}-\xi_j)}{z} + (\theta_{j+1}-\theta_j) \qquad (26)$$

$$w_p = \frac{z}{2\pi}\frac{(\sigma_{j+1}-\sigma_j)}{(\xi_{j+1}-\xi_j)}\ln\frac{r_{j+1}}{r_j} + \frac{\sigma_j(\xi_{j+1}-\xi_j) + (\sigma_{j+1}-\sigma_j)(x-\xi_j)}{2\pi(\xi_{j+1}-\xi_j)} + (\theta_{j+1}-\theta_j) \qquad (27)$$

Note that Equations (26) and (27) can be divided into velocity induced by σ_j and by σ_{j+1} such that

$$(u, w)_p = (u^a, w^a)_p + (u^b, w^b)_p \qquad (28)$$

where the subscript $(\ )^a$ and $(\ )^b$ represent the contribution due to the leading and trailing singularity strengths, respectively. If Equations (26) and (27) are arranged we can separate the $(\ )^a$ part of the velocity components as,

$$u_p^a = \frac{\sigma_j(\xi_{j+1}-x)}{2\pi(\xi_{j+1}-\xi_j)}\ln\frac{r_j}{r_{j+1}} + \frac{z}{2\pi}\left(\frac{\sigma_j}{\xi_{j+1}-\xi_j}\right)\left[\frac{(\xi_{j+1}-\xi_j)}{z} + (\theta_{j+1}-\theta_j)\right] \qquad (29a)$$

$$w_p^a = \frac{z}{2\pi}\left(\frac{\sigma_j}{(\xi_{j+1}-\xi_j)}\right) \ln \frac{r_{j+1}}{r_j} + \frac{\sigma_j(\xi_{j+1}-x)}{2\pi(\xi_{j+1}-\xi_j)}(\theta_{j+1}-\theta_j) \quad (29b)$$

from the $(\;)^b$ part of the velocity components,

$$u_p^b = \frac{\sigma_{j+1}(x-\xi_j)}{2\pi(\xi_{j+1}-\xi_j)} \ln \frac{r_j}{r_{j+1}} - \frac{z}{2\pi}\left(\frac{\sigma_{j+1}}{\xi_{j+1}-\xi_j}\right)\left[\frac{(\xi_{j+1}-\xi_j)}{z} + (\theta_{j+1}-\theta_j)\right] \quad (29c)$$

$$w_p^b = -\frac{z}{2\pi}\left(\frac{\sigma_{j+1}}{\xi_{j+1}-\xi_j}\right) \ln \frac{r_{j+1}}{r_j} + \frac{\sigma_{j+1}(x-\xi_j)}{2\pi(\xi_{j+1}-\xi_j)}(\theta_{j+1}-\theta_j) \quad (29d)$$

To transform these velocity components back to the (x, z) coordinates, a rotation by the panel orientation angle α_i is performed by the following equation:

$$\begin{bmatrix} u \\ w \end{bmatrix} = \begin{bmatrix} \cos\alpha_i & \sin\alpha_i \\ -\sin\alpha_i & \cos\alpha_i \end{bmatrix}\begin{bmatrix} u \\ w \end{bmatrix}_p \quad (30)$$

The velocity at each collocation point is influenced by the two edges of the j-th panel. Thus, adding the influence of the $(j+1)$-th panel and each subsequent panel gives the local induced velocity at the first collocation point

$$\begin{aligned}(u, w)_1 &= (u^a, w^a)_{11}\sigma_1 + [(u^b, w^b)_{11} + (u^a, w^a)_{12}]\sigma_2 \\ &\quad + [(u^b, w^b)_{12} + [(u^a, w^a)_{13}]\,\sigma_3 + \ldots\ldots \\ &= [(u^b, w^b)_{1,N-1} + [(u^a, w^a)_{1N}]\sigma_N + (u^b, w^b)_{1N}\sigma_{N+1}\end{aligned}$$

This equation can be reduced to a form

$$(u, w)_1 = (u, w)_{11}\sigma_1 + (u, w)_{12}\sigma_2 + \ldots\ldots + (u, w)_{1N+1}\,\sigma_{N+1}$$

such that for the first and last terms

$$(u, w)_{11} = (u^a, w^a)_{11} \quad (31a)$$

$$(u, w)_{1,N+1} = (u^b, w^b)_{1N}\sigma_{N+1} \quad (31b)$$

and for all other terms

$$(u, w)_{1,j} = [(u^b, w^b)_{1,j-1} + (u^a, w^a)_{1,j}]\;\sigma_j \quad (31c)$$

From this point the procedure is similar to the constant-strength source method. The influence coefficient is calculated when $\sigma_j = 1$ and

$$a_{ij} = (u, w)_{ij} \cdot n_i \quad (32)$$

For each collocation point there will be $N+1$ such coefficients and unknowns σ_j. The free-stream normal velocity components RHS_i is found at the collocation point

$$\mathrm{RHS}_i = -U_\infty \sin\alpha_i \quad (33)$$

where α_i is the panel inclination angle. Specification of the boundary condition for each $(i = 1 \to N)$ of the collocation points result in N linear algebraic equations with the unknowns σj $(j = 1 \to N+1)$. The additional equation can be found by requiring that the flow leaves parallel to the trailing edge: thus

$$\sigma_1 + \sigma_{N+1} = 0 \quad (34)$$

Another option that will yield similar results is to establish an additional collocation point slightly behind the trailing edge and require that the velocity will be zero there (stagnation point for finite-angle trailing edges). A combination of Equation (21), (33) and (34) with the N boundary conditions result in following $(N+1)$ linear equations:

$$\begin{pmatrix} a_{11} & a_{12} & \cdot & \cdot & \cdot & \cdot & \cdot & a_{1.N+1} \\ a_{21} & a_{22} & \cdot & \cdot & \cdot & \cdot & \cdot & a_{2.N+1} \\ a_{31} & a_{32} & \cdot & \cdot & \cdot & \cdot & \cdot & a_{3.N+1} \\ \cdot & \cdot & \cdot & \cdot & \cdot & \cdot & \cdot & \cdot \\ \cdot & \cdot & \cdot & \cdot & \cdot & \cdot & \cdot & \cdot \\ \cdot & \cdot & \cdot & \cdot & \cdot & \cdot & \cdot & \cdot \\ a_{N1} & a_{N2} & \cdot & \cdot & \cdot & \cdot & \cdot & a_{N.N+1} \\ 1 & 0 & \cdot & \cdot & \cdot & \cdot & \cdot & 1 \end{pmatrix}\begin{pmatrix} \sigma_1 \\ \sigma_2 \\ \sigma_3 \\ \cdot \\ \cdot \\ \cdot \\ \sigma_N \\ \sigma_{N+1} \end{pmatrix} = \begin{pmatrix} \mathrm{RHS}_1 \\ \mathrm{RHS}_2 \\ \mathrm{RHS}_3 \\ \cdot \\ \cdot \\ \cdot \\ \mathrm{RHS}_N \\ 0 \end{pmatrix} \quad (35)$$

The above set of algebraic equations has a well-defined diagonal and can be solved for σ_j by using standard methods of linear algebra.

3.2.1. Calculation of Pressures and Loads

Once the strength of the sources σ_j is known, the velocity at each collocation point can be calculated and the pressure coefficient can be calculated by using Equation (19).

4.0 RESULTS AND DISCUSSIONS

The numerical algorithms outlined before have been applied to a number of hydrofoils such as van de Vooren and NACA 0012 in order to analyse the hydrodynamic characteristics at various depths of water. In the first case, source based lower order panel method with Neumann boundary condition is applied to the 15% thick symmetric van de Vooren hydrofoil with an angle of attack, $\alpha = 0°$. The hydrofoil is discretised by $M = 90$ panels. The predicted pressure on van de Vooren hydrofoil is compared with its analytical results in Figure 4 and the agreement is quite satisfactory. The pressures on this hydrofoil at various depths of water such as respectively are plotted in Figure 5 and we can see that the effect of the depths of water is insignificant. Discretising the hydrofoil by 40, 90 and 180 panels respectively, source based lower order panel method has also been applied to van de Vooren hydrofoil at a depth of water $h/c = 0.4$. Note that this method is derived here for nonlifting shapes and the Kutta condition is not used. Consequently, the circulation of the hydrofoil will be zero and hence no lift and drag will be produced. However, the pressure distribution is well predicted in *Figure 6* and they are convergent to one another. The numerical solution presented here does not assume a symmetric solution. But it appears that the solution is symmetric about the x-axis and the number of unknowns can be reduced by M/2 by a minor modification in the process of influence co-efficient.

A comparison of pressure distribution on van de Vooren hydrofoil with an angle of attack, $\alpha = 0°$ calculated from source based higher order panel method is drawn in Figure 7. It is noted that each computational method depends on the grid and on various other parameters. Therefore, each technique must be validated first before it can be applied to unknown cases. The sensitivity of the linear higher order panel method with Neumann boundary condition is presented in Figure 8. Both methods will have problems near the trailing edge. The calculated values of C_p on NACA 0012 hydrofoil are also compared with Fletcher's numerical as well as Amick's experimental results (Fletcher, 1991) in Figure 9. The agreement between the experimental result and that of lower order method is better in compared to higher order method. Higher order method can achieve a prescribed level of accuracy but the code is more complicated and the required amount of computation per panel is higher. However, the relative merits of low and high order methods depend on the specific problem and on the fundamental method being used.

The computation times measured in seconds (of Intel Celeron computer, 2.00 GHZ and 248 MB of RAM) versus the number of panels is presented in Figure 10. These data indicate that the lower order panel method is the faster and computational effort increases with increasing the order of the method.

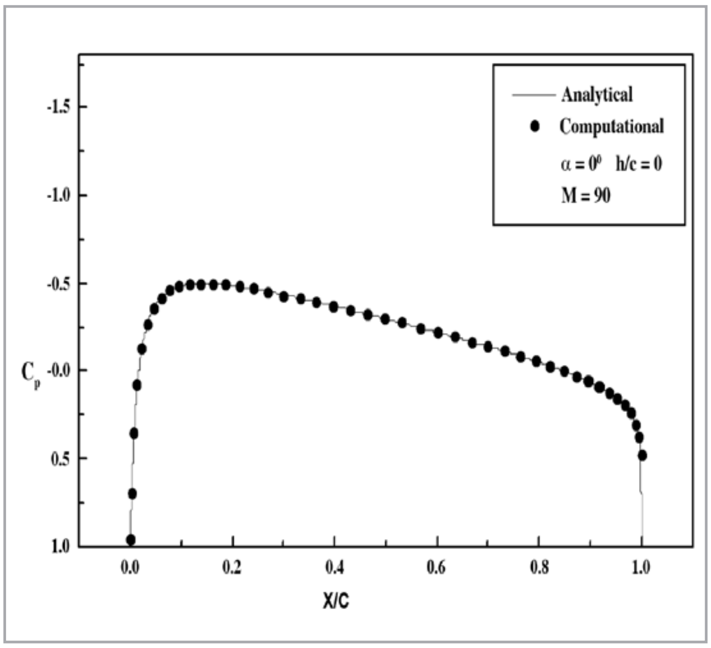

Figure 4 : Pressure on van de Vooren hydrofoil at h/c = 0 by the lower order panel method

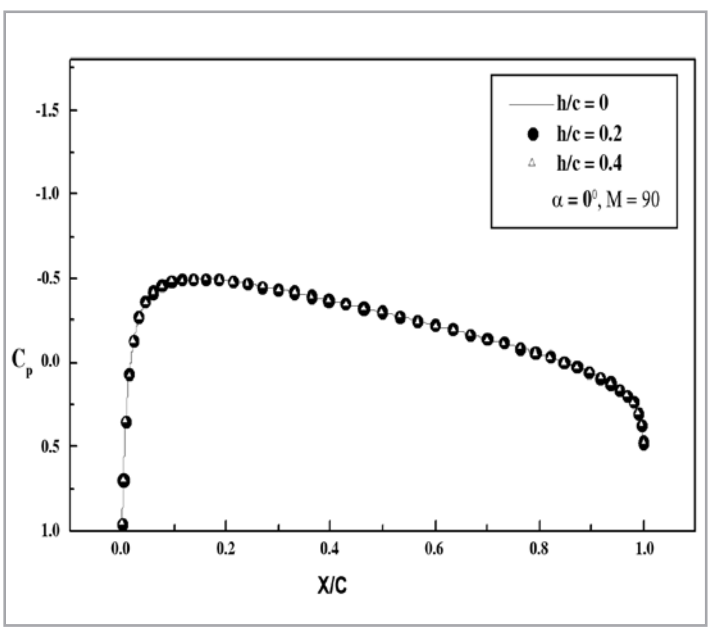

Figure 5 : Water depth effect on the pressure on van de Vooren hydrofoil by the lower order panel method

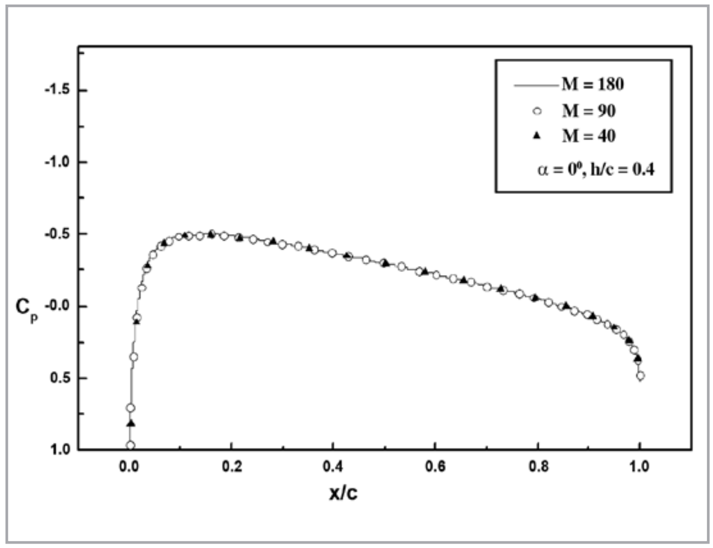

Figure 6 : Panel size effect on the pressure on van de Vooren hydrofoil at h/c = 0.4 by the lower order panel method

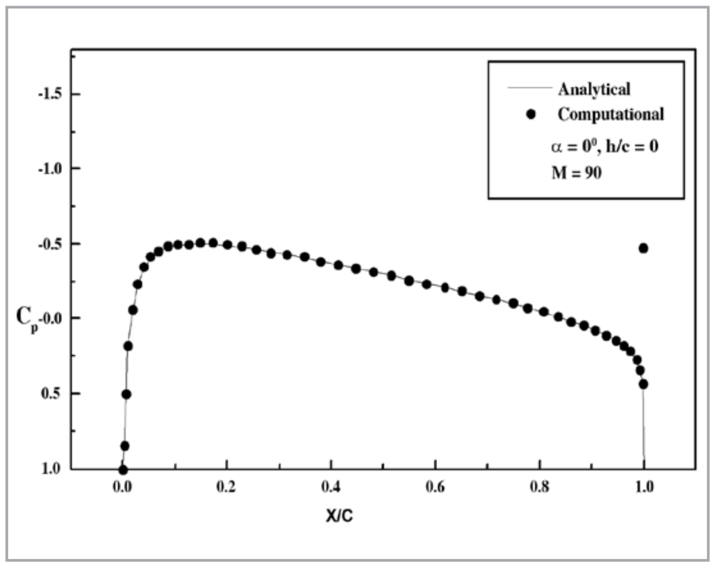

Figure 7 : Pressure on van de Vooren hydrofoil at h/c = 0 by the higher order panel method

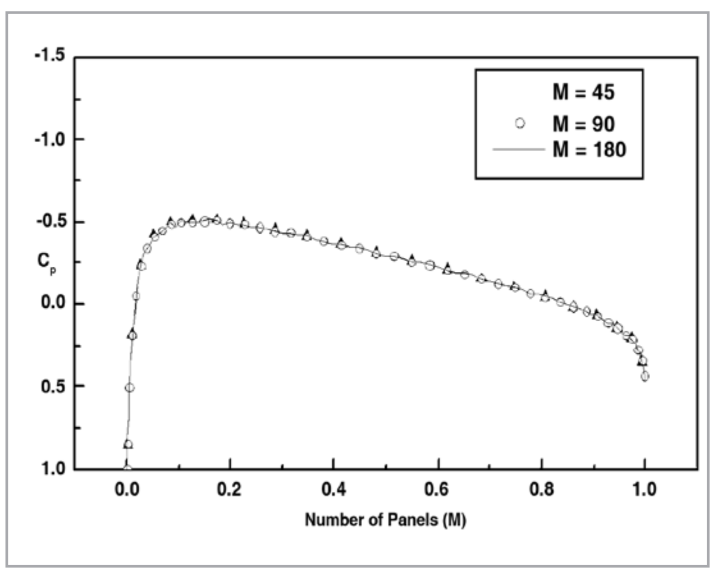

Figure 8 : Panel size effect on the pressure on van de Vooren hydrofoil at h/c = 0 by the higher order panel method

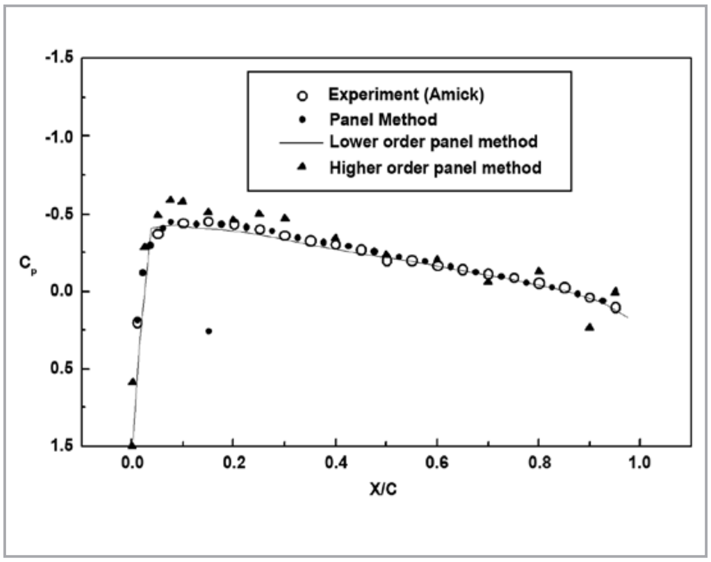

Figure 9 : Comparison between calculated and experimental Pressures on NACA 0012 hydrofoils at h/c = 0

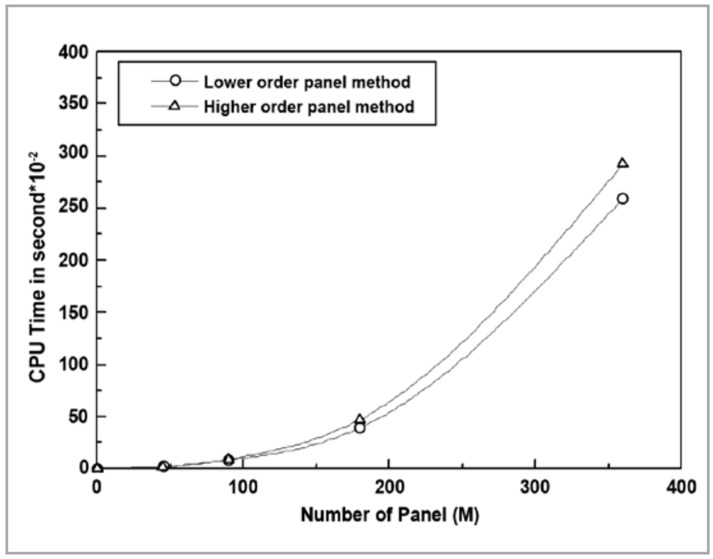

Figure 10 : Comparison of CPU time for Lower and higher order panel methods

5.0 CONCLUSIONS

The paper deals with the source based lower and higher order panel methods for computing the potential flow around the hydrofoil moving with a uniform speed in an unbounded fluid. The following conclusions can be drawn from the present study:

(i) In general, the use of the lower order method results in fewer numerical manipulations and hence less computational time. The use of higher order method requires more computational effort and is justified when the velocity near the body is continuous.

(ii) Each computational method depends on the grid and on various other parameters. Therefore, each technique must be validated before it is applied to unknown cases.

(iii) Both the methods have the problems near the cusped trailing edge of the hydrofoil. Such problems may be avoided by modeling a finite angle there (instead of zero angle) and this may be achieved by simply having larger trailing-edge panels.

(iv) The agreement between the present numerical results with the analytical as well as experimental results is quite satisfactory. ■

APPENDIX

INFLUENCE CO-EFFICIENT

Lower Order Panel Method

Consider a source distribution along the ξ axis as shown in Figure 11. It is assumed that the source strength per unit length is constant such that $\sigma(\xi) = \sigma =$ const. The influence of this distribution at a point $P(x, z)$ is an integral of the influences of the point elements along the segment $\xi_1 - \xi_2$ (see Islam, 2008):

$$\Phi = \frac{\sigma}{2\pi}\int_{\xi_1}^{\xi_2} 1\text{n}\sqrt{(x-\xi)^2 + z^2}\; d\xi \qquad \text{(A1)}$$

Differentiating Equation (A1) with respect to x and z

$$u(\xi, \eta) = \frac{\sigma}{2\pi}\int_{\xi_1}^{\xi_2} \frac{x-\xi}{(x-\xi)^2 + z^2}\, d\xi \qquad \text{(A2)}$$

$$w(\xi, \eta) = \frac{\sigma}{2\pi}\int_{\xi_1}^{\xi_2} \frac{z}{(x-\xi)^2 + z^2}\, d\xi \qquad \text{(A3)}$$

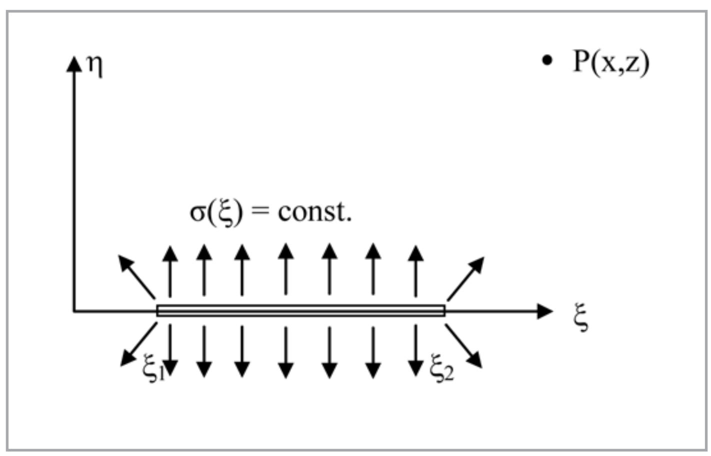

Figure 11: Constant-strength source distributions along the x - axis.

The integral for the velocity potential in terms of the corner points $(\xi_1, 0)$ and $(\xi_2, 0)$ of a generic panel element as shown in Figure 12, the distances r_1, r_2 and the angles θ_1, θ_2 it becomes

$$\Phi = \frac{\sigma}{4\pi}\left[(x-\xi_1)\, 1\text{n}\, r_1^2 - (x-\xi_2)\, 1\text{n}\, r_2^2 + 2z(\theta_2 - \theta_1)\right] \qquad \text{(A4)}$$

where

$$\theta_k = tan^{-1}\frac{z}{x-\xi_k} \qquad k = 1, 2 \qquad \text{(A5)}$$

$$r_k = \sqrt{(x-\xi_k)^2 + z^2} \qquad k = 1, 2 \tag{A6}$$

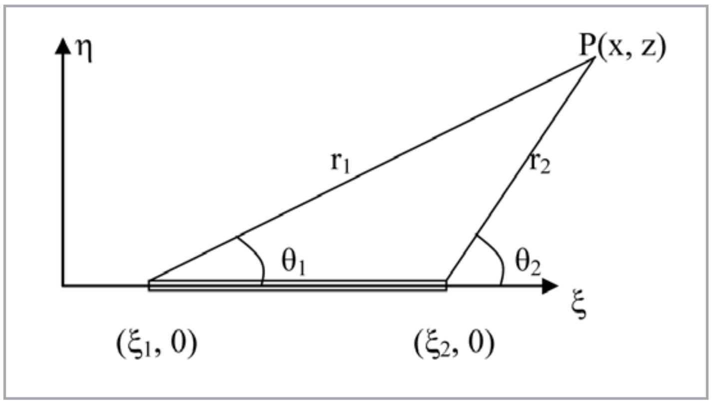

Figure 12 : Nomenclature for the panel influence coefficient derivation

The velocity components are obtained from Equation (A2) and (A3) as

$$u = \frac{\sigma}{2\pi} \ln \frac{r_1}{r_2} = \frac{\sigma}{4\pi} \ln \frac{r^2_1}{r^2_2} \tag{A7}$$

$$w = \frac{\sigma}{2\pi} (\theta_2 - \theta_1) \tag{A8}$$

Returning to *x, z* variables we obtain

$$\Phi = \frac{\sigma}{4\pi} \{(x-\xi_1) \ln[(x-\xi_1)^2 + z^2]$$

$$-(x-\xi_2) \ln[(x-\xi_2)^2 + z^2$$

$$+ 2z\,(tan^{-1} \frac{z}{x-\xi_2} - tan^{-1} \frac{z}{x-\xi_1})\} \tag{A9}$$

$$u = \frac{\sigma}{4\pi} \ln \frac{(x-\xi_1)^2 + z^2}{(x-\xi_2) + z^2} \tag{A10}$$

$$w = \frac{\sigma}{2\pi} \left[tan^{-1} \frac{z}{x-\xi_2} - tan^{-1} \frac{z}{x-\xi_1} \right] \tag{A11}$$

HIGHER ORDER PANEL METHOD

Let us consider a linear source distribution along the ξ axis ($\xi_1<\xi<\xi_2$) with a source strength of $\sigma(\xi) = \sigma_0 + \sigma_1(\xi-\xi_1)$, as shown in Figure 13. Based on the principle of superposition, this can be divided into a constant-strength element and a linearly varying strength element with the strength $\sigma(\xi) = \sigma_1\xi$. Therefore, for the general case as shown in the left-hand side of Figure 13, the results of this section must be added to the results of the constant-strength source element.

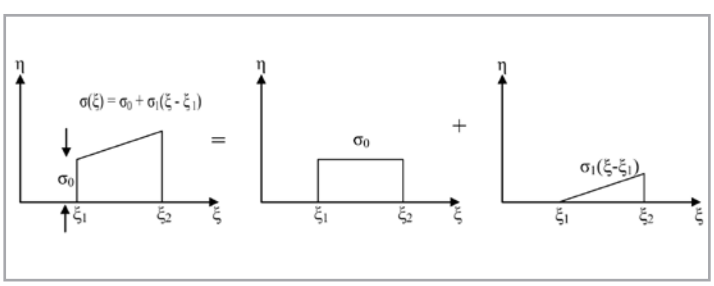

Figure 13 : Decomposition of a generic linear strength element to constant-strength and linearly varying strength elements

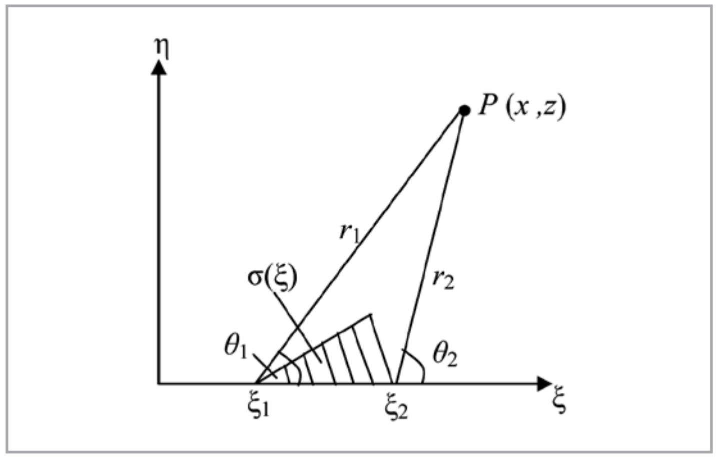

Figure 14 : Nomenclature for calculating the influence of linearly varying strength source

The influence of the simplified linear distribution source element, where $\sigma(\xi) = \sigma_1\,\xi$, at a point *P* is obtained by integrating the influences of the point elements between ξ_1 and ξ_2 (see Figure 14):

$$\Phi = \frac{\sigma_1}{2\pi} \int_{\xi_1}^{\xi_2} \xi \ln\sqrt{(x-\xi)^2 + z^2}\, d\xi \tag{A12}$$

$$u = \frac{\sigma_1}{2\pi} \int_{\xi_1}^{\xi_2} \frac{\xi(x-\xi)}{(x-\xi)^2 + z^2}\, d\xi \tag{A13}$$

$$w = \frac{\sigma_1}{2\pi} \int_{\xi_1}^{\xi_2} \frac{\xi z}{(x-\xi)^2 + z^2}\, d\xi \tag{A14}$$

The integration of the velocity potential can be represented as

$$\Phi = \frac{\sigma_1}{2\pi} \left[\frac{x^2 - \xi_1{}^2 - z^2}{2} \ln r_1{}^2 - \frac{x^2 - \xi_2{}^2 - z^2}{2} \ln r_2{}^2 \right.$$

$$\left. + 2xz(\theta_2 - \theta_1) - x(\xi_2 - \xi_1) \right] \tag{A15}$$

where r_1, r_2, θ_1 and θ_2 are defined by Equations (A5) and (A6). The velocity components are obtained by Equations (A13) and (A14) as follows:

$$u = \frac{\sigma_1}{2\pi} \left[\frac{x}{2} \ln \frac{r^2_2}{r^2_1} + (\xi_1 - \xi_2) + z(\theta_2 - \theta_1) \right] \tag{A16}$$

$$w = \frac{\sigma_1}{2\pi} \left[z \ln \frac{r^2_2}{r^2_1} + 2x(\theta_2 - \theta_1) \right] \tag{A17}$$

Substitution of r_k and θ_k from Equations (A6) and (A7) results in

$$\Phi = \frac{\sigma_1}{4\pi} \left[\frac{x^2 - \xi_1{}^2 - z^2}{2} \ln\, [(x-\xi_1)^2 + z^2] \right.$$

$$- \frac{x^2 - \xi^2{}_2 - z^2}{2} \ln\, [(x-\xi_2)^2 + z^2]$$

$$\left. + 2xz(tan^{-1} \frac{z}{x-\xi_2} - tan^{-1} \frac{z}{x-\xi_1}) - x(\xi_2 - \xi_1) \right] \tag{A18}$$

$$u = \frac{\sigma_1}{2\pi}\left[\frac{x}{2}\ 1n\frac{(x-\xi_1)^2+z^2}{(x-\xi_2)^2+z^2} + (\xi_1-\xi_2) + z\left(tan^{-1}\frac{z}{x-\xi_2} - tan^{-1}\frac{z}{x-\xi_1}\right)\right] \quad \text{(A19)}$$

$$w = \frac{\sigma_1}{4\pi}\left[z\ 1n\frac{(x-\xi_1)^2+z^2}{(x-\xi_2)^2+z^2} + 2x\left(tan^{-1}\frac{z}{x-\xi_2} - tan^{-1}\frac{z}{x-\xi_1}\right)\right] \quad \text{(A20)}$$

REFERENCES

[1] Giesing, J.P. and Smith, A.M.O. (1967): Potential flow about two-dimensional hydrofoils, Journal of Fluid Mechanics, Vol. 28, pp.113-129.

[2] Hough, G.R. and Moran, S.P. (1969): Froude number effects on two-dimensional hydrofoils, Journal of Ship Research, Vol.13, pp.53-60.

[3] Salvesen and Von Kerczek, C. (1975): Numerical solution of two-dimensional nonlinear body-wave problems. Proceedings, 1st International Conference on Numerical Ship Hydrodynamics, Bethesda, pp. 279-293.

[4] Salvesen and Von Kerczek, C. (1976): Comparison of numerical and perturbation solution of two-dimensional nonlinear water-wave problems, Journal of Ship Research, Vol. 20(3), pp.160-170.

[5] Bai, K.J. (1978): A localized finite-element method for two-dimensional steady potential flows with a free surface, Journal of Ship Research, Vol. 22, pp.216-230.

[6] Yeung, R.W. and Bouger, Y.C. (1979): A hybrid-integral equation method for steady two-dimensional ship waves, International Journal of Numerical Methods in Engineering, Vol.14, pp.317-336.

[7] Kennell, C. and Plotkin, A. (1984): A second order theory for the potential flow about thin hydrofoils, Journal of Ship Research, Vol. 28, pp.55-64.

[8] Forbes, L.K. (1985): A numerical method for non-linear flow about a submerged hydrofoil, Journal of Engineering Mathematics, Vo.19, pp.329-339.

[9] Bai, K.J. and Han, J.H. (1994): A localized finite element method for the nonlinear steady waves due to a two-dimensional hydrofoil, Journal of Ship Research, Vol.38, pp.42-51.

[10] Wu, G.K. and Eatock Taylor, R. (1995): Time stepping solutions of the two dimensional nonlinear wave radiation problem, International Journal of Ocean Engineering, Vol.22, pp.785-798.

[11] Bal, S. (1999): A panel method for the potential flow around 2-D hydrofoil, Transactions of Journal of Engineering and Environmental Science, Vol. 23, pp.349-361.

[12] Bal, S. (2005): Lift and drag characteristics of cavitating swept and V-type hydrofoils, International Journal of Maritime Engineering, The Royal Institute of Naval Architects.

[13] Tarafder, M. S., Khalil, G. M. and Mahmud, S. M. I. (2006): Free surface potential flow around Hydrofoils by Rankine source panel method, The Journal of National Oceanographic and Maritime Institute, Vol. 23, No. 2, pp.57-75.

[14] Hsin, C.Y. and Chou, S.K. (1998): Applications of a hybrid boundary element method to the analysis of free surface flow around lifting and non-lifting bodies, Proceedings of the 22nd Sympossium on Naval Hydrodynamics, Washington DC, USA.

[15] Kim, B.K. (1992): Computation of hydrodynamic forces on a submerged lifting body, Proceedings of the 2nd International Offshore and Polar Engineering Conference, ISOPE, San Francisco, USA, June 14-19, pp 367-374.

[16] Ragab, S.A. (1998): Inviscid non-cavitating flow over shallowly submerged swept hydrofoils, Proceedings of the 8th International Offshore and Polar Engineering Conference, ISOPE, Montreal, Canada, May 24-29, pp. 253-259.

PROFILES

DR MD SHAHJADA TARAFDER
Dr Md. Shahjada Tarafder is now working as an Associate Professor in the Department of Naval Architecture and Marine Engineering of Bangladesh University of Engineering and Technology, Dhaka. Dr Tarafder obtained the Degree of B Sc Engg. in 1994 and M Sc Engg. in 1996 from the same university. He obtained the Degree of Doctor of Engineering from Yokohama National University, Japan in September 2002.

DR GAZI M KHALIL
Dr Gazi M. Khalil is serving as a Professor in the Department of Naval Architecture and Marine Engineering of Bangladesh University of Engineering and Technology, Bangladesh. He has been teaching and doing research in this university for more than 35 years. Dr Khalil has to his credit more than 100 research papers published in various national and international journals and proceedings of the conferences. He has been serving as the Editor of the Journal of NOAMI published by the National Oceanographic and Maritime Institute, Bangladesh since 1997 to till to-date.

MR. MUHAMMAD RABIUL ISLAM
Mr. Muhammad Rabiul Islam is an Assistant Naval Architect of Bangladesh Inland Water Transport Authority (BIWTA), Ministry of Shipping of Bangladesh. Currently, he is doing his Ph D in Yokohama National University, Japan. He received the Degree of M Sc Engg. in 2008 and B Sc Engg. in 2003 from the Department of Naval Architecture and Marine Engineering of Bangladesh University of Engineering & Technology, Dhaka.

DESIGN AND ANALYSIS OF MULTI-CAVITY TRADITIONAL AND H-BRANCHING RUNNERS FOR PLASTIC INJECTION MOLD

(Date received: 20.11.2007)

Mohd. Rizwan Hamsin, Azuddin Mamat and Aznijar Ahmad-Yazid
Department of Engineering Design and Manufacture
Faculty of Engineering, University of Malaya,
50603, UM, Kuala Lumpur
E-mail: aznijar@um.edu.my

ABSTRACT

This paper describes the design and analysis of plastic injection mold balancing runner. The runners were designed based on Ellis Model, a viscosity model of flow network consisting of elements and nodes. 4-coefficients viscosity model and temperature dependence Ellis Model were used in order to reduce the amount of computational analysis by FEA software. A Cross WLF viscosity model was used in the FEA analysis. FEA simulation of injection molding was conducted for 8 and 16 cavity runners. Runner layout was assumed as pressure at the end of each element acting as an initial and final boundary condition. The length and size of the runner can be adjusted to fit the boundary condition that had been chosen. Flow rates at each element leading to gates were set to simulate the desired pressure drop. The final boundary condition for the first element was set as the initial boundary condition for the next element. By employing Ellis model, it was shown that the calculated results are similar to the result obtained through simulation. The model employed has successfully shown an equal filling time for each cavity, an equal pressure at each gate as well as uniform part filling. A predictive FEA performed prior to actual manufacturing is helpful in order to produce good molds.

Keywords: *Ellis Model, Flow Analysis, Plastic Injection Mold, Runner Design, Simulation*

1.0 INTRODUCTION

Injection molding is one of the most important manufacturing processes in the industry. It leads to a higher manufacturing rate, shorter product cycle and low percentage of scrap, excellent product surface and easy molding of complicated shapes [1]. An important aspect in good injection molding process is the runner and gating system design. The main function of runner and gating system is to deliver molten plastic into the mould through all sections of the mold cavities. Poor runner and gating design can lead to defects such as gas porosity, shrinkage porosity, flow line cold shut, and poor surface quality. With good runner and gating design, one may control the filling pattern and prevents over-packing. Incidences of faulty molded parts can be reduced, hence increasing productivity.

A runner is defined as an at least one-dimensional element that connects two nodes. In most cases, the elements within a runner have constant diameter. However, if the diameters vary, re-sizing will be performed proportionally. Demands for tighter tolerances, near-zero reject, and ever-lower costs that were once limited to automotive and medical jobs are now required even for molders of common consumer product. Molders have often responded by limiting themselves to molds of low cavities because they are the easiest way to balance naturally. But the use of low cavities molds would result in the increase of the numbers of molds, using more machines. This eventually results in an increase of floor space for the machines and people. However, to remain competitive in a global marketplace, cost can only be reduced by producing parts faster consistently and reduce the number of scrap. Hitherto, the importance of runner analysis on design and molding seems to have been long overlooked. Many flow analyses have been conducted, but the focus tends to be mainly on the part and cavity. However, many researchers have indicated that the runners play a much more significant role than many might realise [2, 3, 4].

Zhao *et al.* [5] performed numerical simulations on coupled fluid flow and heat transfer in a thin liquid slag or flux layer. Steady state Navier–Stokes equations were solved using a commercial finite volume software, FLUENT. The combined effects of natural convection, bottom shear velocity and strongly temperature dependent viscosity were investigated.

Lee and Lin *et al.* [6] designed a runner and gating system for a multi-cavity injection mould using Finite Element Method (FEM) and neural network. In order to select the optimal runner system parameter to minimise the warp of an injection mould, FEM, Taguchi's method and an adductive network were used. A satisfactory result as compared to the corresponding finite element verification was obtained. Fan *et al.* [7] studied real time flow rate estimation in injection molding. Experimental and analytical methods were employed in this study in order to estimate the flow rate and pressure at multiple points in an injection mold. In the experiments, melt pressure transducers were positioned at the inlet and the outlets of the feed system. A non-Newtonian, non-isothermal, faster than real time simulation utilised the feedback from the experiments to estimate the flow rates delivered through each branch of the feed system, and also provided feedback with regards to the apparent viscosity of the polymer melt provided by the molding machine. A two-cavity mold with a valve-gated hot runner system was studied.

Kumar *et. al*. [8] performed a computer simulation for the transport processes during an injection mold filling and managed to optimise the molding condition. The computer simulation of injection mold filling at constant flow rate was modeled for the production of a cylindrical part under isothermal and non-isothermal conditions. The finite difference method used to solve the governing differential equation for both the processes yield good agreement with the analytical solutions.

Plastics injection molding has been limited by the lack of observability and controllability, such that it is impossible to identify or control flow rates and pressures at multiple locations of a mold. An analysis method is available to estimate the flow rate and pressure at multiple points in an injection mold. Poorly designed runner systems are often the main cause for many molding issues that could be solved by re-designing/modifying the runners without making any changes to other parts of the mold.

The research aims to investigate the feasibility of adopting a simulation, in this case, MoldFlow software, during a mold design exercise, rather than to keep on relying on trial and error technique currently used. By using two different runner configurations, it is also desired to identify the appropriate runner system to be adopted in order to achieve best flow-rate within the runners. In the following sections of this paper, the design and analysis of traditional and h-branching runners for plastic injection mold are explained in detail and the results obtained are discussed.

2.0 NUMERICAL BACKGROUND

To model the injection mold runner, a viscosity models for flow analysis function is required. A number of well known models such as Power law models, Carreau model, Cross model and Ellis model are available. The aim in employing a viscosity model is to match the observed behavior of the material as closely as possible.

2.1 ELLIS MODEL

For this work, an Ellis model is used. The runner system in injection mold is modeled as a flow network, consists of elements and nodes. Each element consists of cylindrical elements of unknown lengths and diameter. An Ellis model in terms of shear rate is written as follows:

$$\left(\frac{\eta_0}{\eta} = 1 + \frac{\tau}{\tau_{\frac{1}{2}}}\right)^{\alpha-1} \tag{1}$$

where $\tau_{1/2}$ is the shear stress at which the viscosity is 50% of the Newtonian limit, η_0, and α-1 is the slope of the viscosity in the power law regime. For the purpose of modeling the temperature dependence of the rheology, the zero shear rate viscosity is modeled with Arrhenius type dependence as:

$$\pi_0 = \mu \exp(T) \tag{2}$$

Where, T is temperature from previous time step.

2.2 DERIVATION FOR RODS

Considering the viscous flow in a rod with an open end, the relationship between flow rate and pressure gradient can be assumed as:

$$Q = \frac{\pi R^4 - \Delta P}{8\eta L}\left[1 + \left(\frac{R\Delta P}{2L\tau_{\frac{1}{2}}}\right)^{\alpha-1}\right] \tag{3}$$

where Q is the volumetric flow rate, R is the rod radius, ΔP is the pressure drop, L is the length of the rod, and other coefficients are from the Ellis model fitting. The shear stress, τ, and shear rate, $\dot{\gamma}$, are, respectively:

$$\tau = \left(\frac{\Delta PR}{2L}\right) \tag{4}$$

$$\dot{\gamma} = \frac{\Delta PR}{2\eta_0 L}\left[1 + \left(\frac{R\Delta P}{2L\tau_{\frac{1}{2}}}\right)^{\alpha-1}\right] \tag{5}$$

For bulk temperature, integrating the shear heating across the radius leads to,

$$P_{x\dot{\gamma}} = 2\pi L \int_0^R \tau\dot{\gamma} R dR = \pi L\left(\frac{\Delta P}{L}\right)^2 \frac{R^4}{8\eta_0} + \pi \mathrm{L}\left(\frac{\Delta P}{L}\right)^{\alpha+1} \frac{\left(2\tau_{\frac{1}{2}}\right)^{1-\alpha}}{2(\alpha+3)\eta_0} \tag{6}$$

2.3 BOUNDARY CONDITION

With a constant mold wall boundary condition instead of a Biot boundary condition, the transient temperature distribution after a time step Δt is solved as:

$$\frac{T(R,t) - T_{wall}}{T_{melt} - T_{wall}} = \sum_{x=0}^{\infty} \frac{2J_0(\beta_n r)}{(\beta_n R)J_1(\beta_n R)} \exp(-\beta_n^2 \Delta ta) \tag{7}$$

where,

T_{melt} The heat conduction between polymers melt with an initial temperature.

T_{wall} Temperature at walls of a cylindrical feed system. a is the thermal diffusivity of the polymer melt. J_0 and J_1 are Bessel functions and β_n is the eigen value. The bulk temperature of the polymer melt, $\bar{T}$, can be estimated as:

$$\frac{\bar{T} - T_{wall}}{T_{melt} - T_{wall}} = \sum_{x=0}^{\infty} \frac{2}{(\beta_n R)J_1(\beta_n R)} \exp(-\beta_n^2 \Delta ta) \frac{2\pi \int_0^R J_0(\beta_n r) rdr}{\pi R^2}$$

$$= \sum_{x=0}^{\infty} \frac{4}{(\beta_n R)_2} \exp(-\beta_n^2 \Delta ta) \tag{8}$$

Neglecting higher order terms and applying the boundary condition for cylinders, where,

$$\beta_n R \cong \frac{3\pi}{4} \tag{9}$$

Therefore,

$$\bar{T} - T_{wall} = T_{melt} - T_{wall}\left(\frac{64}{9\pi^2}\right)\exp\left(\frac{\frac{-9}{16}\pi^2 a\Delta t}{R^2}\right) \tag{10}$$

This equation does not include the effect of temperature rise due to viscous heating by melting plastic. In order to take into account of viscous heating, the temperature rise due to viscous heating is:

$$\rho C_p \frac{\Delta \bar{T}}{\Delta t} = \frac{P_{xy}}{V} = \left(\frac{\Delta PR}{L}\right)^2 \frac{1}{8\eta_0} + \left(\frac{2\tau_{\frac{1}{2}}}{2(\alpha+3)\eta_0}\right) \tag{11}$$

Effect of viscous heating will indicates that the change in the bulk temperature is:

$$\Delta\bar{T}\,\frac{\Delta T}{\rho C_p} = \left[\left(\frac{\Delta PR}{L}\right)^2 \frac{1}{8\eta_0} + \frac{\Delta PR}{L}^{\alpha+1} \frac{(2\tau_{\frac{1}{2}})^{1-\alpha}}{2(\alpha+3)\eta_0}\right] \tag{12}$$

It can be concluded that, bulk temperature of a plastic flow with Ellis viscosity model for flow in a rod, taking into viscous heating and heat conduction with an estimated pressure drop is:

$$\bar{T} = T_{wall} + (T_{melt} - T_{wall})\,\frac{64}{9\pi^2}\exp\left(\frac{\frac{-9}{16}\pi^2 a\Delta t}{R^2}\right) + \frac{\Delta t}{\rho C_p}$$
$$\left[\left(\frac{\Delta PR^2}{L}\right)\frac{1}{8\eta_0} + \left(\frac{\Delta PR}{L}\right)^{\alpha+1}\left(\frac{(2\tau_{\frac{1}{2}})^{1-\alpha}}{2(\alpha+3)\eta_0}\right)\right] \tag{13}$$

3.0 RESEARCH DESIGN

This section explains in details, the runner size, runner layout, processing condition, boundary condition and rules of estimation used in this work. Figure 1 shows the research design flow chart that was followed.

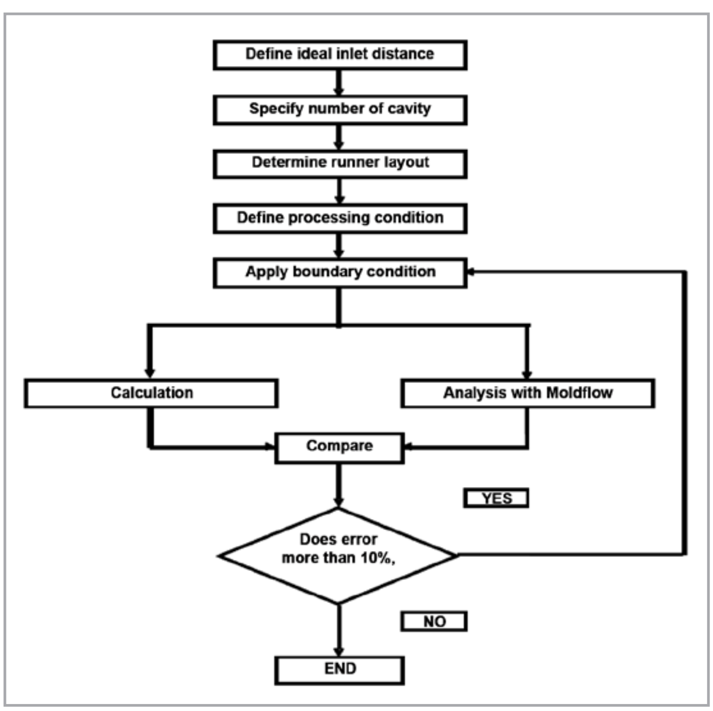

Figure 1 : Research design flow chart

3.1 RUNNER DIAMETER AND LENGTH ESTIMATION

The purpose of this technique is to control the pressure and flow rate in runner elements. This is performed by estimating the pressure drop within an element, the end pressure at gates and achieving equal flow rate at each runner approaching to gate. Consider part shown in Figure 2.

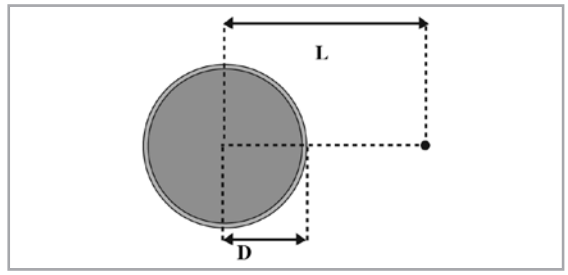

Figure 2 : Estimation of length from inlet to 1st branch

From element 1, taken as starting point, the ideal distance, *L* between injection points parallel to inlet is determined. This is known as length of the first element. Assuming at inlet, plastic flow is injected with 6 MPa at melt temperature of 230°C. Molten plastic will flow from position 0 to position 1 in 0.5 sec. Note that position 0 is inlet, and position 1 is 1st. branch. At 1st. branch, the assumed pressure is at 5.5MPa. Thus, flow rate across element 1 and bulk temperature can be calculated. But, these values can be adjusted by changing the radius of runner. For the first element, these values are taken. Since 1st. branch leads to elements 2, 3 and 4, final condition of element 1 will be used as initial condition for elements 2, 3 and 4. Between elements 2 and 3, only element 2 will be used to analyzes the flow condition because both elements have similar length and radius. Therefore, flow in element 2, pressure at final condition is assumed to be equal to all gate entrance. For that reason, a proper value must be selected to avoid too large or too small pressure drop in other element.

3.2 RUNNER LAYOUT AND CONFIGURATION

A technique to calculate desired length and radius of a runner is already available. By following Kazmer method [9], the entire runner network layout was modeled as a flow network, consists of elements and nodes. For research purpose, a traditional and H-branching will be used. Since this layout is symmetrical, analysis will be taken on the half side of the runner, with assumption that melt will flow equally to the other half. Also, on the half side, analysis will be performed on the lower half of the runner. For example, Figure 3 shows a numbered elements and nodal used for the analysis in a typical 8 cavity runner layout. Therefore, elements that will be observed are elements 1, 2, 4 and 5. The elements 2 and 5, which lead to the gate will be used as comparison. This current work is focused on 8 and 16 cavity for traditional and *H*-branching runner layout.

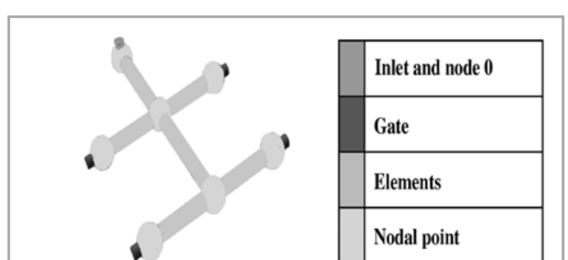

Figure 3 : General runner layout

3.3 PROCESSING CONDITION

Processing condition should satisfy Equations (3) and (13). Material used is polypropylene. The material constant can be obtained from experimental process using viscometer, fitting the Ellis model to material data or the Cross-WLF model database from MoldFlow [6]. For this work, the coefficient is chosen by fitting the Ellis model to the material data in Moldflow Database. The properties are shown below:

a	Mold surface temperature	40°C
b	Mold temperature	60°C
c	Melt temperature	240°C
d	Mu	9980 Pa-S
e	Specific heat	2740J/Kg-C
f	Thermal conductivity	0.164 W/m-C
g	Density	775Kg/m^3
h	Material diffusivity	7.72 x 10-8
i	Tau1/2	24200 Pa.s
j	Temperature constant	0.01564 1/C
k	Alpha	2.54
l	Wall temperature	230°C
m	Filling time	Depended on estimated value obtained through the estimated parameter table

3.4 BOUNDARY CONDITION

Each element was then analysed as a symmetrical cylindrical shape. The cylinder is divided into *n* number of sub elements. The number of sub elements depends on the length of the element and mesh size. Boundary conditions were set up at each end of the element. The desired parameters were pressure, temperature and plastic flow rate. Figure 4 shows plastic flow from positions 0 to 1 at a time step Δt.

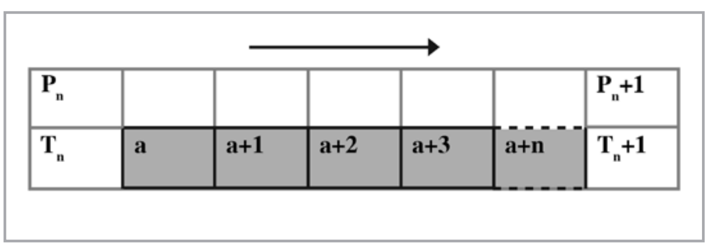

Figure 4 : Element 1 boundary conditions

Pressure drop can be defined by:

$$\Delta p = P_n - P_n + 1 \qquad (14)$$

Temperature is defined by:

$$\Delta T = T_n - T_n + 1 \qquad (15)$$

Equation (3.11) with coefficient from Ellis Model fitting is used to find the bulk temperature at T_n+1. Melt flow rate, *Q* between *n* and *n*+1 is define by using equation (3). Length, *L* and radius, *R* is selected randomly, according to size of part. Temperature dependence viscosity, can be defined by

$$\eta_{n+1} = \mu \exp (CT_n) \qquad (16)$$

Figure 5 shows an example of boundary condition used for a traditional runner and Figure 6, for an *H*-branching runner.

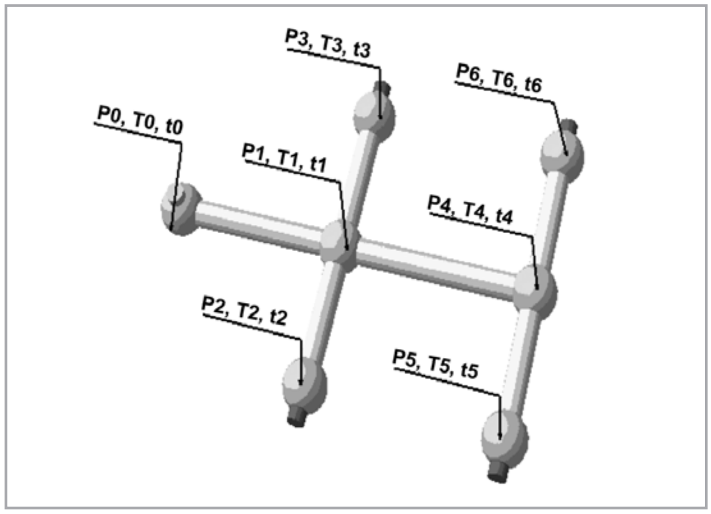

Figure 5 : Boundary condition for traditional runner

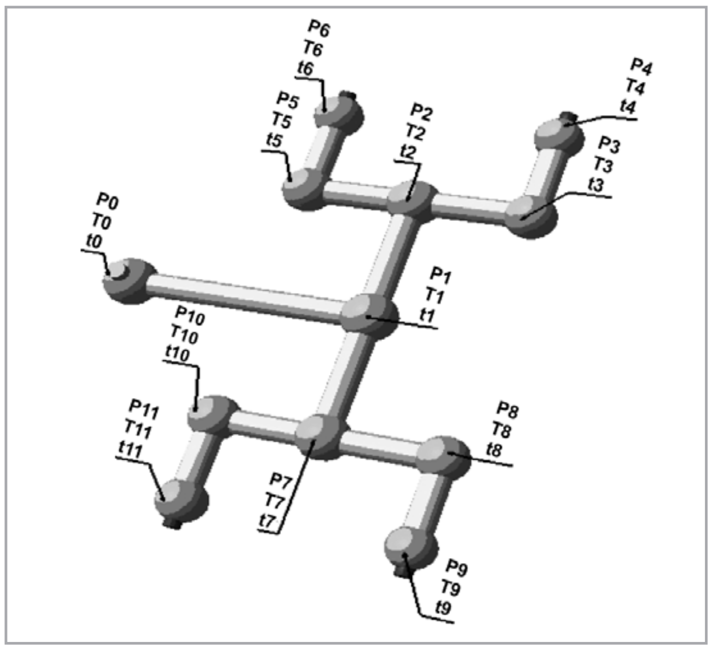

Figure 6 : Boundary condition for H-branching runner

3.5 RULES OF ESTIMATION

The estimation process of each boundary condition to achieve certain desired runner length and diameter is governed by flow rate and pressure distribution. In order to complete the equation, melt flow rate and pressure distribution need to be known. Figure 7 shows an example of the estimated condition for melt flow rate and pressure drop used for traditional runner while Figure 8 is for an *H*-branching runner. The color-shaded area represent elements and nodal in runner layout.

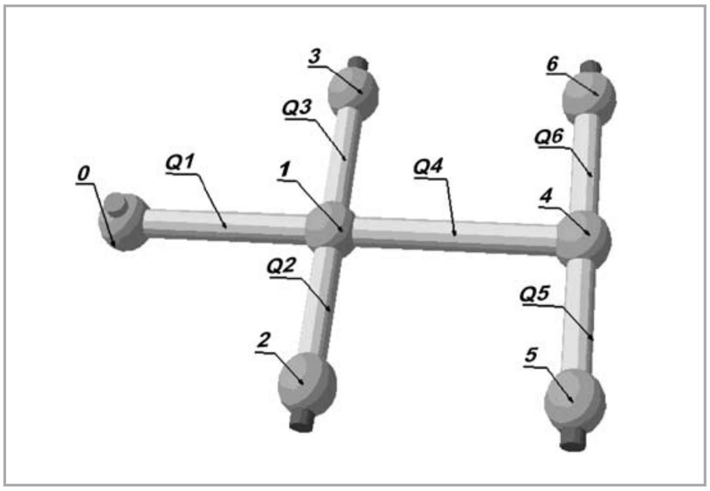

Figure 7 : Melt flow rate distribution for 8 cavity traditional runner

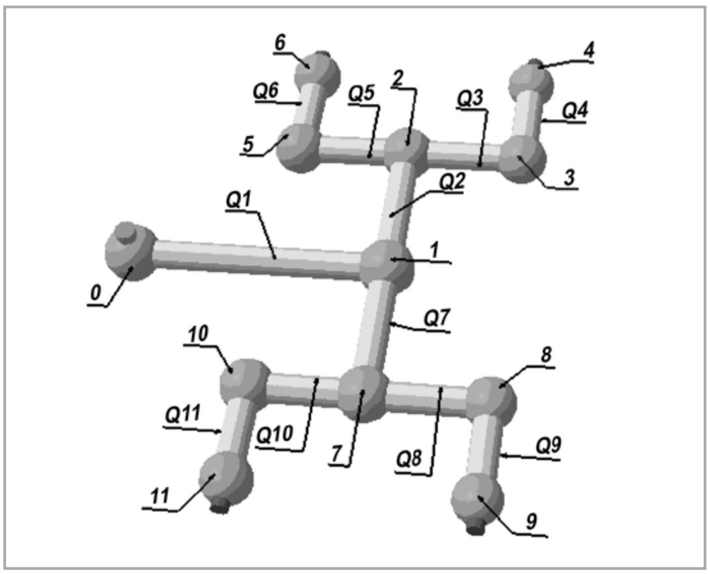

Figure 8 : Melt flow rate distribution for 16 cavity H-branching runner

For traditional runner layout, the melt flow rate;

$$Q_1 \approx 2Q_4 + Q_2 + Q_3 \tag{17}$$

$$Q_1 \approx 4Q_2 \approx 4Q_3 \approx 4Q_5 \approx 4Q_6 \tag{18}$$

Meanwhile, for H type runner layout, the melt flow rate;

$$Q_1 \approx 4Q_2 \approx 8Q_3 \tag{19}$$

$$Q_3 \approx Q_4 \approx Q_5 \approx Q_6 \tag{20}$$

Pressure at each nodal entrance to cavity, must equal approximately

For traditional runner layout, the pressure is approximated,

$$P_2 \approx P_3 \approx P_5 \approx P_6 \tag{21}$$

Meanwhile, for H type runner layout, the pressures,

$$P_4 = P_6 \tag{22}$$

4.0 RESULTS AND DISCUSSIONS

Results obtained through simulation using a Cross-WLF model were compared with the calculation performed based on modified Ellis model. The results are divided into 4 sections: 8 cavities traditional runner, 16 cavities traditional runner, 8 cavities *H*-branching runner and 16 cavities *H*-branching runner and represented in various tables and figures.

4.1 RESULTS FOR 8 CAVITIES TRADITIONAL RUNNER

4.1.1 SIMULATION FOR 8 CAVITY RUNNER

Figure 9 shows a half side layout for 8 cavity traditional runner. The runner layout with numbered flow rate in each element and nodal points is also shown.

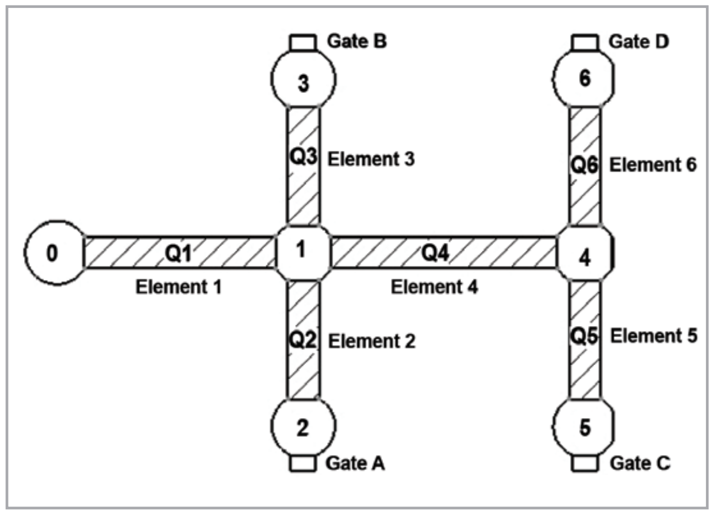

Figure 9 : Half side layout for 8 cavity traditional runner

Table 1 shows the estimated parameters that have been calculated. The first and second rows, represent the initial pressure and the final pressure at each element. In pressure flow path, it is found that one of the cavity exhibit lower pressure at the end of the filling process. In temperature and fill time flow path, all cavities show equal capacity.

Table 1: Parameters for 8 cavity traditional runner

	Elements			
	1	2	4	5
$P_{initial}$ (MPa)	4.00	3.50	3.50	3.00
P_{final} (MPa)	3.50	2.50	3.00	2.50
P_{drop} (MPa)	0.50	1.00	0.50	0.50
Radius (m)	0.0055	0.0037	0.0059	0.0049
Length (m)	0.03	0.03	0.05	0.03
$T_{initial}$ (°C)	240.00	235.94	235.94	232.50
T_{final} (°C)	235.94	239.00	232.50	232.67
Time step (sec)	0.500	0.500	0.500	0.500

Mesh size (m)	0.008	0.008	0.008	0.008
No. of element	3.750	3.750	6.250	3.750
Element time-step	0.133	0.133	0.080	0.133
η (°C)	233.864	249.176	249.176	262.962
Flow rate (m^3/s)	7.505E-05	3.986E-05	3.780E-05	3.753E-05
Flow rate (cc/s)	75.051	39.864	37.802	37.535

4.1.2 MELT FLOW PATH FOR 8 CAVITY RUNNER

Result of fill time for traditional 8 cavity runner shown in Figure 10, with the pressure distribution plot shown in Figure 11, and the temperature distribution plot in Figure 12.

Similar-colored plots shown in Figures 10, 11 and 12 indicated an equal fill time, pressure and temperature at each gate. Comparisons of the pressure drops for 8 cavity runner obtained through the simulation and estimated values are shown in Figure 13. For element 2, error recorded was 4.77% and 4.16% for element 5. Figures 14 and 15 show the estimated and the simulated flow rate values at two elements, elements 2 and 5 respectively.

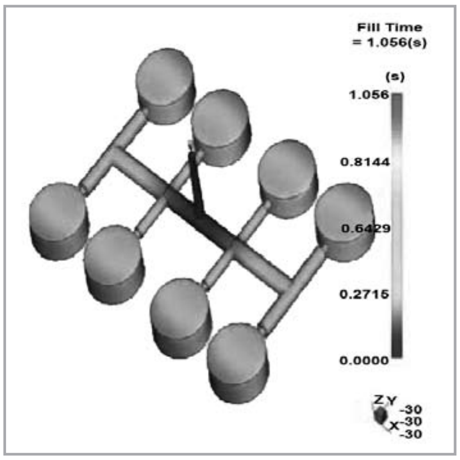

Figure 10 : Fill time distribution for 8 cavity traditional runner

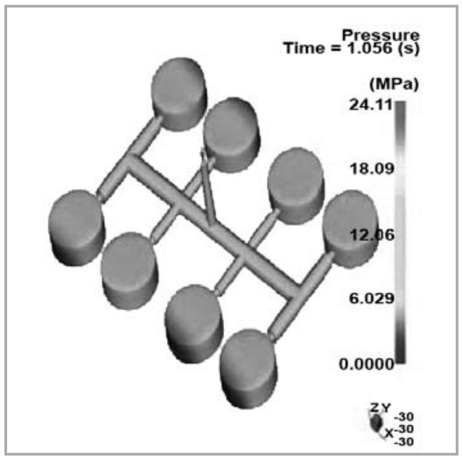

Figure 11 : Pressure distribution for 8 cavity traditional runner

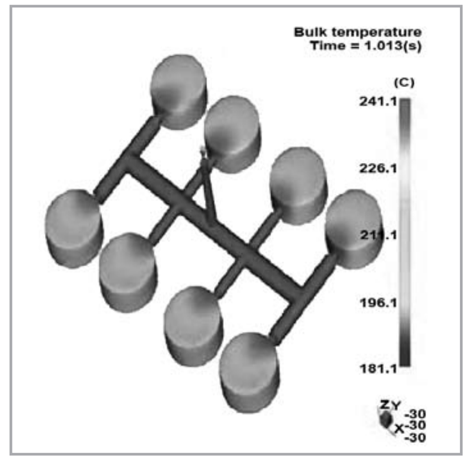

Figure 12 : Temperature distribution for 8 cavity traditional runner

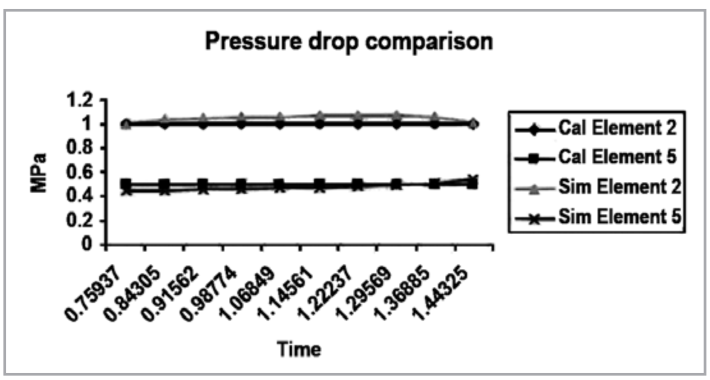

Figure 13 : Pressure drop comparison in elements 2 and 5 for 8 cavity traditional runner

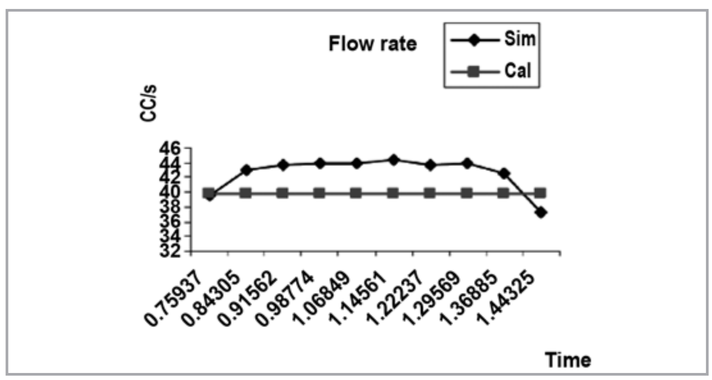

Figure 14 : Flow rate comparison in elements 2 for 8 cavity traditional runner

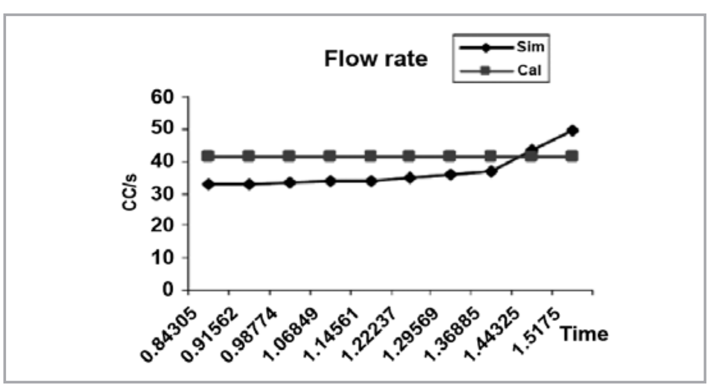

Figure 15 : Flow rate comparison in elements 5 for 8 cavity traditional runner

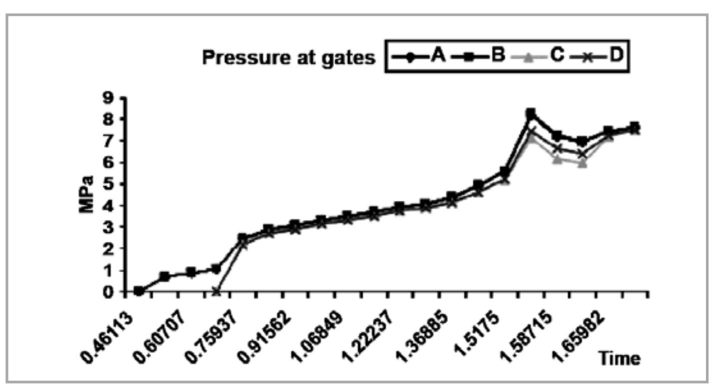

Figure 16 : Pressure at gates for 8 cavity traditional runner

The error recorded for the melt flow rate at elements 2 was 6.42% and for element 5 was 11.73%. Figure 16, meanwhile shows the pressure distribution at gates A, B, C and D.

4.2 RESULTS FOR 16 CAVITY TRADITIONAL RUNNER

4.2.1 SIMULATION FOR 16 CAVITY RUNNER

In this simulation, a traditional type of runner layout was used. The cavity is placed at a desired position inside the mold with distance that has been derived using values from Table 2.

Table 2: Parameters for 16 cavity traditional runner

	Elements			
	1	**2**	**4**	**5**
$P_{initial}$ (MPa)	6	5.5	5.5	5
P_{final} (MPa)	5.5	3.5	5	3.5
P_{drop} (MPa)	0.5	2	0.5	1.5
Radius (m)	0.0058	0.0021	0.0067	0.0024
Length (m)	0.03	0.03	0.05	0.03
$T_{initial}$ (°C)	240	243.64	243.64	242.34
T_{final} (°C)	243.64	253.43	242.34	248.09
Time step (sec)	0.5	0.5	0.5	0.5
Mesh size (m)	0.008	0.008	0.008	0.008
No. of element	3.75	3.75	6.25	3.75
Element time-step	0.133	0.133	0.08	0.133
η (°C)	233.864	220.922	220.922	225.458
Flow rate (m^3/s)	9.80E-05	1.09E-05	7.85E-05	1.13E-05
Flow rate (cc/s)	98.026	10.846	78.494	11.335

	Elements			
	7	**8**	**10**	**11**
$P_{initial}$ (MPa)	5	4.5	4.5	4
P_{final} (MPa)	4.5	3.5	4	3.5
P_{drop} (MPa)	0.5	1	0.5	0.5
Radius (m)	0.0058	0.0028	0.0052	0.0037
Length (m)	0.05	0.03	0.05	0.03
$T_{initial}$ (°C)	242.34	241.52	241.52	241.06
T_{final} (°C)	241.52	243.81	241.06	241.31
Time step (sec)	0.5	0.5	0.5	0.25
Mesh size (m)	0.008	0.008	0.008	0.008
No. of element	6.25	3.75	6.25	3.75
Element time-step	0.08	0.133	0.08	0.067
η (°C)	225.458	228.359	228.359	230.005
Flow rate (m^3/s)	3.85E-05	1.05E-05	2.27E-05	1.09E-05
Flow rate (cc/s)	38.516	10.517	22.712	10.925

Using the same boundary condition, it was found that equal filling has been achieved in all the three desired parameters of fill time, pressure and temperature. Figure 17 shows runner layout with numbered element, nodes and gates.

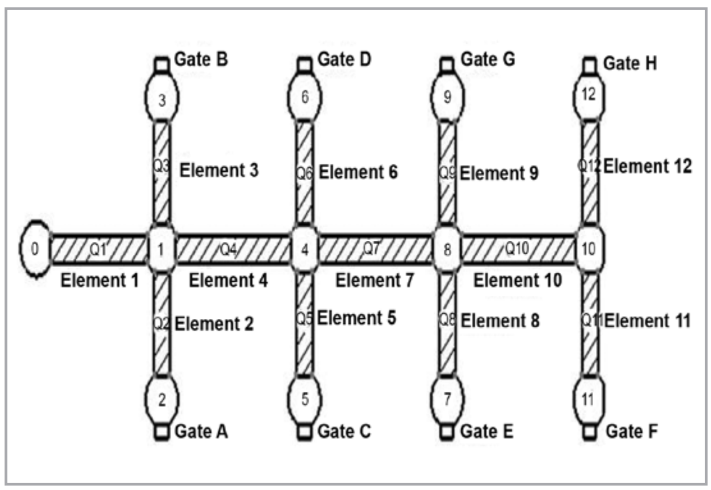

Figure 17 : Half side layout for 16 cavity traditional runner

4.2.2 MELT FLOW PATH FOR 16 CAVITY RUNNER

Figure 18 shows the result of fill time for traditional 16 cavity runner. The pressure distribution for the same 16 cavity runner is shown in Figure 19 while the temperature distribution is shown in Figure 20.

A similar plot of colors was again observed in Figures 18, 19 and 20; similar to the observation made on the 8 cavity runner earlier on. This observation indicated, again, that equal fill time, pressure and temperature were achieved. When comparing the simulated and calculated results of the pressure drop at each element leading to the gate, as shown in Figure 21, errors for elements 2, 5, 8 and 11 were considerably low, at 6.83%, 3.36%, 1.23% and 1.23% respectively.

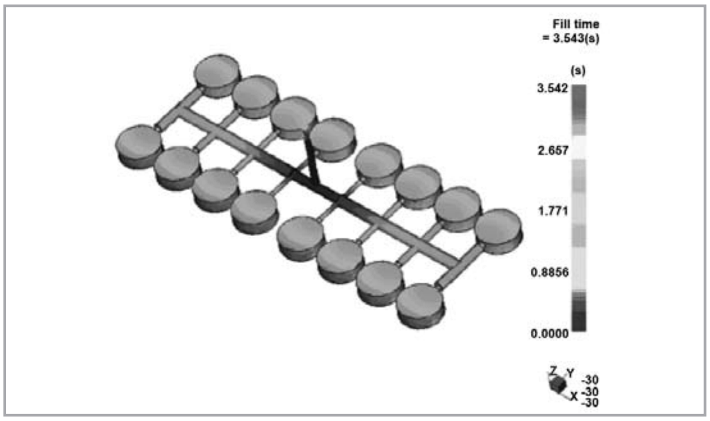

Figure 18 : Fill time distribution for 16 cavity traditional runner

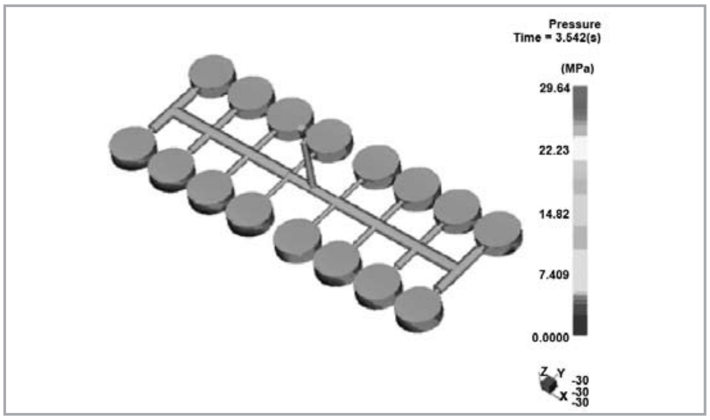

Figure 19 : Pressure distribution for 16 cavity traditional runner

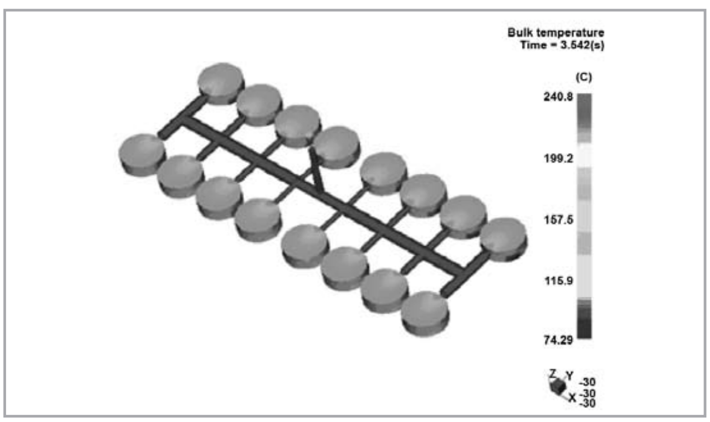

Figure 20 : Temperature distribution for 16 cavity traditional runner

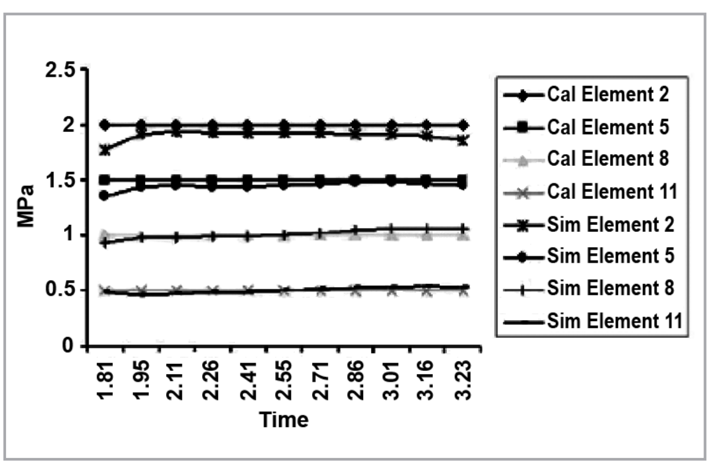

Figure 21 : Pressure drop comparison for 16 cavity traditional runner

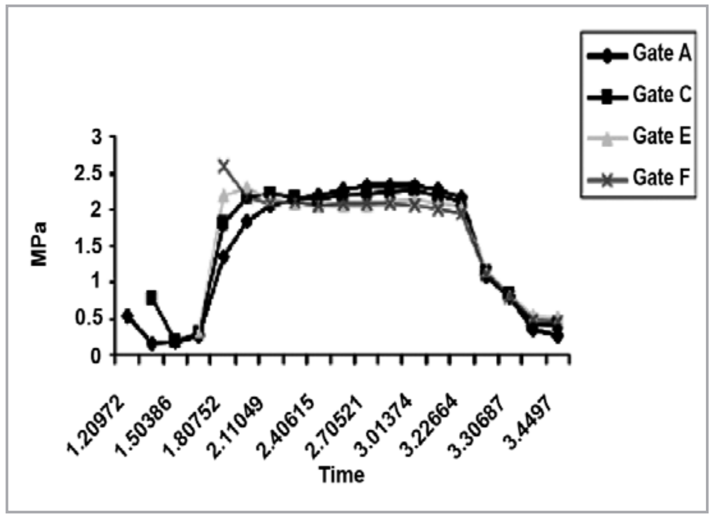

Figure 22 : Pressure at each gates for 16 cavity traditional runner

At the same time, an almost identical value of pressure distribution at each gate throughout the filling process, as indicated in Figure 22.

The calculated and simulated flow rate values in the elements leading to each gate are shown in Figure 23 (for element 2), Figure 24 (for element 5), Figure 25 (for element 8) and Figure 26 (for element 11). The observed error was noted to be low at 4.50%, 4.93%, 0.96% and 4.62 % for elements 2, 4, 8 and 11 respectively.

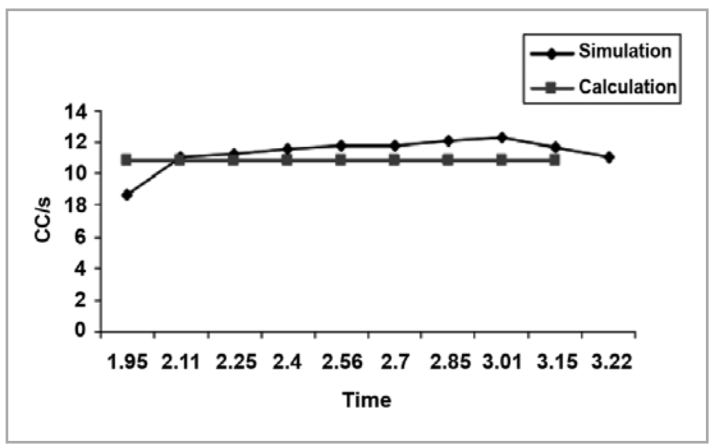

Figure 23 : Flow rate comparison in element 2 for 16 cavity traditional runner

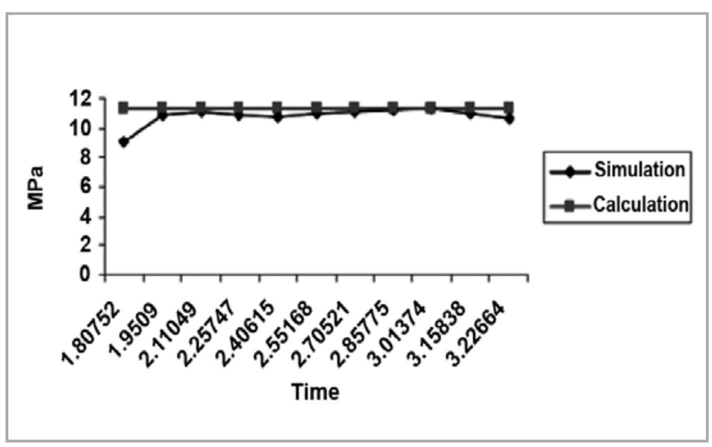

Figure 24 : Flow rate comparison in element 5 for 16 cavity traditional runner

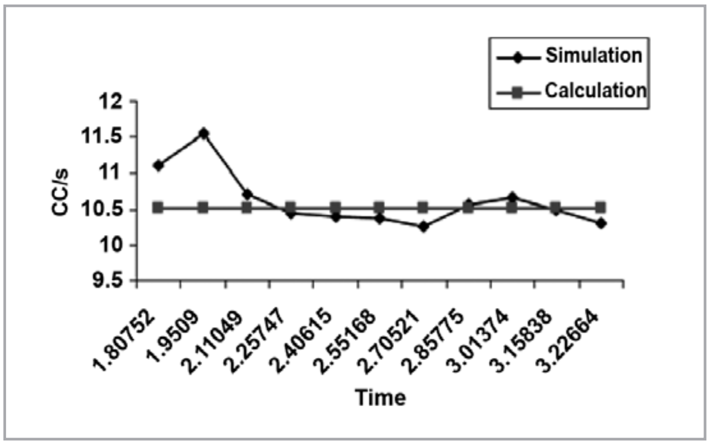

Figure 25 : Flow rate comparison in elements 8 for 16 cavity traditional runner

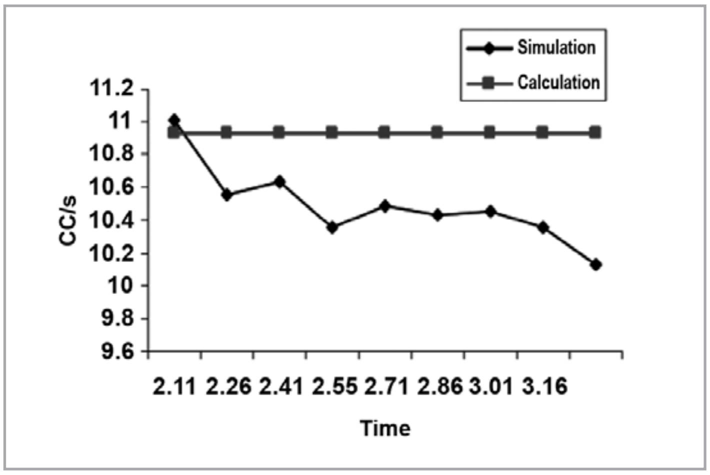

Figure 26 : Flow rate comparison in elements 11 for 16 cavity traditional runner

4.3 RESULTS FOR 8 CAVITY H-BRANCHING RUNNER

4.3.1 SIMULATION FOR 8 CAVITY RUNNER

In this simulation, *H*-branching type of runner layout was used. This type of runner is different to the one that has been discussed earlier on. This type of runner actually split the flow twice if compared to the single flow within a traditional runner layout. Figure 27 shows the runner layout with numbered elements, nodes and gates.

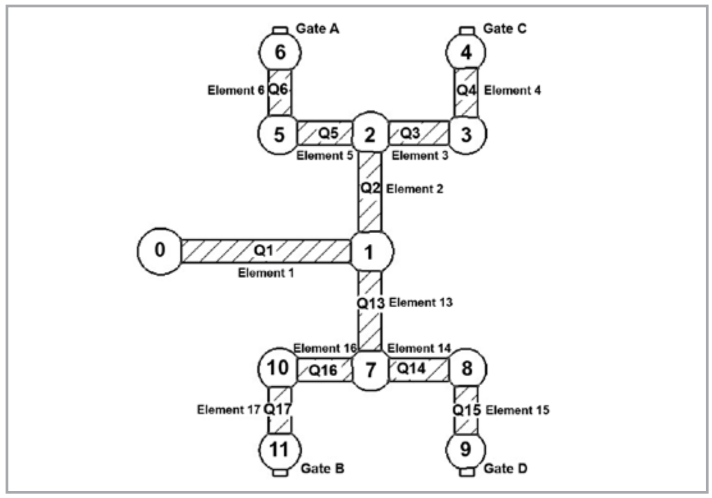

Figure 27 : Half side layout for 8 cavity H-branching runner

Results of fill time, pressure and temperature distribution for *H*-branching 8 cavity runner are shown in Table 3. In the pressure flow path, one of the cavity shows low pressure at the end of the filling while in temperature and fill time flow path, all cavities show equal filling capacity. The ratio between each element to gate is taken as the measuring index.

Table 3: Parameters for 8 cavity H-branching runner

	Elements					
	1	**2**	**3**	**4**	**5**	**6**
$P_{initial}$ (MPa)	6	5	4.5	4	4.5	4.25
P_{final} (MPa)	5	4.5	4	3	4.25	3
P_{drop} (MPa)	1	0.5	0.5	1	0.25	1.25
Radius (m)	0.005	0.004	0.003	0.0027	0.0039	0.0024
Length (m)	0.05	0.03	0.02	0.03	0.02	0.03
$T_{initial}$ (°C)	240	244.04	242.47	242.51	242.47	241.25
T_{final} (°C)	244.04	242.47	242.51	243.8	241.25	244.5
Time step (sec)	0.5	0.5	0.5	0.5	0.5	0.5
Mesh size	0.008	0.008	0.008	0.008	0.01	0.01
No. of element	6.25	3.75	2.5	3.75	2.5	3.75
Element time-step	0.08	0.133	0.2	0.133	0.2	0.13
η (°C)	233.864	219.555	225.012	224.861	225.01	229.33
Flow rate (m^3/s)	6.73E-05	1.67E-05	8.54E-06	8.90E-06	8.73E-06	7.59E-06
Flow rate (cc/s)	67.323	16.654	8.543	8.9	8.73	7.59

4.3.2 MELT FLOW PATH FOR 8 CAVITY RUNNER

Figure 28 shows the simulation results of fill time for the 8 cavity runner. The simulated result for the pressure drop is shown in Figure 29, meanwhile Figure 30 shows the temperature distribution.

While satisfactory filling occurs for fill time and temperature, it is shown in Figure 29 that one of the cavities has smaller pressure at the end of fill. In order to show the differences between the calculated and simulated results for H-branching runner, comparison will be made through the ratio of element leading to gate at each branch. This was performed because flow rate is divided into two parts. Ratio comparison produced more acceptable results. Figure 31 shows the ratio of pressure drop between elements 4 and 6 while Figure 32 show the flow rate between elements 4 and 6. Error recorded for ratio of pressure drop is 8.474% and for the flow rate at 3.56%. The pressure at each gate is shown in Figure 33.

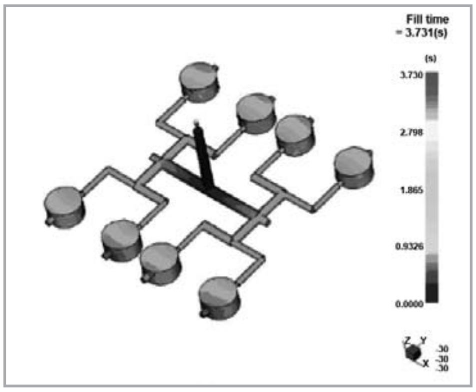

Figure 28 : Fill time distribution for 8 cavity H-branching runner

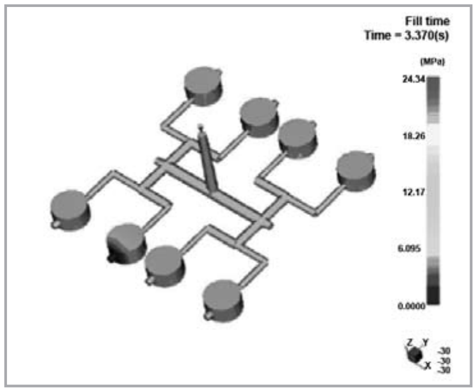

Figure 29 : Pressure drop distribution for 8 cavity H-branching runner

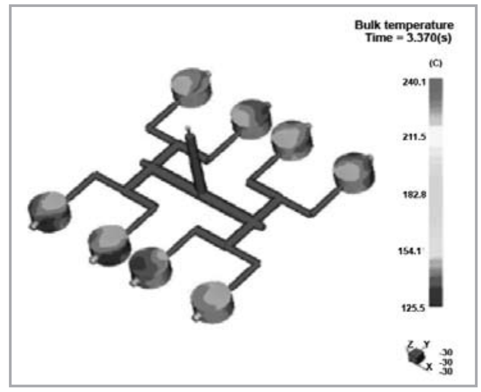

Figure 30 : Temperature distribution for 8 cavity H-branching runner

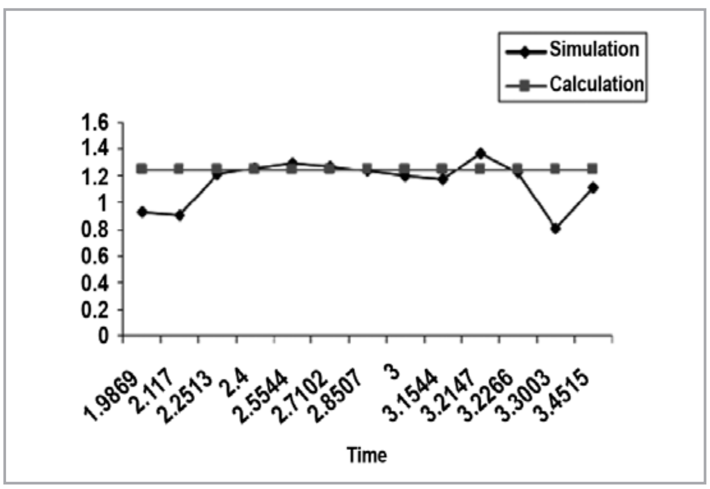

Figure 31 : Pressure drop ratio between elements 4 and 6 for 8 cavity H-branching runner

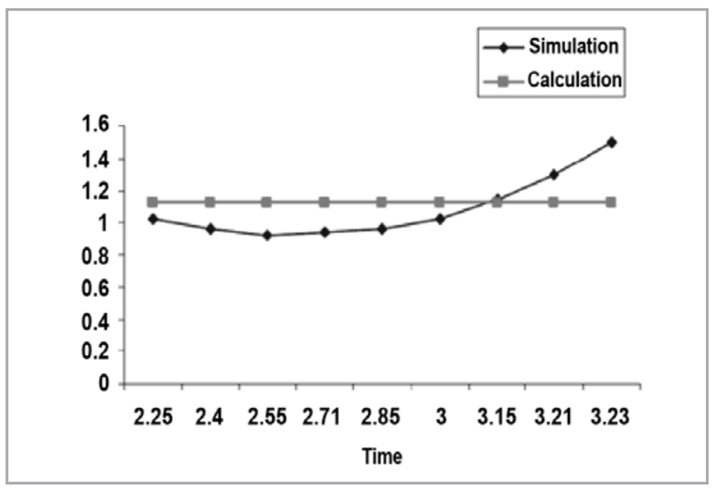

Figure 32 : Flow rate ratio between elements 4 and 6 for 8 cavity H-branching runner

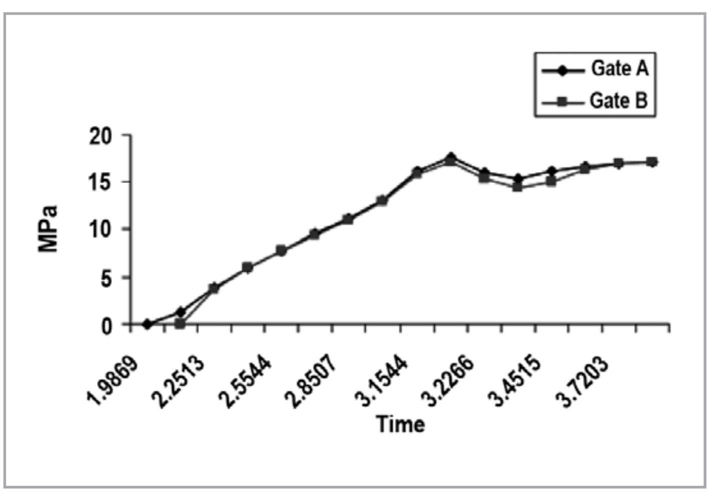

Figure 33 : Pressure at gates for 8 cavity H-branching runner

4.4 RESULTS FOR 16 CAVITY H-BRANCHING RUNNER

4.4.1 SIMULATION OF 16 CAVITY RUNNER

This runner layout is an extension of the 8 cavity runner simulated earlier. As shown in Figure 34, it also has the feature of traditional runner layout, where the flow rate in primary runner is divided into two secondary runners. This runner has the largest number of element. Therefore, in the estimation process, it is required for users to follow the melt flow rate distribution rules discussed earlier. In the simulation results, it was found that equal cavity fillings has been achieved at all but one cavity, where at this cavity there is a slightly lower pressure at the end of the filling.

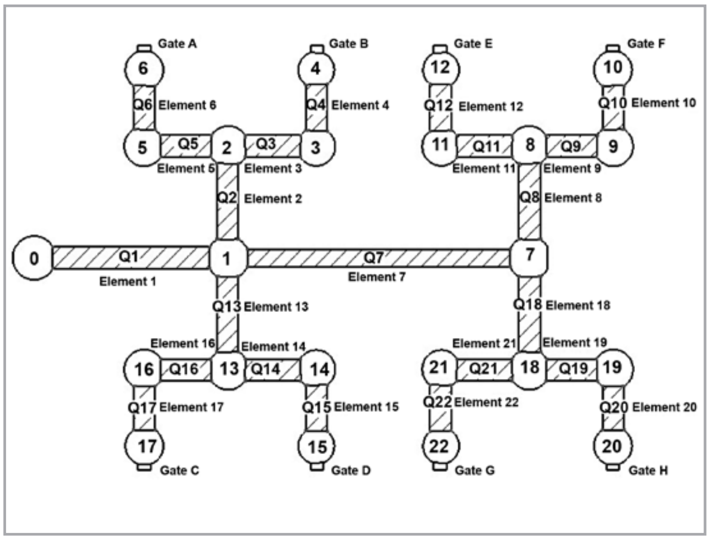

Figure 34 : Half side layout for 16 cavity H-branching runner

4.4.2 MELT FLOW PATH FOR 16 CAVITY RUNNER

Figure 35 shows the result of fill time for 16 cavity H-branching runner. The pressure distribution result for the same configuration is shown in Figure 36 and temperature distribution shown in Figure 37. At each gate, it was observed that similar color was plotted indicating an equal fill time and temperature has been achieved. However, on the flow path, it was seen that one of the cavities has slightly lower pressure compared to the others.

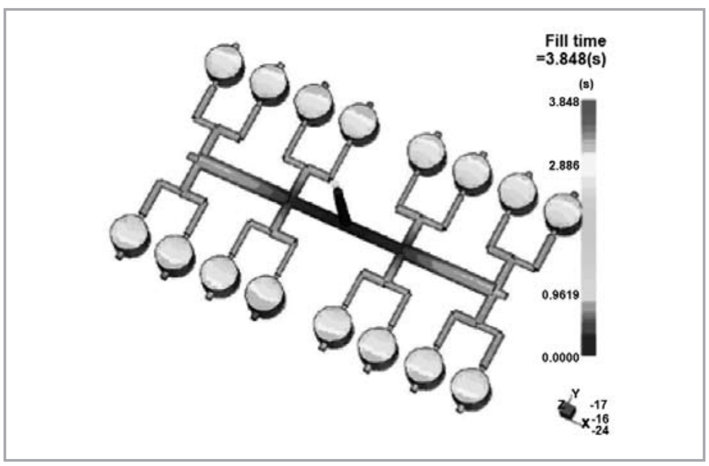

Figure 35 : Fill time distribution for 16 cavity H-branching runner

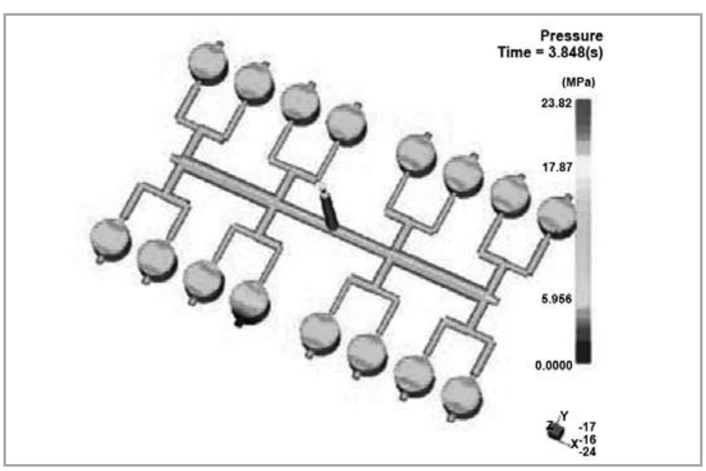

Figure 36 : Pressure distribution for 16 cavity H-branching runner

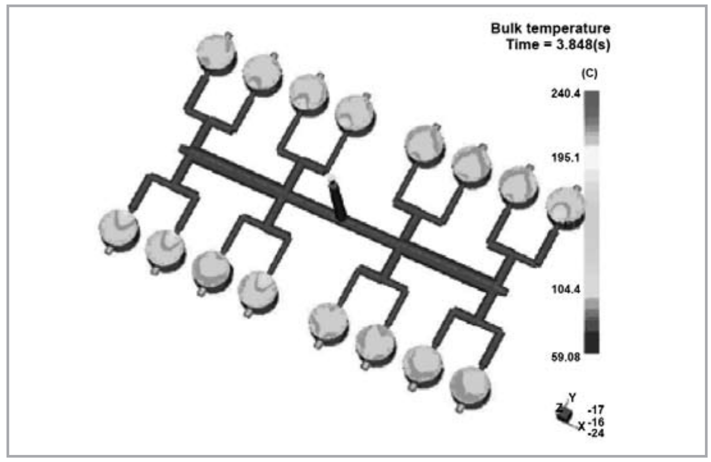

Figure 37: Temperature distribution for 16 cavity H-branching runner

Figure 38 shows the calculated and simulated ratio of pressure drop between elements 4 and 6, and elements 10 and 12. Errors recorded were 5.476% and 2.214% respectively. Figure 39 shows the ratio of flow rate element between elements 4 and 6 and Figure 40 shows the ratio of flow rate between elements 10 and 12.

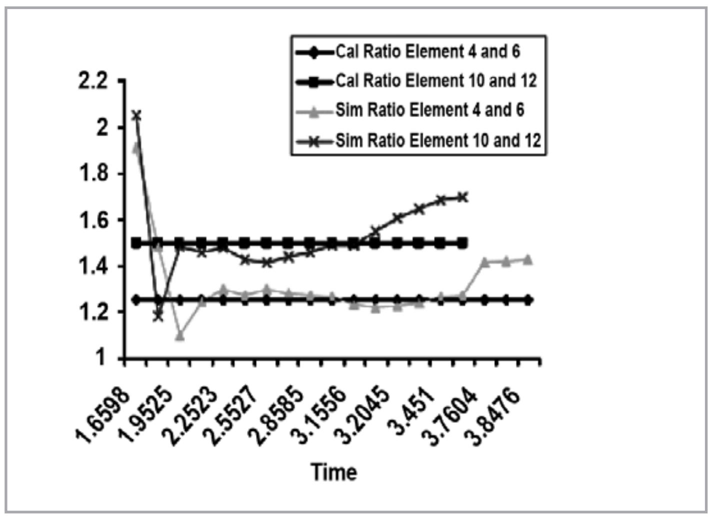

Figure 38 : Ratio of element comparison for 16 cavity H-branching runner

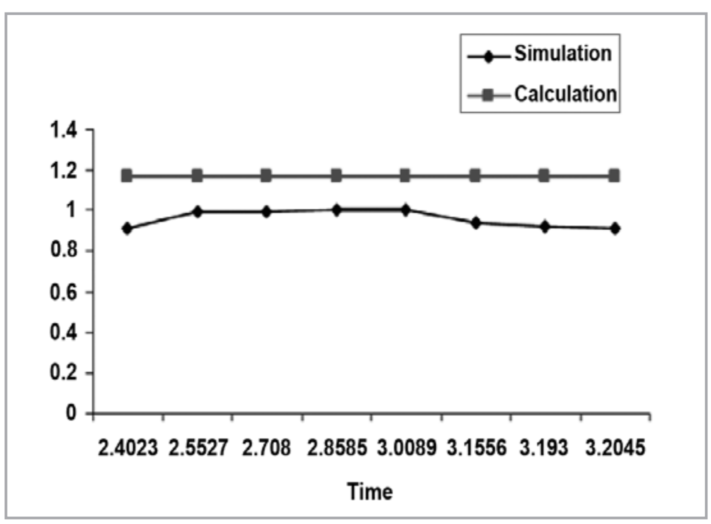

Figure 39 : Flow rate ratio between elements 4 and 6 for 16 cavity H-branching runner

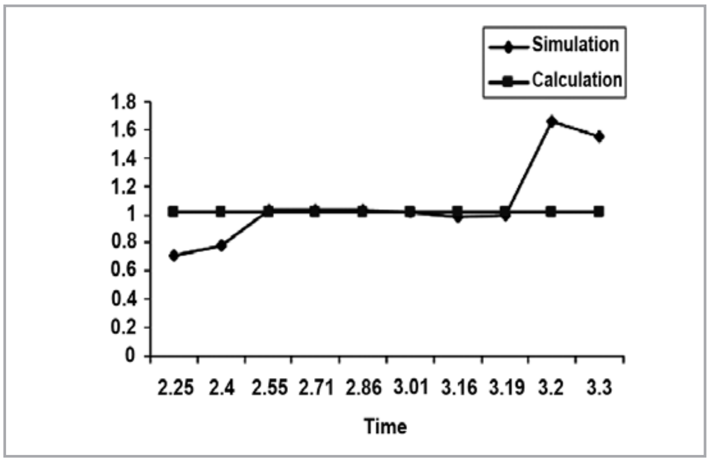

Figure 40 : Flow rate ratio between element 10 and 12 for 16 cavity H-branching runner

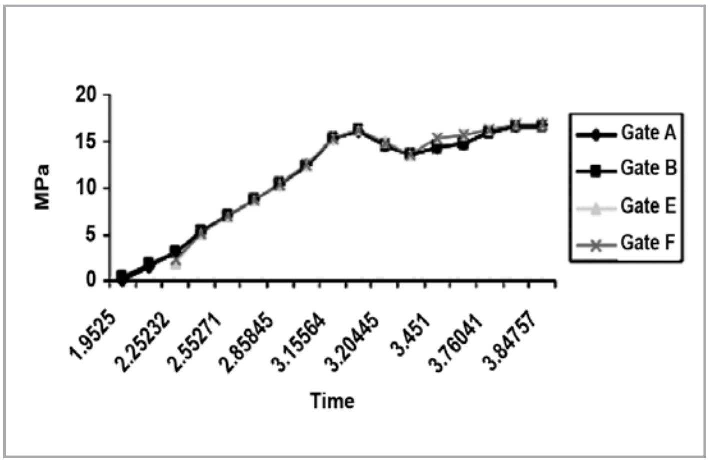

Figure 41 : Pressure at gates for 16 cavity H-branching runner

The errors when comparing the calculated and simulated ratio of flow rate between elements 4 and 6 was 9.7%, while the error for the ratio of flow rate between elements 10 and 12 was 5.14%. An equal pressure at each gate for this configuration was still observed as shown in Figure 41.

4.5 DISCUSSIONS

Overall, both the predicted parameters obtained from calculation and the values produced by MoldFLow analysis were in general agreement. However, there were few departures of values such as at the initial and final values of the flow rate, shown in Figures 15, 25, 31, 38 and 40. These were due to the adoption of different viscosity models by both techniques employed; the calculations were based on Ellis Model while the MoldFLow analysis employs the cross WLF model.

4.5.1 TRADITIONAL RUNNER LAYOUT

The described calculation technique discussed earlier was compared against values obtained from the Moldflow software with the assumed parameters in the listed table for each case. Each cavity is situated 30-mm from the mold center. Pressure measurement at each gate was also obtained. The predicted melt flow path was also shown to provide an insight of what actually happened in the injection process. From the inlet, melt flow freely into the first branch and separated into three parts. When considering an 8 cavity mold in section 4.1, as an example, the melt filled the cavity in the first branch first before filling into the next branch. On the first branch, the melt flow into element 2 at 0.188s and reached the end of the element at 0.4249s, at which, at the same time, the melt would then flow into element 5. At this point, since equation 11 is in viscosity terms of shear stress and shear rate, it was found that shear stress at the wall in element 2 was larger than those in element 5.

Referring to Table 1, although the flow rate was equal but the diameter of element 5 at 98 cm was significantly larger than the element 2 diameter of 74 cm. Therefore, at gate A, only small volume of melt appears to trickle into the cavity, while waiting for element 5 to be fully-filled. Once element 5 is fully-filled, only then will the melt flow in continuously at an equal flow rate. The calculated and simulated values start exactly at the time when the two elements have been filled. Therefore it satisfies equation 13 that compensate for runner wall temperature. Wall temperature for this condition was assumed at 240°C which mean the melt doesn't experience temperature drop at the wall. For the 8 cavity mold, at element 2, the shear stress was 0.0363MPa and the shear rate was 52.86/s. In element 5, the shear stress and shear rate is at 0.0184MPa and 16.19/s respectively.

4.5.2 H-BRANCHING RUNNER LAYOUT

One problem that has been perceived is that the cause of filling imbalance is mainly due to the flow imbalance between the cavities when there are non-uniform material properties entering into each cavity. Figure 42 can help to clarify this claim.

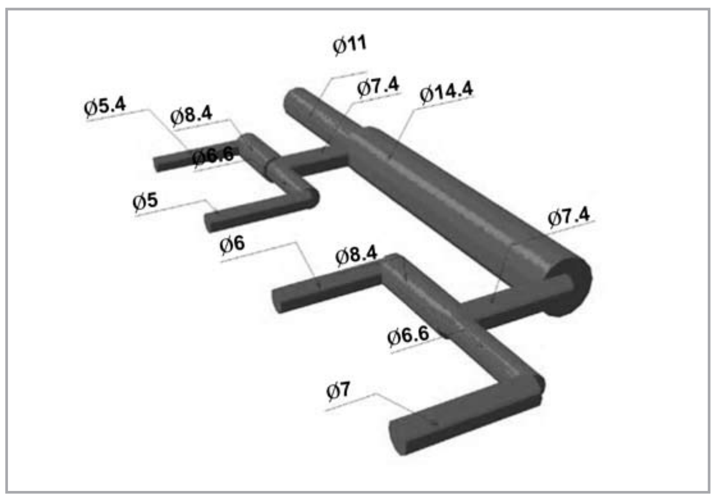

Figure 42 : Size for 16 cavity H-branching runner

In a mold with a single branch in the runner, the velocity, shear rate, temperature, and viscosity distribution across the branching runner will become non-symmetrical from side to side in the secondary runner. The hotter outer laminates on one side of the primary runner will flow along the left wall of the secondary runner. The cooler center laminates will go to the opposite right side of the secondary runner. Similarly, the hotter outer laminates at the bottom portion of the primary runner will follow along the wall of the left side of tertiary runner. The cooler center laminates will go to the opposite right edge of tertiary runner. One half of the secondary runner will be hotter than the other half. Therefore, using this technique molders can control the variation in flow rate and shear distribution inside the branched runner. Table 4 shows, almost identical melt flow rate are set at element leading to the gate. Thus, by having equal flow rate, the melt is "forced" to have desired shear rate and shear stress, stimulated by runner diameter and length.

Table 4: Parameters for 16 cavity H-branching runner

	Elements					
	1	2	3	4	5	6
$P_{initial}$ (MPa)	6	5	4.5	4	4.5	4.25
P_{final} (MPa)	5	4.5	4	3	4.25	3
p_{drop} (MPa)	1	0.5	0.5	1	0.25	1.25
Radius (m)	0.005	0.004	0.003	0.0027	0.0039	0.0024
Length (m)	0.05	0.03	0.02	0.03	0.02	0.03
$T_{initial}$ (°C)	240	244.04	242.47	242.51	242.47	241.25
T_{final} (°C)	244.04	242.47	242.51	243.8	241.25	244.5
Time step (sec)	0.5	0.5	0.5	0.5	0.5	0.5
Mesh size	0.008	0.008	0.008	0.008	0.01	0.01
No. of element	6.25	3.75	2.5	3.75	2.5	3.75
Element time-step	0.08	0.133	0.2	0.133	0.2	0.13
η (°C)	233.864	219.555	225.012	224.861	225.01	229.33
Flow rate (m^3/s)	6.73E-05	1.67E-05	8.54E-06	8.90E-06	8.73E-06	7.59E-06
Flow rate (cc/s)	67.323	16.654	8.543	8.9	8.73	7.59

	Elements					
	7	8	9	10	11	12
$P_{initial}$ (MPa)	5	4.5	4	3.5	4	3.75
P_{final} (MPa)	4.5	4	3.5	3	3.75	3
P_{drop} (MPa)	0.5	0.5	0.5	0.5	0.25	0.75
Radius (m)	0.0066	0.004	0.003	0.004	0.0039	0.003
Length (m)	0.08	0.03	0.02	0.03	0.02	0.03
$T_{initial}$ (°C)	244.04	241.499	241.683	242.256	241.683	241.019
T_{final} (°C)	241.5	241.68	242.26	241.53	241.02	242.04
Time step (sec)	0.5	0.5	0.5	0.5	0.5	0.5
Mesh size	0.01	0.01	0.01	0.01	0.01	0.01
No. of element	10	3.75	2.5	3.75	2.5	3.75
Element time-step	0.05	0.13	0.2	0.13	0.2	0.13
η (°C)	219.56	228.44	227.79	225.76	227.79	230.17
Flow rate (m^3/s)	3.32E-05	1.60E-05	8.44E-06	8.54E-06	8.63E-06	8.35E-06
Flow rate (cc/s)	33.18	16.01	8.44	8.54	8.63	8.35

5.0 CONCLUSIONS

An Ellis model with Arrhenius temperature dependence has four coefficients, and the Cross model with WLF temperature dependence has six coefficients. As the number of model coefficients increases, it is easier to model the melts recital. However, the increased number of model coefficients significantly increases the analysis time. This approach is to assume Ellis Viscosity model with temperature dependence for a given material. Added to flow rate with Ellis model relationship, a number of estimations can be made in the feed system of injection molding. This thereby reduce the number of rheological parameters *e.g.* the Newtonian limit and the critical shear stress.

The results have shown, especially for pressure in elements, that molders can predict and control the shape and size requirements of molds in order to achieve the required parameter at the entrance of the gate. Initial pressure at the inlet was not that important; in that any values depending on number of cavity can be used. This was true given that larger number of cavity requires larger injection pressure. Flow rate at each element entering the gate, must be equal so that, it can achieve the required pressure drop. From all these constraints, size of runner length and diameter can be adjusted to achieve the desired results. These findings concur with the works of Lin and Tai, Sulaiman and Keen, and Hu *et. al.*, all indicating that runners do play a significant role in the mold design exercise [2,3,4].

In conclusion, the runner sizing general formula for a traditional runner layout for 8 to 20 cavities can then be described as:

For n cavity with m branches, the flow-rate at primary runner

$$Q_1 \approx Q_{(y+2m-2)}$$

Where, $y = \dfrac{n}{4}$

Then, $\dfrac{1}{2} Q_{y+2m-2} \approx Q_2 \approx Q_5 \approx Q_8 \approx Q_{11} \approx Q_{14}$

and Q_{y+2m-2} is the last element on the primary runner

While the runners sizing general formula for an H-branching runner layout with 16 cavities yield the flow-rate at runners as:

$$Q_1 = 4Q_2 \qquad Q_1 = 2Q_7$$
$$Q_2 = 2Q_3 = 2Q_5 \qquad Q_8 = 2Q_9 = 2Q_{11}$$
$$Q_3 = Q_4 = Q_5 = Q_6 \qquad Q_9 = Q_{10} = Q_{11} = Q_{12}$$

This paper has also shown that, similar to the works of Zhao *et. al.*, Lee and Lin, Fan *et. al.* and Kumar *et. al.*, [5, 6, 7, 8] that the simulation techniques and calculations performed during a mold design process is helpful in producing better molds. It is also proven that the better runner configuration to be adopted is the H-branching runner layout configuration. ■

REFERENCES

[1] M. Zhai, Y. C. Lam and C. K. Au, "Runner sizing and weld line positioning for plastics injection molding with multiple gates", *Engineering with Computers*, Vol. 21, No. 3, pp. 218-224, May, 2006.

[2] J. C. Lin and C. C. Tai, "The Runner Optimization Design of a Die-Casting Die and the Part Produced", *International Journal of Advance Manufacturing Technology*, Vol. 14, No. 2, pp. 133-145, Feb, 1998.

[3] S. Sulaiman and T.C. Keen, "Flow analysis along the runner and gating system of a casting process", *Journal of Materials Processing Technology*, Vol. 63, No. 1-3, pp. 690-695, Jan, 1997.

[4] B. H. Hu, K. K. Tong, X. P. Niu and I. Pinwill, "Design and optimisation of runner and gating systems for the die casting of thin-walled magnesium telecommunication parts through numerical simulation", *Journal of Materials Processing Technology*, Vol. 105, No. 1-2, pp. 128-133, Sep, 2000.

[5] B. Zhao, S.P. Vanka and B.G. Thomas, "Numerical study of flow and heat transfer in a molten flux layer", *International Journal of Heat and Fluid Flow*, Vol. 26, No. 1, pp. 105-118, Feb, 2005.

[6] K.S. Lee and J.C. Lin, "Design of the runner and gating system parameters for a multi-cavity injection mould using FEM and neural network", *The International Journal of Advanced Manufacturing Technology*, Vol. 27, No. 11-12, pp. 1089-1096, Feb, 2006.

[7] B. Fan, D. Kazmer and R. Mukhari, "Real Time Flow Rate Estimation in Injection Molding", *Molding Technology Symposium at the 20th Annual Meeting of the Polymer Processing Society*, Akron, OH, June, 2003.

[8] A. Kumar, P. S. Ghoshdastidar and M. K. Muju, "Computer simulation of transport processes during injection mold-filling and optimization of the molding conditions", *Journal of Materials Processing Technology*, Vol. 120, No. 1-3, pp. 438-449, Jan, 2002.

[9] D. O. Kazmer, "Professor David Kazmer for Plastic Part Design and Manufacturing", *WebMaster Mag.*, [Online]. Website: http://kazmer.uml.edu/, Oct. 21, 2005.

ESSENTIAL QUALITY PRACTICES IN INDONESIAN MANUFACTURING SMEs

(Date received: 19.2.2008)

Mohd. Nizam Ab. Rahman[1], Hernadewita[2], Baba Md. Deros[3] and Ahmad Rasdan Ismail[4]
Department of Mechanical and Materials Engineering
Faculty of Engineering, National University of Malaysia, 43600 UKM, Bangi, Selangor
E-mail: mnizam@eng.ukm.my[1] / hadeita@yahoo.com[2]

ABSTRACT

The importance of quality practices has considerably increased over the last years, on both a practical and theoretical levels. In competitive and global business environment, companies should create a need for managers in manufacturing sector to effectively and continually improve quality, capability and process efficiency. This paper presents the findings from the survey on the current status of fundamental 5-S quality practices and the implementation of total quality management (TQM) in Indonesian SMEs. The aims are to determine whether the essential quality practices such as 5-S quality practices have a significant contribution to the successful TQM implementation and any differences in the implementation of 5-S can be attributed mainly to the maturity of the 5-S programme. This paper outlines the results of the 5-S survey conducted among 36 Indonesian manufacturing SMEs with a total of 78 per cent are applying 5-S in their environment. The main finding from the study proved that 5-S activities provide an essential total quality environment.

Keywords: *5-S, Indonesia, Total Quality Environment, TQM*

1.0 INTRODUCTION

Total Quality Management (TQM) provides the overall concept that promotes continuous improvement in an organisation. TQM philosophy stresses a systematic, integrated, consistent, organisation-wide perspective involving everyone and everything. It focuses primarily on total satisfaction for both the internal and external customers, within a management environment that seeks continuous quality improvement of all systems and processes. Total quality management and/or quality practices theory has been influenced by the contributions, mainly made by quality pioneers and/or quality leaders such as Crosby, Deming, Ishikawa, Juran, Feigenbaum, Oakland and many others. The development by all these quality experts shows significant improvement in manufacturing process and system. Improvements in the manufacturing system can lead to direct and indirect improvements to company environmental management practices, particularly in overall waste reduction. Positive relationships have been established between environmental performance and improvements to the following aspects of the manufacturing system; including quality management [1,2]; lean manufacturing practice [1,3]; worker involvement [4]; environmental technologies and advanced manufacturing technologies [1,5]; and supply strategies [4,6].

There are many manufacturing practices which are labelled as 'Japanese'. Quality practices for the Japanese manufacturer are not only linked to customer satisfaction but also to the efficiency of the production process. One of the famous Japanese quality practices is 5-S. 5-S practice is a technique employed to establish and maintain a high-quality environment in an organisation. The 5-S offers some basic practices and requirements for producing quality of products and services with high productivity and with little or no waste, which they are, involve organisation, neatness, cleanliness, standardisation and discipline at the workplace. The technique has been practised in Japan for a long time in manufacturing systems. Most Japanese 5-S practitioners consider the 5-S useful not just for improving their physical environment but for improving their thinking processes as well [7]. Many of the everyday problems could be solved through adoption of this practice.

In an era where global competition is highly intense, countries apply quality methodologies in the form of strategic quality management, quality systems, quality assurance and quality control, to gain or sustain a competitive edge. Quality must be managed and controlled in order to be an effective system for integrating the quality development, quality maintenance, and quality improvement efforts at various groups in organisation. This will enable marketing, engineering, production and service provided at the most economical levels for achieving customer satisfaction.

Having reviewed the quality practices, the importance of Kaizen concept is necessary to be described. Kaizen is a Japanese word describing the approach of continuous improvement involving everybody. Kaizen is everybody's business, and many systems have been developed to make managers and workers Kaizen-conscious. Continuous Improvement (CI) starts with the suggestions for improvement being made, value-added changes being implemented in the organisation, and resulting in an increase in company profits being realised [8]. In the words of the guru of Kaizen, Masaaki Imai [9], Kaizen means step-by-step gradual improvement in the nature of refinements or enhancements, doing little things better, continuously setting and achieving ever-higher standards, and is as important as breakthrough innovations. Kaizen is the truth behind Japan's economic miracle and the real reason the Japanese have become the masters of 'flexible manufacturing' technology – the ability to quickly adapt manufacturing processes to changing customer and market requirements. Indeed, most of the Japanese business philosophy is based on a successful combination of two strategies: Kaizen and innovation.

Again, in competitive markets and global environment, the possibility of an enterprise achieving and maintaining a lasting quality leadership is tied both with the capability of offering a real quality (*Q*), and the ability of applying innovative skill in renewing the products at a fast rate [10]. Concerning the time to market, design contraction offers some important competitive advantages, such as:

1. On the once hand, a shorter time allows lower investments and, therefore, asks for a shorter payback period with a reduction in risk.
2. On the other hand, a shorter time to market allows one to drug the market, artificially accelerating competitors product aging and then damaging them under the commercial profile.

This paper reports a survey conducted among a sample of Indonesian SMEs, as an initial output of the research, which ultimately aims to develop an approach to facilitate Cleaner Production (CP) implementation in Indonesia, including recommendations for public policy and considerations of infrastructure. Hence this study aimed to provide some important lessons for these companies, on improving their quality practices, 5-S and TQM implementation process. With this knowledge and the awareness of quality practices as well as global competition, SME owners and managers will be able to establish strategies that help the organisation moving towards better quality management implementation. The authors believe that the results might be relevant to SMEs in other countries; who are in the process of adopting advanced quality management and business excellence concepts or perhaps in developing networks or business joint-venture with other countries or other SME companies. SMEs are an important sector for the growth of any country, as they are the life blood of modern economies. Their survival will actually assist in improving the competitiveness of the large companies. Besides their flexibility and ability to innovate, SMEs play a significant role in providing employment opportunities. Therefore, there is a need to study and improve the quality practices in SME companies in order to enhance their quality environment and competiveness. The study can be started with a basic of quality practices; *i.e* 5-S as a part towards better quality management implementation, for example TQM.

2.0 5-S AND TQM

2.1 THE 5-S (SEIRI, SEITON, SEISO, SEIKETSU AND SHITSUKE) DEFINITIONS

The 5-S is the acronyms of five Japanese words: *Seiri, Seiton, Seiso, Seiketsu* and *Shitsuke*. As mentioned earlier, 5-S is a technique used to establish and maintain quality environment in an organization towards the success factor for the implementation of TQM. The meaning and English equivalents are shown in Table 1 [7].

Another Japanese quality leader, Hirano [11] has used different words for 5-S, which are *Seiri* – structurise, sort. *Seiton* – straighten, simplify. *Seiso* – sanitise, shine. *Seiketsu* – standardise, systemise. Shitsuke – self-discipline, custom and practice. Commitment from the top management to all operation management in the organisation is the highest compulsory, and the importance of having a 5-S competition to improve the organisation environment is crucial. The 5-S should be practiced at managerial level and keep their commitment.

2.2 TQM DEFINITION

Quality has always been the key to business success and long-term survivability. Quality has been synonymous with the philosophies of experts such as Dr W. Edwards Deming, Dr Joseph M. Juran, Dr Genichi Taguchi and others. Each expert possesses his own sound philosophy and approached for the improvement of quality.

The word quality means different things to different people and therefore there are many definitions and approaches. Quality culture varies, not only amongst the different organizations or countries, but also among the different divisions of the same organisation. In a TQM culture, the customer is the most important part of the process, and if the process quality is attained, customer satisfaction should be assured. Quality is the system, which, when implemented, yields increased market share and reduced scrap and rework. Deming [12] stated that quality is the umbrella of a plethora of process improvement techniques and theories that starts with a company's vendors and extends beyond the sales of that company's products and services to the consumer. Quality is built on these provable process improvement techniques, which serve as components under the umbrella.

Table 1: 5-S Meanings and English Equivalent

Japanese	English	Meaning	Examples (out of 50 points of 5-S checklist)
Seiri	Structurise	Organisation	Throw away rubbish or return to store
Seiton	Systematise	Neatness	30-second retrieval of document
Seiso	Sanitise	Cleaning	Individual cleaning responsibility
Seiketsu	Standardise	Standardisation	Transparency of storage
Shitsuke	Self-discipline	Discipline	Do 5-S daily

Source: Ho (7)

Quality is somewhat of an intangible based on perception. The determination of quality will most likely be based on perception with the manufacturer or organisation determining performance and the customer or user determining expectations. The concept of quality can be concluded that must concern customer satisfaction and as a predictable degree of uniformity and dependability at low cost and suited to the market. It comprises a set of tools, techniques and process whose output yields customer satisfaction and continuous improvement or Kaizen. TQM requires that the executives are involved and committed, interested, and really focus on its development and implementation.

Results of TQM include error-free processes, which deliver products and services fit for use, on time, with competitive pricing and good value. In any business, there are both internal as well as external customers. Companies with a commitment to excellence need to satisfy their customer requirements in every level, internal as well as external. They should develop a corporate (or organisational) culture for continuous improvement and a customer-driven-attitude. The quality approaches highlighted above are low-cost. For instance, the 5-S is easy to apply and do not require major capital investment and they should quickly identify possible areas for further productivity-improvement drives. A gradual implementation of selected tools in the 5-S activities should lead to reduction in production waste and improve the morale of employees involved as they see the immediate visual impact of their productivity improvement and working areas.

Management has to outline the top priority of the quality goals, policies and customer satisfaction, so that employees are always reminded, not only focus on the product [13]. CI is striving organisation toward the achievement of the vision [14]. The improvement system must be applied continuously and consistently conformance to the requirement of a self-disciplined, with everyone in the organisation motivated to improve the quality of system [15]. As a conclusion, Kaizen or CI activity is required to ensure that appropriate changes are made on an ongoing basis, so that the organisation continues to respond effectively to the changing demands made of it. CI strategy is well established that can meet the company business objectives.

2.3 INDONESIAN SMEs PROFILE

The abbreviation SME occurs commonly in the European Union and in international organisations, such as the World Bank, the United Nations and the World Trade Organisations (WTO). The term Small or

Medium-sized Business or SMB has become more standard in a few other countries. Small and Medium Enterprises or SMEs are companies whose headcount or turnover falls below certain limits, as categorised in Table 2. The terms ‘small and medium scale industries’ (SMIs) and ‘small and medium sized enterprises’ (SMEs) appear to have been used interchangeably. The authors would like to note here that in economics perspective, an ‘industry’ addresses a group of organisations or companies producing the same type of products, whereas an ‘enterprise’ addresses a business company or an organisation. SMEs can be found in almost all industries. Therefore, the term ‘enterprises’ is the more accurate and suitable term to be applied in this paper.

In Indonesia, small enterprises have grown mainly on the initiatives of private sector and its share in the manufacturing sector is more than 35 percent. It has provided the employment opportunities to be more than 13.6% (7,592,510 manpower) from the total of absorption employment [17], which is higher than other major economy/country (for example India with an employment growth rate around 5 percent only). However, the implementation and growth have been largely noticed in urban area and labor productivity has also showed undeceive. Small enterprises produce a wide range of products numbering over 7000 items in capital goods, intermediate goods and consumer items. It has been noticed that the goods produced in small scale sector do not have a good quality image and efforts have been taken for a decade now to improve the quality aspects.

Table 2 : SME definitions by number of employee and structure of capital

Country	SME Definitions by number of employees			Structure of the SME Capital		
	Micro	Small	Medium	Micro	Small	Medium
European Union [16]	less than 10 employees	fewer than 50 employees	fewer than 250 employees	Turnover ≤ Euro 2 million	Turnover ≤ Euro 10 million	Turnover ≤ Euro 50 million
Indonesia (Ministry of Industry of Indonesia [17]	1-10 employees	11-99 employees	100-300 employees	Turnover not exceeding 200 Million IDR	Turnover 200 million IDR to 10 Billion IDR	Turnover more than 10 Billion IDR
Japan [18]	≤ 300 Employees			Turnover Yen 300 million or less		
Malaysia [19]	Less than 5 employees	5 -50 employees	51 -150 employees	Turnover < RM250K	Turnover RM250K - < 10M	Turnover RM10M - < 25M
World Bank [20]	Less than 50 employees, with assets not exceeding US$ 150,000			Medium size define as 50-199 employees, with assets US$ 150,000 – US$ 750,000		

Note: US$ 1 = IDR 9,000; US$ 1 = RM 3.42; US$ 1 = Yen 82
Sources: European Union [16], Ministry of Industry Indonesia [17], Japan [18], SMIDEC [19], and World Bank [20]

Table 3 : GDP ratio by type of enterprises and manpower

No.	Type of Enterprises	Unit Industry (1000)	Manpower (1000)	GDP (IDR. Billion)	GDP Ratio by	
					Industry (IDR.million/unit)	Manpower (IDR. Million/MP)
1.	Small	2,874.58	7,592.51	55.69	19.37	7.34
2.	Medium	11.44	3,771.25	54.38	4,751.92	14.42
3.	Large	0.76	249.25	218.34	366,489.31	1,111.60
	Total	2,886.58	11,613.01	328.41	134.12	33.34

Note: US$ 1 = IDR 9,000.
Source: Ministry of Industry of Republic Indonesia [17]

It has shown that the small scale sector created large number for employment and support the economics growth in developing country like Indonesia. The absorption of employment in Indonesian SMEs by year 2006, as shown in Table 3.

The implementation of TQM in Indonesian SMEs has appeared from implementation of the ISO 9000 some two decades ago. The ISO 9000 series of quality standards was introduced in Indonesia since 1980s but the involvement of Indonesian companies is still low compare to others developed countries [21]. For the last 20 years, a great amount of effort and promotion has been put into quality development of Indonesian SMEs. More than 10 agencies/institutions from various ministries have been involved in these efforts. The Indonesia government hopes that SMEs will play a crucial role, such as suppliers of parts and components to larger industries, for the production of final products, is crucial in the process of strengthening and expanding Indonesian manufacturing industry. The Indonesian government is well aware that SMEs constitute a very important element of the industrial community, and considers that a strong SME sector in manufacturing can help assure that industrial foundations in Indonesia are firm. Like governments in some developed countries, Indonesia's policy aims to actively assist manufacturing SMEs to upgrade their business performance to a world-class standard. A key factor in upgrading SME competitiveness is considered to be quality performance. The opening of national markets to global competition and the adoption of the ASEAN Free Trade Area (AFTA) policy indicates that Indonesian SME companies are urged to survive in the highly-competitive modern business situation.

3.0 METHODOLOGY

This research aims to describe an investigation into the 5-S and TQM implementation in Indonesian SMEs. The approach was focused on development, implementation and the operation evaluation at the selected manufacturing SMEs. The research was carried out in the SMEs in Jakarta and Bekasi, Indonesia. Mainly, the SMEs are producing variety of parts and components for various industries such as consumer, electronic and automotive.

The 5-S methodology relies on the creation and keeping well organised, clean, high effective and high quality workplace. This research has been carried out in the selected of 36 commercial development product industries, denoted as parts and components. The case- study companies were selected because they provided specific insights into the subject of inquiry [22]. The company performance was considered essential for increasing the product's competitiveness. This research uses questionnaire survey and interviews [23, 24], and literature search in gaining empirical evidences. During these research it was executed the selection of things in production process, on each workplace. The 5-S methodology was introduced to workers and 5-S checklist score have been explained. The 5-S score was: 5–Extremely Good; 4–Very Good; 3–Good; 2–Poor; 1–Extremely Poor.

In the aim of execution the inspection of the 5-S rules' activity, it is applied from the 50 checklist [7]. The each rule of 5-S has been implemented and applied in consequence to the great changes as follows:-

- (1S): daily "things-to-do" list, one set of tools, "needed things" stored: low, medium and high usage, better usage of the working area, prevention of losing tools;
- (2S): Neat notice boards (include zoning and labels), zoning, placement marks, signage and badges, first-in-first-out arrangement, functional placement for leaflets, tools and material;
- (3S): clean the places most people do not notice, individual cleaning responsibility assigned, maintenance the clean workplace, cleaning inspections and correct minor problems, make cleaning and inspection easy (15cm);
- (4S): transparency (minimise doors, covers and locks), energy preservation (air-conditional temperature. mark/ switch), physical handling standards and instructions; 5-S responsibility labels on floor plan or at site, and;
- (5S): execute individual 5-S responsibilities, good communication and phone call (magic-word), wear if necessary (safety helmet/ gloves/ shoes/ etc), organisation chart and performance indicators.

The questionnaire was designed to obtain background information about the surveyed company, including: ownership of the company; existing workforce; management perception of existing system; methods used for improving quality; quality training frequency, the 5-S rule practice and TQM. The TQM implementation review on customer satisfaction; continuous improvement; reduce cost; reward and recognition; error prevention on not good (NG) or rejected product; co-operation and teamwork, and the implementation of quality standard (ISO 9000 series).

3.1 SELECTION OF COMPANIES

The companies were all selected based on their willingness to participate in the study. This research is focused on the SMEs in Jakarta and Bekasi as a centre and represented industrial estate area in Indonesia. Based on Japan International Cooperation Agency (JICA) [21], they are categorized into four groups based on the stage of business development and the contract situation with customers:

Stage 1 Products (parts and components) are for after-market.

Stage 2 Quality, Cost, and Delivery (*Q*CD) of the products which have not reached the audit level of the particular customer yet.

Stage 3 Contract with the particular customer is unstable.

Stage 4 Contract with the particular customer is stable.

They are also grouped into four stages based on general features of manufacturer levels as shown below:

Stage-4 Stable parts/components suppliers. In this stage, manufacturers supply their products to assemblers regularly. The product acknowledged as genuine parts.

Stage-3 Viable suppliers. In this stage, manufacturers receive orders from particular customers (assemblers or first tier customers), occasionally (unstable).

Stage-2 Potential customers. Customers target post-sales and maintenance-purpose market because their *Q*CD does not meet the requirement of assemblers.

Stage-1 Manufacturers apply only basic skills for aftermarket production.

The research analysis was applied and compared with the company criteria based on equipment and technology application which developed by Japan International Cooperation Agency (JICA) [21], as in Table 4.

Table 4 : Company criteria based on technology applied

Score (Mark)	Rating Criteria for Sub-Items	International Comparison
5	Equipment and Technology appropriate from the viewpoint of quality product requirement	Average level of Original Equipment Manufacture (OEM) part Industries in industrialised countries
4	Mostly appropriate equipment and technology are used, though some of them need improvement	Top level in ASEAN parts industries except for companies with foreign capital
3	Inappropriate equipment and technology are used at a considerably high rate. Some are missing	Average level in ASEAN parts industries except for companies with foreign capital
2	Inappropriate equipment and technology are used, causing poor quality of products	Lower level in ASEAN parts industries except for companies with foreign capital
1	Obsolete and out-of-date equipment and technology are used. Cottage industry level	The lowest level in ASEAN parts industries

(Source : Japan International Cooperation Agency JICA [21])

Table 5 : 5-S Implementation at company

Type of Company	5S-Score					Total
	1	2	3	4	5	
Medium	-	1 (2.8%)	15 (41.7%)	3 (8.3%)	3 (8.3%)	22
Small	1 (2.8%)	6 (16.7%)	6 (16.7%)	1 (2.8%)	-	14
Total	1 (2.8%)	7 (19.5%)	21 (58.4%)	4 (11.1%)	3 (8.3%)	36

4.0 SURVEY RESULTS

4.1 COMPANY BACKGROUND

Companies selected in this study have been in operation since 1970s and has a workforce of more than 50 employees. Thirty six factories located at different sites (Jakarta and Bekasi), and involved in the manufacturing of small and medium-size lots of the same parts and components. The machines are arranged according to their specific manufacturing technologies which defining a process layout. The wide spread of production job orders (more than 7000 item numbers) together with working cycle interferences give rise to very complex production flows among different companies.

The first aspect analysed was the general company profile. The breakdown of the companies is based on the size of the companies. A proportion of 14 companies (38.9%), classified into medium-sized enterprises and employing between 100 to 300 employees. The other 22 companies (61.1%) classified into small sized enterprises and having less than 99 employees. Based on company ownership, 5 companies (13.9%) are classified into joint venture and 31 companies (86.1%) classified as local investment.

4.2 RESULT OF ANALYSIS ON 5-S IMPLEMENTATION

From the 5-S practice, out of 36 companies, 29 companies (80.6%) have practiced the 5-S concept (5S score: 3, 4 and 5) in their organisations. About 7 companies (19.4%) have not come across the 5-S concept (5S score: 1 and 2). The breakdown of 5S implementation is shown in Table 5. Most of the companies believe by practising the 5-S will enhance the working environment. The remaining non-5-S companies claimed that they would increase their capabilities by conducting internal training, due to lack of awareness and company budget. Throughout the visits, the authors have convinced the companies about the benefits of 5-S implementation, as a foundation or stepping stone towards total quality environment.

4.3 RESULTS OF ANALYSIS ON TQM IMPLEMENTATION

This section examines the effects of ISO certification and 5-S-TQM implementation on company's activities and performance, as shown in Table 6. It shows that, out of 36 companies, 30 companies (83.3%) indicate that they are certified by the quality standard system (ISO 9000 series). However, out of these 30 ISO certified companies, only 12 companies (33.3%) claimed that they have continuously implemented ISO 9000 in their organisations. Meanwhile, 36 companies (100%) admitted their involvement in the TQM implementation at their organisations. Majority of the companies have actually built the concept into their day-to-day activities without realising that it is a well established quality technique. Some SMEs may claim to have adopted TQM, which was only due to the fact that the issues and requirements for a genuine TQM company were not fully understood. Other companies do not claim to be TQM companies, but have implemented many important quality-related activities, using their own approach. However, in this study, the analysis of TQM implementation in the companies was identified by; 1) provided TQM training for the employee upon they join the company; 2) weekly TQM meeting conducted in the company (early week); and 3) daily production meeting was conducted in the company (early morning). Therefore, the cross tabulation analysis on TQM implementation versus ISO practices was carried out in the four categories as shown in Table 7.

Table 6 : TQM implementation at company

Type of Company	ISO 9000 Certification	Continuously Practicing ISO 9000 Procedure	TQM Implementation
Medium	19 (52.8%)	10 (27.8%)	22 (61.1%)
Small	11 (30.6%)	2 (5.6%)	14 (38.9%)
Total	30 (83.3%)	12 (33.3%)	36 (100%)

Table 7 : Company 5-S and TQM implementation

Company	5-S-TQM	Non-5-S-TQM	Total
ISO	12 (33.3%)	1 (2.8%)	13
Non-ISO	5 (13.9)	18 (50.0%)	23
Total	17 (47.2%)	19 (52.8%)	36

Table 8 : ANOVA list of TQM implementation in 5S-TQM and non-5S-TQM companies

Impact		N	Mean	F	Sig
Quality training	5-S-TQM Non5S-TQM Total	35 1 36	2.722 1.831	1.487	0.231
Customer satisfaction	5-S-TQM Non5S-TQM Total	35 1 36	0.347 0.614	0.566	0.457
Reduce cost	5-S-TQM Non5S-TQM Total	35 1 36	0.056 0.387	0.143	0.707
Reward and recognition	5-S-TQM Non5S-TQM Total	35 1 36	0.347 0.614	0.566	0.457
Error prevention	5-S-TQM Non5S-TQM Total	35 1 36	0.056 0.498	0.112	0.740
Teamwork	5-S-TQM Non5S-TQM Total	35 1 36	0.239 0.949	0.251	0.619
Continuous improvement	5-S-TQM Non5S-TQM Total	35 1 36	4.500 0.926	4.857	0.034

Table 7 showed that, out of 36 companies, only 12 companies (83.3%) claimed, they are both certified by the ISO 9000 certification and implementing the 5-S-TQM practices in their organisations. About 18 companies (50.0%) indicated that they have neither implemented the ISO 9000 and 5-S-TQM in their organisations. The data was further analysed using the analysis of variance (ANOVA) procedure, produced by the Statistical Package for Social Sciences (SPSS) version 15.0. The ANOVA list of 5-S and TQM implementation at companies as shown in Table 8. With the use of ANOVA test, the differences within each set of variables were tested at 95 per cent confidence level. The ANOVA test revealed that, out of 7 quality performance variables, 3 variables: reduce cost, error prevention, and teamwork show statistically significant differences in mean at 95 per cent confidence level. The remaining 4 variables: quality training, customer satisfaction, reward and recognition and continuous improvement show no significant differences in mean. This implies that TQM practices have significant positive effects on company performance in both categories, and regardless of ISO certification. These findings are in contrast with those of Sohail and Hoong [25], but in accord with the findings of Rahman [26]. According to Rahman [26] (who conducted a larger postal survey on Australian SMEs), there is no significant difference between SMEs with and without ISO 9000 series certification, with regard to the impact of company performance. Sohail and Hoong [25] studied a small sample of Malaysian SMEs, and identified that customer management and quality satisfaction, and strategy planning had significant positive effects on company performance in ISO 9000 series certified companies.

From the questionnaire survey, all 36 companies (100%) have claimed that they are currently implementing TQM in their organisation, however the current situation showed that the average rejected/NG product is still performed at high percentage. As shown in Table 9, 14 companies showed the highest, indicated about or more than 15% of producing rejected/NG products, meanwhile 17 companies indicated the rejected/NG products with a range between 10% and 14.9%; and only 5 companies that claimed for both 5-S and TQM implementation, indicated the rejected/NG products with percentage of less than 10%. Percentage of the rejected/NG products for each company is also tabulated in Figure 1.

Table 9 : Percentage NG product in 5-S and TQM Implementation by Company

Company	Percentage of NG Product			Total
	$(1x \geq 15\%)$	$(10\% \leq x \leq 14.9\%)$	$x \leq 10\%$	
5-S-TQM	6 (16.7%)	15 (41.7%)	5 (13.9%)	26
Non-5-S-TQM	8 (22.2%)	2 (5.6%)	-	10
Total	14 (38.9%)	17 (47.3)	5 (13.9%)	36

Another reason may be related to the lack of TQM implementation. Part of that, the number of years for TQM involvement is considerably low or in a short period. This can be seen from the survey as 14 companies (38.9%) have been involved in TQM for less than two years. However, the findings have shown that both 5-S and TQM practices have a significant contribution to improve quality performance in organisations. There is no doubt that the implementation of the various quality initiatives can continuously improve business performance, sustain productivity and competitiveness in organisations. Hopefully, it would motivate more Indonesian organisations looking forward and implementing various quality practices in their daily manufacturing operations and activities.

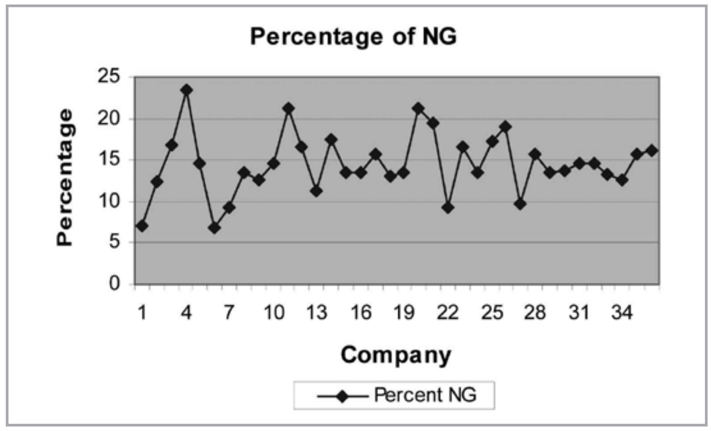

Figure 1 : Percentage of rejected/NG products

5.0 CONCLUSION

Relatively little academic research, it appears, is currently being devoted to the subject of improving quality management for Indonesian SMEs. The result of the study provides some useful information about quality management practices in Indonesian SMEs. The findings collected give a good foundation, describing essential of quality implementation levels and potential for development. Clearly, this is a great scope for the application of 5-S in the Indonesian manufacturing environment as their workplace are expected for cleanliness and orderliness. The logic behind the 5-S practice is that organisation (structurise), neatness (systemise), cleanliness (sanitise), standardisation (standardise) and discipline (self-discipline) at the workplace are basic requirements for producing high quality products and services, with little or zero waste and zero defect, while maintaining high levels of productivity.

The analysis of the survey results based on these 36 companies that manufacturing and producing parts/components, has provided evidence for the correlation between the 5-S and TQM benefits. The main finding is that the 5-S provides an essential total quality environment which is an important base for TQM implementation successfully. TQM training policy should incorporate the 5-S practice guidelines. The study also provides pertinent information about the current issues for Indonesian SME companies which are implementing 5-S and TQM, and also companies that are moving in the direction of ISO 9000 or attempting a TQM transformation. The survey methodology used in this study especially for questionnaire had several limitations. Due to time and resource constraints, the number of respondents (*i.e.* 36) from the thirty six case study companies that participated in the survey was quite a small sample size, therefore, the results of this study must be treated with caution. ■

REFERENCES

[1] R. Klassen, "Just-In-Time Manufacturing and Pollution Prevention Generate Mutual Benefits in The Furniture Industry", *Interfaces*, Vol.30, No.3, pp. 95-106, 2000.

[2] H. Kitazawa, and J. Sarkis, "*Benchmarking for Agility", Benchmarking An International Journal*, Vol. 8, No. 2, pp. 88-107, 2000.

[3] A.A. King, and M.J. Lenox, "Lean and Green? An Empirical Examination of the Relationship between Lean Production and Environmental Performance", *Production and Operations Management*, Vol. 10, No. 3, pp. 244-256, 2001.

[4] C. Geffen, and S. Rothenberg, "Suppliers and Environmental Innovation – The Automotive Paint Process", *International Journal of Operations and Production Management*, Vol. 20, No.2, pp. 166-186, 2000.

[5] R. Florida, "Lean And Green: the Move To Environmentally Conscious Manufacturing", *California Management Review*, Vol. 39, No.1, pp. 80-105, 1996.

[6] R. Min, and F.J. Galle, "The Linkage Among Management System, Practices and Behavior in Successful Manufacturing Strategy", *International Journal of Operations and Productions Management*, Vol.7, No.10, pp. 967-983, 2001.

[7] S.K. Ho, "Business Excellence through 5-S and 6-Sigma", *Oxford Business and Economics Conference*, 2007.

[8] T. Hirzel, "Measuring the Productivity Impact of ICT at the Firm Level", *Discussion Paper*, Mannheim, 1997.

[9] M. Imai, KAIZEN: The Keys to Japan's Competitive Success, New York: Van Nontrand and Company, 1986.

[10] F. Franceschini, and S. Rossetto, "*Design for Quality: Selecting Product's Technical Features*", Quality Engineering, Vol. 9, No.4, pp. 681-688, 2002.

[11] H. Hirano, *Handbook of Factory Rationalization*, Productivity Press: Oregon, 1984.

[12] W.E. Deming, *Quality Productivity & Competitive Position*, MIT Center for Advanced Engineering Study: Cambridge, M.A., 1990.

[13] D.H. Basterfield, *Total Quality Management*, New Jersey: Prentice Hall, 1995.

[14] T. Richardson, *Total Quality Management*, New York: Delmar Publishing, 1997.

[15] P. Crosby, *Quality is Free*, New York: McGraw-Hill, 1979.

[16] European Union, E.U. *Census Bureau: European Fact Finder, Profiles of Selected Economic Characteristic*, 2003.

[17] Ministry of Industry of Indonesia, *Strategic Planning for Indonesian Industry*, Jakarta, Indonesia, 2006.

[18] Japan, *Overview of Japanese SMEs*, Unico International Corporation, Tokyo, Japan, 2006.

[19] Small and Medium Industries Development Corporation SMIDEC, www.smidec.gov.my, 2008.

[20] World Bank, *Statistical Annual Report: Indonesian Economic Review*, Jakarta, Indonesia, 2004.

[21] Japan International Cooperation Agency JICA, *Follow-up Study of SMEs Development Focused on Manufacturing Industries in Republic of Indonesia*, Unico International Corporation, Tokyo, Japan, 2005.

[22] R.K. Yin, *Case Study Research: Design and Methods*, California: Sage Publications, Inc., Thousand Oaks, CA, 1994.

[23] W. Diamond, *Practical Experiment Designs*, New York: John Wiley and Sons, Inc, 2001.

[24] K. Hinkelmann, *Experimental Design, Statistical Models, and Genetic Statistics*, New York: Marcel Dekker, Inc, 1984.

[25] M.S. Sohail, and T.B. Hoong, "TQM practices and organizational performances of SMEs in Malaysia", *Benchmarking. An International Journal*, Vol. 10 No. 1, pp. 37-53, 2003.

[26] S. Rahman, "A comparative study of TQM practice and organizational performance of SMEs with and without ISO 9000 certification", *International Journal of Quality and Reliability Management*, Vol. 18 No. 1, pp. 35-49, 2001.

PROFILES

DR MOHD. NIZAM AB. RAHMAN

Dr Mohd. Nizam Ab. Rahman is a senior lecturer in Quality and Operations Management at the Department of Mechanical and Materials Engineering, UKM. His research interests include quality operations, modern quality management such as supply chain, BSC, Six sigma, Production SPC. He graduated in Industrial Physics in 1996 and obtained an MSc in 1999 from Universiti Teknologi Malaysia.

ASSOC. PROF. BABA MD. DEROS

Assoc. Prof. Baba Md. Deros is a graduate member of IEM and holds BSc (Hons) in Mechanical Engineering from University of Glamorgan, United Kingdom, Master of Science in Manufacturing Systems Engineering from University of Warwick, United Kingdom and PhD in Manufacturing Management. He has been working as a lecturer in several Polytechnics and currently as an Associate Professor in the Department of Mechanical and Materials Engineering, Faculty of Engineering, UKM.

HERNADEWITA

Hernadewita is a postgraduate student at Mechanical and Materials Engineering, UKM, under supervision of Dr. Mohd Nizam Ab Rahman and Assoc. Prof. Hj Baba Md Deros. She is doing a research on Productivity and Cleaner Production in Indonesian SMEs. She has worked with foreign company for thirteen years in Indonesia and currently as a lecturer in School of Management of Industry under Ministry of Industry, Republic of Indonesia.

ENGR. AHMAD RASDAN ISMAIL

Engr. Ahmad Rasdan Ismail is a professional engineer registered with the Board of Engineers Malaysia BEM, and holds a BEng. (Hons) (UKM), as well as a Masters of Science in Manufacturing Systems Engineering (UPM). He has been working in the engineering field including as a design engineer at R&D PROTON and also as a consultant for many projects under UKM. Currently a lecturer in manufacturing engineering at the UKM.

INVESTIGATION OF TRANSIENT PERFORMANCE OF CAPACITOR VOLTAGE TRANSFORMER (CVT)

(Date received: 19.2.2008)

Associated Prof. Dr Saad Mekhilef[1], Mr. Cheng Hock Lim[2] and Dr Ab. Halim Abu Bakar[3]
[1,2,3]*Department of Electrical Engineering,*
University of Malaya, 50603 UM, Kuala Lumpur
E-mail: saad@um.edu.my.[1]

ABSTRACT

This paper reports the digital-time domain studies on a typical 132kV Capacitor Voltage Transformer (CVT) model. The transient studies are conducted using Alternative Transient Program (ATP-EMTP). Simulation results corresponding to the CVT transient response under both system fault and ferroresonance condition are reported in this paper. Transient studies are performed (1) to identify the CVT components that contribute to the transient response of CVT, (2) to determine system condition that affect the CVT transient response. A lightning simulation case study is also presented to demonstrate the ferroresonance oscillation sustained inside a CVT due to lightning strike as affected by the factors of lightning current amplitude and distance between CVT and lightning arrester.

Keywords: *ATP-EMTP, CVT and Ferroresonance*

1.0 INTRODUCTION

Capacitive Voltage Transformers (CVTs) are the predominant source of voltage signals for monitoring, protection relays and control application at transmission and subtransmission voltage level. For the past few years, electric utility in Malaysia has reported a big number of CVT failures and explosions in the substations. These have affected the reliability of the power system [1-4].

Theoretically, the output waveform of a CVT should be an exact replica of the input waveform under all operating system conditions [5-8]. This requirement can easily be satisfied under steady-state condition. However, electric power systems are subjected to many types of disturbances that results in electric transients due to lightning, system fault, line energization and deenergisation, switching of inductive or capacitive load. Under such transient conditions, the CVT output waveform may not follow closely to its input waveform due to internal storage elements such as capacitive, inductive and non-linear components (saturable magnetic core) of the CVT [9-12]. They take time to dissipate their stored energy. Electromechanical relays can cope with unfavorable CVT transients due to their natural mechanical inertia at the expense of slower operation. Digital relays are designed for high-speed tripping and therefore they face certain CVT related transient problem [13-15].

The phenomenon of ferroresonance is of particular concern during CVT transients because it may cause thermal overstress and consequently deterioration of CVT components due to transient overvoltages produced inside the CVT. The transient errors produced can have major impact on the dependability and security of the protective relay which may affect the overall protection performance [16].

In order to have a better access to the above issues, a thorough investigation of the CVT transient performance is needed. In this work, a typical 132kV CVT model to be used in connection with the ATP-EMTP is presented. Digital time domain simulations corresponding to system fault and ferroresonance condition are carried out. The objectives of this work are (1) to identify the CVT transients' contribution factors, and (2) to investigate the impact of power system transient *e.g.* system faults and lightning on the transient performance of CVT [17-19].

Lightning stroke near the high voltage (H.V.) transmission line is one of the most common transient disturbances found in high voltage substation. The transient disturbances always transmitted through instrument transformer to the complex and distributed protection circuit, connected at their secondary terminals and seriously affect their workings [20-23]. To realise the above problem, a lightning case study was carried out to investigate the ferroresonance oscillations sustained inside a CVT, which are of serious concern, predominantly because of causing possible damage to CVT.

2.0 CVT MODEL

Figure 1 shows the circuit diagram of the typical 132kV CVT model used for the studies. Switches S1 and S2 are not part of the CVT circuitry, it's included in the model to simulate various transient scenarios imposed on the CVT.

Basically, the CVT model is composed of Capacitive Voltage Divider (C1 and C2), Step-down Transformer (SDT), Compensating Series Reactor (SR), Ferroresonance Suppression Circuit (Cf, Rf, Lf), and Overvoltage Protection devices (Vgap, Rgap).

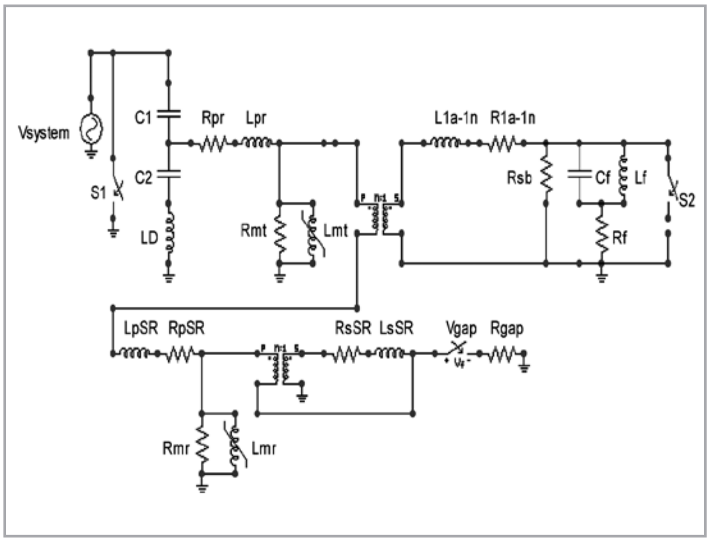

Figure 1 : CVT circuit diagram

It should be noted that Vgap represents either a spark gap with pre-specified break-down voltage or voltage-controlled switch which is triggered at a pre-specified voltage level. This CVT model utilises a voltage-controlled switched as available in ATPDraw. The voltage-controlled switch is open originally, and tries to close after T ≥ Tclose. The closing is successful as soon as the voltage across the switch is ≥ Flashover Voltage. After the switch has closed, it will wait until the time delay Tdelay has elapsed and then tries to open again.

3.0 DIGITAL TIME DOMAIN STUDIES

Digital time domain simulations corresponding to ferroresonance tests (short-circuit across secondary winding) and system fault are conducted on the CVT model to investigate the transient contribution factor.

3.1 FERRORESONANCE TESTS

To investigate the transient response contribution factors under ferroresonance condition, short-circuit across secondary winding is imposed by closing S2 at peak voltage and then opening S2 after 1 sec. The tests are carried out under different cases to investigate the effect of CVT components, and system condition on the ferroresonance response.

Case 1: CVT Burden

This case investigates the effect CVT burden (system condition) on the CVT ferroresonance phenomena. CVT burden is one of the dissipating paths for energy accumulated in the CVT circuitry. Its effect is so profound that it can dominate the CVT transient behavior. The tests make use of two types of burdens as suggested by [3] for transient response test as follow:

(i) *Pure Resisitive Burden*

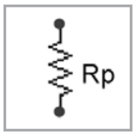

(ii) *Series Burden*

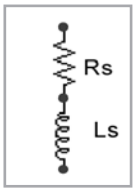

Figure 2(a) shows the CVT output response is subjected to ferroresonance oscillation after the secondary short circuit is cleared (no load is connected). The ferroresonance is cleared after nearly 10 cycles. Figures 2(b) and 2(c) show the CVT response to ferroresonance test when pure resisitive burden of 100VA and 400VA is included on the secondary winding of the CVT as load respectively. Figure 2(b) shows that the ferroresonance is cleared after nearly 7 cycles. Whereas, Figure 2(c) shows that the ferroresonance is cleared after 2 cycles. These indicate that, the ferroresonance can be more effectively damped out when we have load with higher VA. Therefore it is recommended that the CVT be fully loaded to avoid extensive transient.

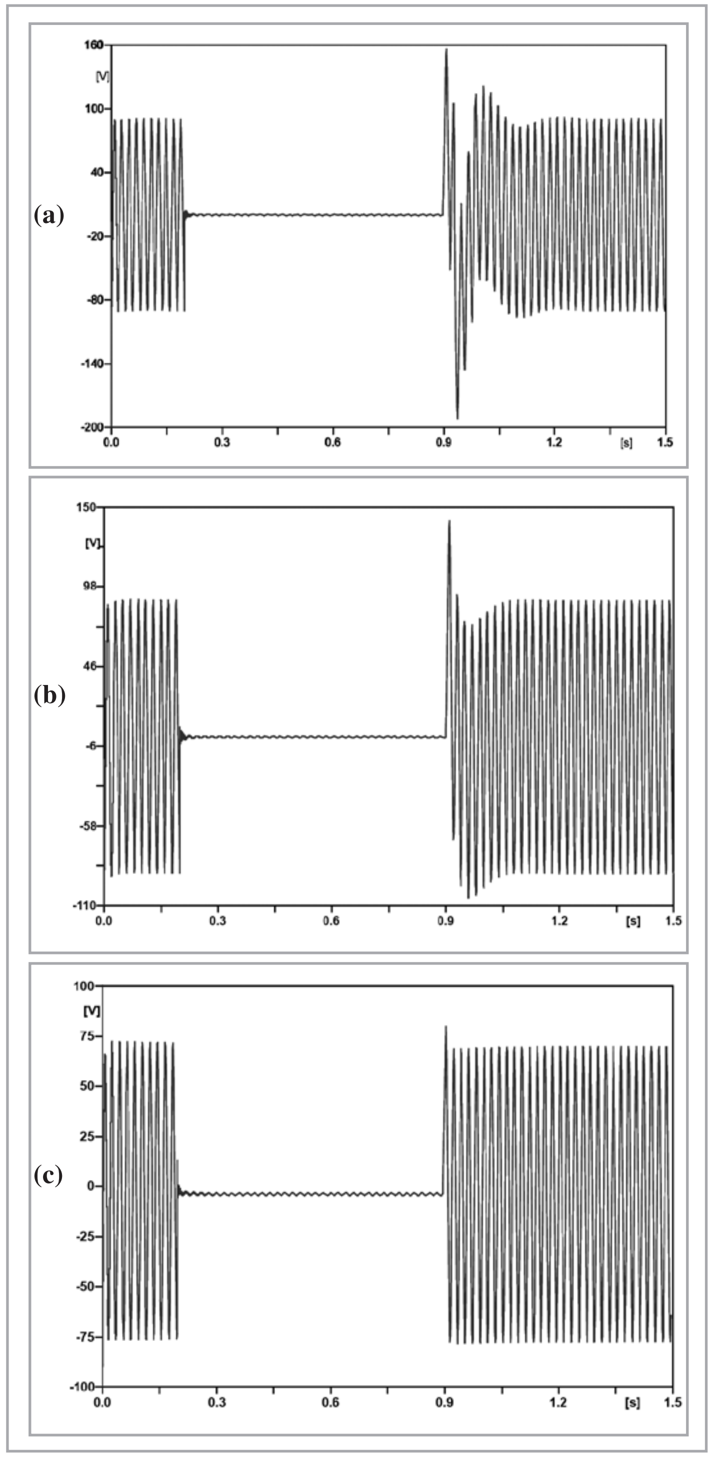

Figure 2 : CVT output voltage response to ferroresonance test for pure resistive burden (a) burden = 0 , VA (b) burden = 100 VA (c) burden = 400 VA

Figures 3(a) and 3(b) show the CVT response to ferroresonance test when series burden with power factor of 0.2 and 0.8 is included on the secondary winding of the CVT as load respectively. By comparing both figures, it is obvious that ferroresonance is more effectively damped out for load with higher power factor. Hence, it is fair to say that higher power factor burden gives better transient response.

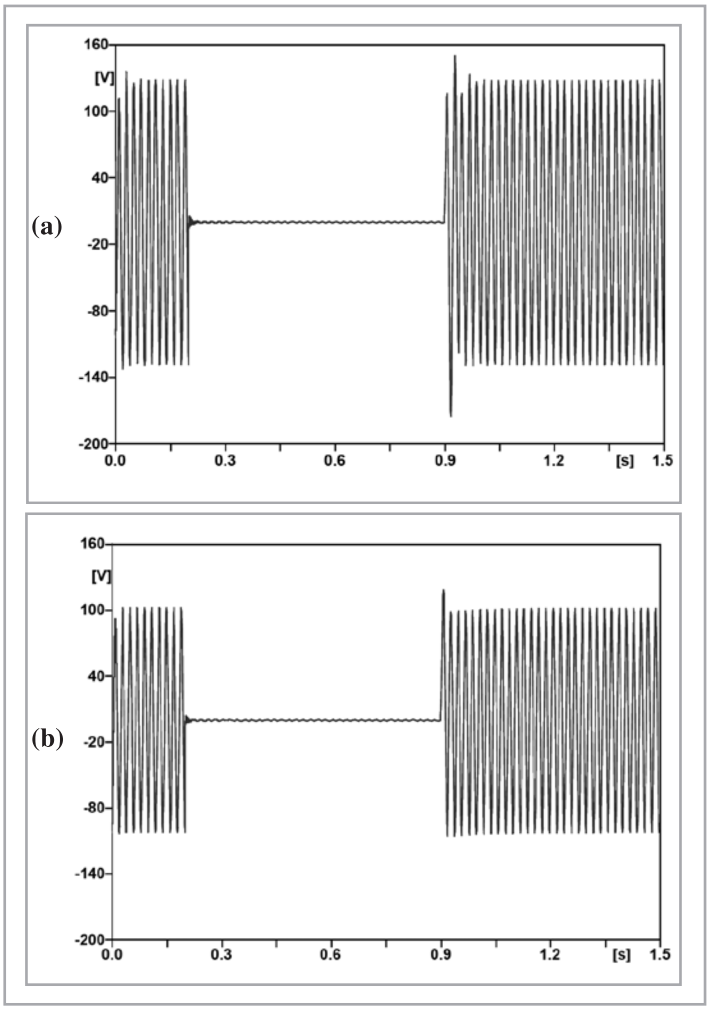

Figure 3 : CVT output voltage response to ferroresonance test for series burden of 200VA (a) power factor = 0.2, and (b) power factor = 0.8.

Case 2: Ferroresonance Suppression Circuit

This case investigates the effect of ferroresonance suppression circuit (FSC) on the CVT transient performance. FSC is designed to avoid dangerous and destructive overvoltages caused by ferroresonance. It loads a CVT and creates an extra path- apart from the burden – for dissipating energy. A specific design of FSC is often treated as proprietary information and is seldom available. However, two generic models of FSC that are commonly used in CVT will be considered here. They are the active ferroresonance circuit (ASFC) and passive ferroresonance circuit (PFSC) as shown in Figures 4(a) and 4(b) respectively.

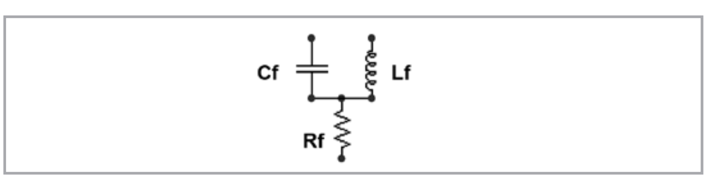

Figure 4(a) : Active ferroresonance suppression circuit

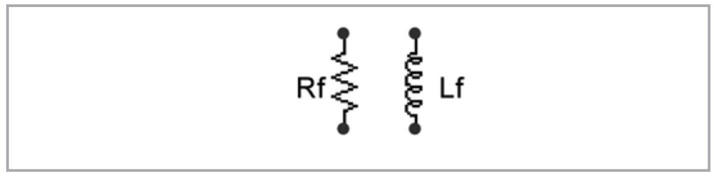

Figure 4(b) : Passive ferroresonance suppression circuit

Figures 5(a) and 5(b) show the transient response of the CVT with AFSC and CVT with PSFC respectively. Note that the CVT with a PFSC has a better, less distorted transient response (lower voltage spike) as compare CVT with an AFSC.

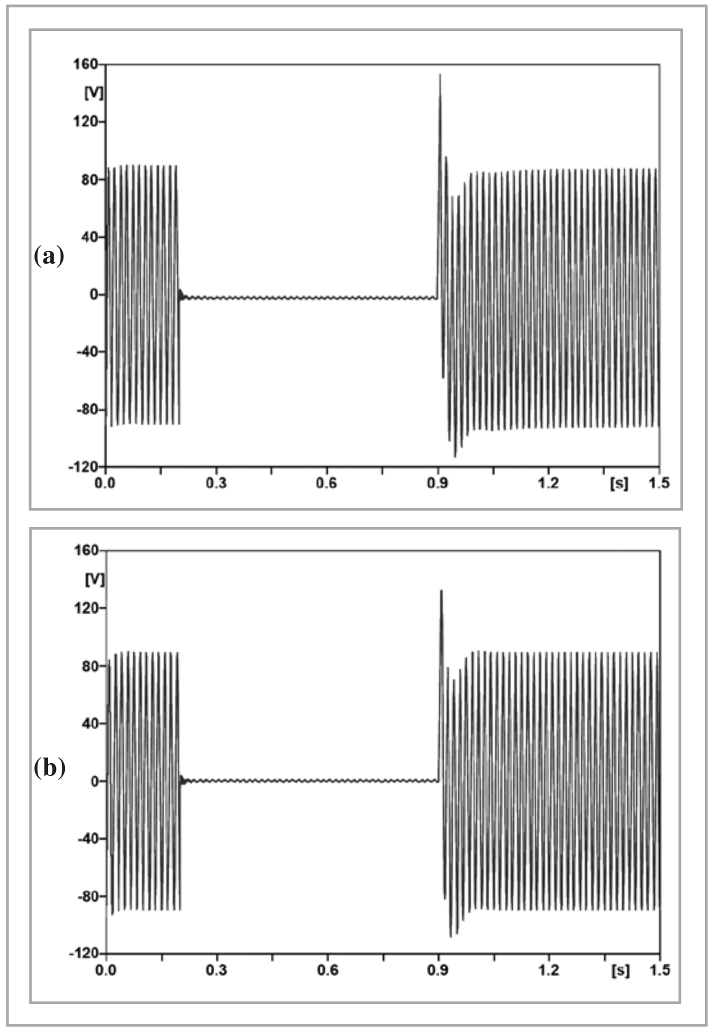

Figure 5 : CVT output voltage responses for (a) CVT with AFSC and (b) CVT with PSFC

3.2 SYSTEM FAULT

A simplified equivalent circuit of the CVT model as shown in Figure 6 is used to investigate the transient response contribution factors during a close-in, line-to-ground fault using ATPDraw simulation. This is imposed by closing and opening switch S1. The tests are carried out under different cases to investigate the effect of CVT components, and system condition on the CVT transient response.

Case 1: Sum of Stack Capacitance

This case investigates the effect of the sum of stack capacitance, (CVT component) on the CVT transient performance.

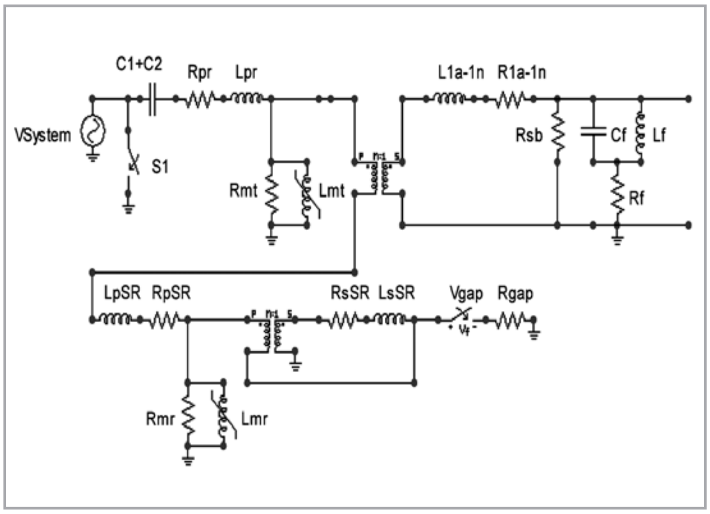

Figure 6: Simplified equivalent circuit of the CVT model

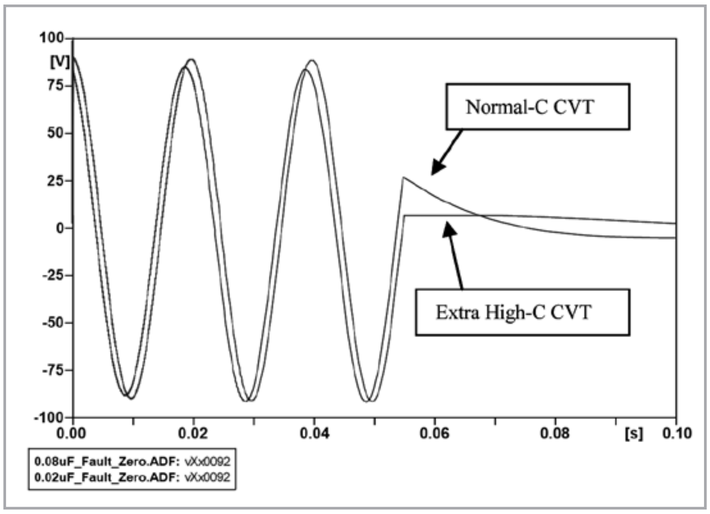

Figure 7: CVT otuput voltage

Figure 7 shows the CVT output voltages for both CVT with normal-Capacitance and Extra-High Capacitance respectively. Note that the higher the sum of stack capacitance, the lower the magnitude of the transients.

Case 2: Point on Wave when Fault Occur

This case investigates the effect of point on wave when fault occur (system condition) on CVT transient.

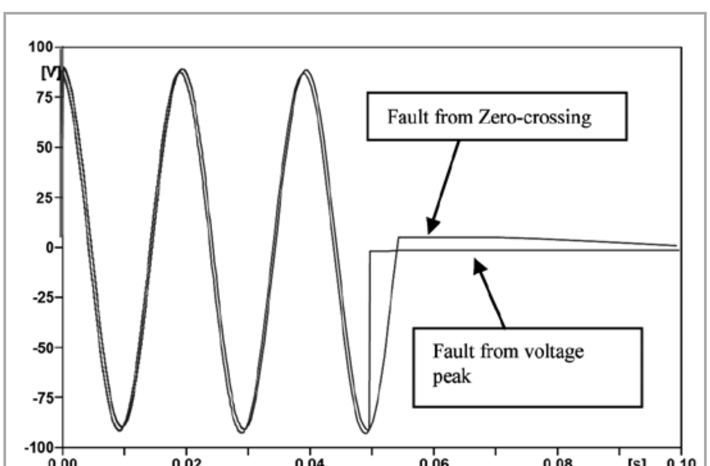

(a)

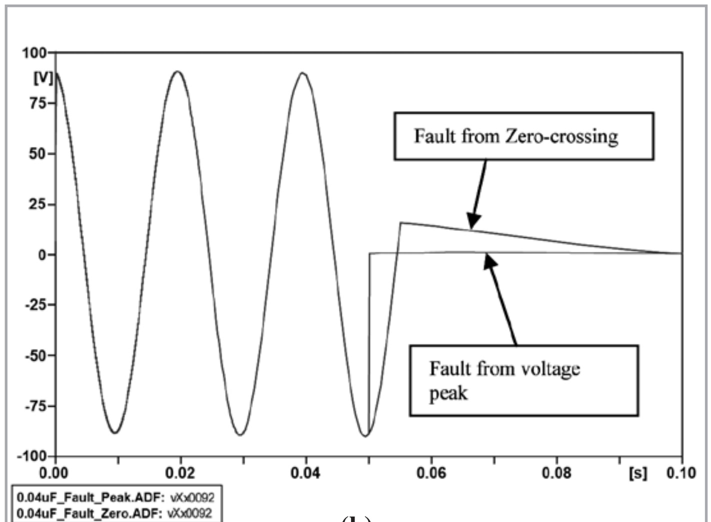

(b)

Figure 8 : CVT Secondary output voltage for (a) Extra-High-C CVT and (b) High-C CVT

Figures 8(a) and 8(b) show the extra-high-C CVT and high-C CVT secondary output voltages for system fault occur at both voltage peak and zero crossing respectively. It clearly shows that most severe transients are generated when a fault occur at the zero crossing of the primary voltage.

4.0 LIGHTNING SIMULATION

Lightning surge analysis is performed on a typical power system configuration in which the CVT model is connected. The lightning source is represented in this study by a single-stroke Heidler-type current source model, with parallel impedance equal to the lightning channel surge impedance. Lightning arrester is modeled using Metal-Oxide Surge arrester. Two different case studies are conducted to investigate the important factors, which affect the CVT transient when a typical power system configuration is subjected to lightning strike. These factors include the lightning current amplitude, and distance between CVT and lightning arrester.

Case 1: Lightning Current Amplitude

Figure 9 shows the CVT secondary output voltages when lightning current is injected at different peak current setting. Each stroke is a triangular current impulse of 1.5/50 µs.

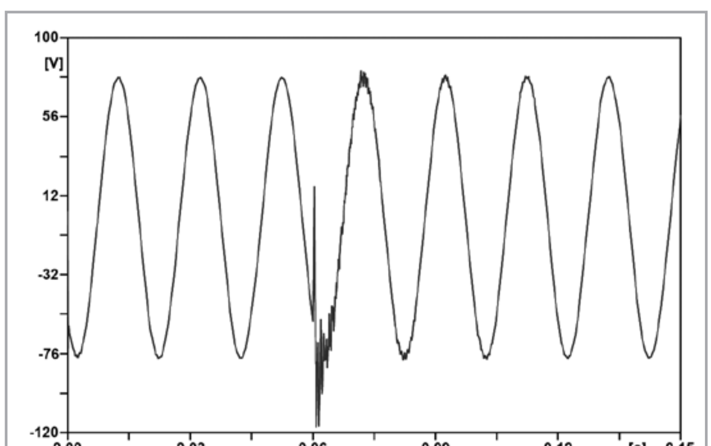

(a)

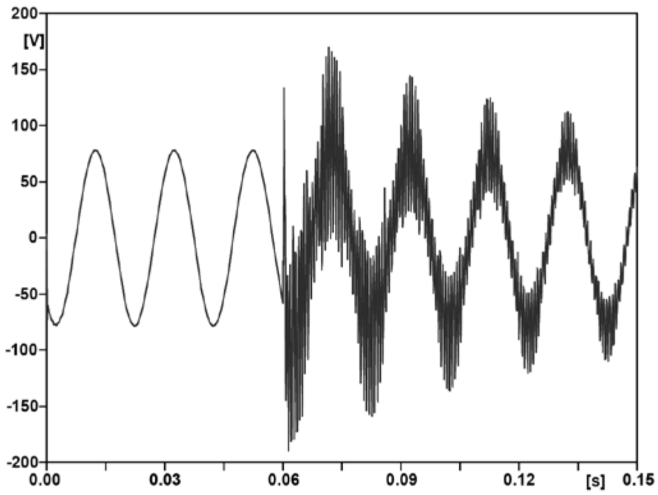

(b)

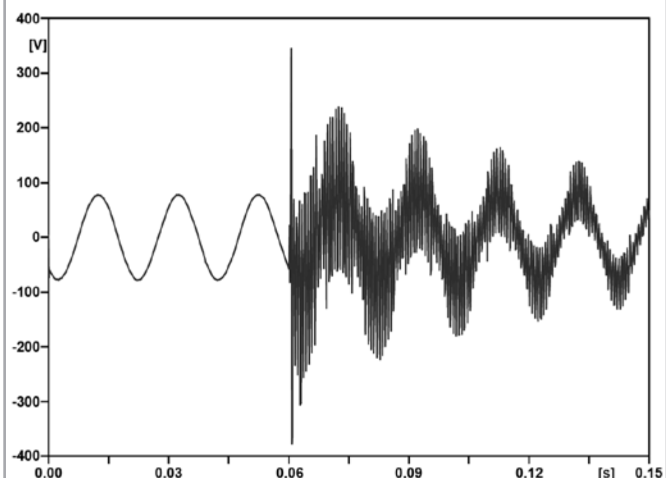

(c)

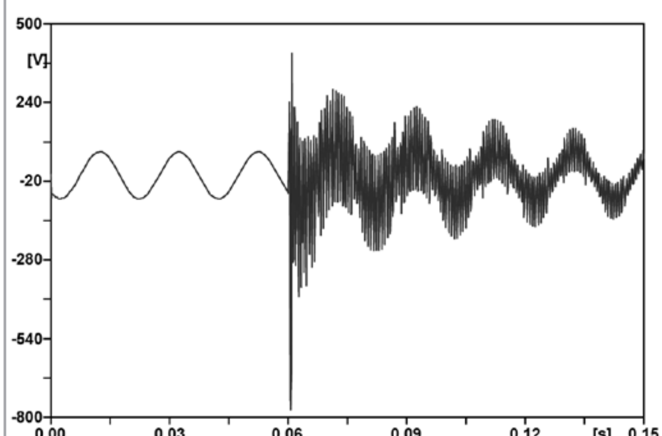

(d)

Figure 9 CVT secondary voltages for (a) lightning peak Current = 4000A, (b) lightning peak current = 20000A, (c) Lightning peak current = 34500A, and (d) Lightning peak current = 200000A.

Figure 9(a) through (d) clearly show that lightning surge can cause ferroresonance oscillation in CVT. The oscillation becomes worse as the lightning peak current increase, involving frequencies higher than the operating frequency of the system. This can lead to heating of transformer. High temperatures inside the transformer may weaken the insulation and cause failure under electrical stress.

Case 2: Distance between Lightning Arrester and CVT

Figure 10(a) and 10(b) show the CVT secondary output voltages for two different distances between the lightning arrester and the CVT.

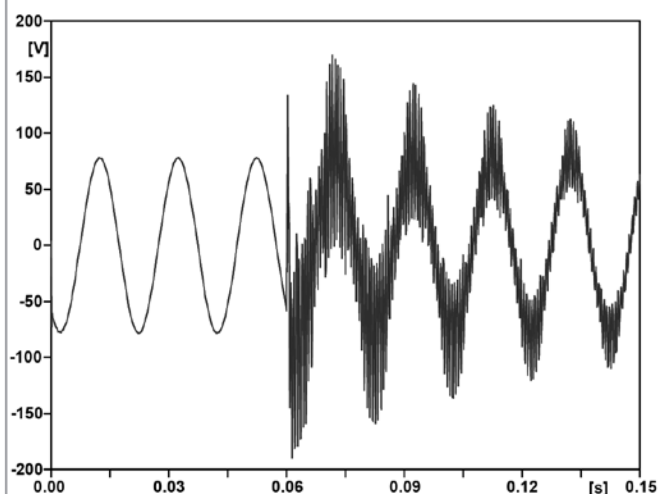

(a)

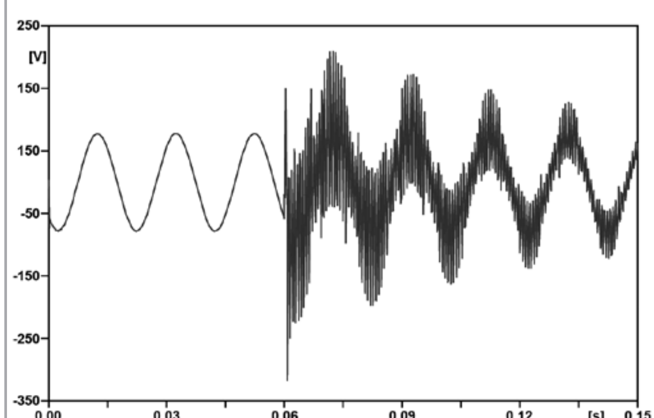

(b)

Figure 10 : CVT secondary output voltages for (a) Distance between lightning arrester and CVT = 3m, (b) Distance between lightning arrester and CVT =10 m

From Figures 10(a) and 10(b), it's obvious that, the CVT is subjected to more severe transient, as the distance between the lightning arrester and CVT increase.

5.0 CONCLUSIONS

This paper presents the simulation results of digital-time domain studies conducted on a typical 132kV CVT model using ATP-EMTP software. It also includes a lightning case study on a typical power system configuration where the CVT is connected. The investigation concludes that:

- Fault occurring at voltage zero-crossing generate the worst-case CVT transient.
- The transient produced by CVTs with PFSC are much less than those produced by CVTs with AFSC.
- The greater the CVT's equivalent capacitance (sum of stack capacitance), the smaller the amplitude of the transient oscillations.
- Burden with high power factor or nearly resistive give better transient response.
- Lightning can cause ferroresonance oscillation, which may lead to CVT failure.
- The possibility of CVT failure will increase as the distance between the CVT and lightning arrester increase. This is because that will cause voltage overstress to take place at the CVT secondary side.

REFERENCES

[1] M.R. Iravani, X. Wang, I. Polishchuk, J. Ribeiro and A. Sarshar, "Digital time-domain investigation of transient behaviour of capacitor voltage transformer," IEEE Trans. on Power Delivery, Vol. 13, No. 2, April 1998, pp.123-133.

[2] Dudurych, I.M.; Gallagher, T.J.; Corbett, J. and Escudero, M.V.; "EMTP analysis of the lightning performance of a HV transmission line" IEE Proceedings Generation, Transmission and Distribution, Volume 150, Issue 4, 14 July 2003 pp. 501 – 506.

[3] Chowdhuri, P.; Anderson, J.G.; Chisholm, W.A.; Field, T.E.; Ishii, M.; Martinez, J.A.; Marz, M.B.; McDaniel, J.; McDermott, T.R.; Mousa, A.M.; Narita, T.; Nichols, D.K. and Short, T.A. "Parameters of lightning strokes: a review" IEEE Transactions on Power Delivery, Volume 20, Issue 1, Jan 2005 pp.346 – 358.

[4] Ghassemi, F.; Gale, P.F.; Clegg, B.; Cumming, T. and Coutts, C.; "Method to measure CVT transfer function" IEEE Transactions on Power Delivery, Volume 17, Issue 4, Oct. 2002 pp.915 – 920.

[5] Instrument Transformer – Part 5: Capacitor Voltage Transformer, IEC/PAS 60044-5.

[6] M. Sanaye-Pasand, R.Aghazadeh, "Capacitive Voltage Substations Ferroresonance Prevention using Power Electronic Devices," International Conference on Power System Transients - IPST 2003 in New Orleans, USA.

[7] Preecha Sakarung, Somchai Chatratana, "Application of PSCAD-EMTDC and Chaos Theory to Power System Ferroresonanace Analysis," International Conference on Power System Transients (IPST'05) in Montreal, Canada, June 19-23, 2005, Paper No. IPST05 - 227.

[8] Alessandro Villa R. and Zulay Romero C., "Failure Analysis of CVT from Substations EL Tablazo and Cuatricentenario up 400 kV," International Conference on Power System Transients (IPST'05) in Montreal, Canada, June 19-23, 2005, Paper No. IPST05 - 150.

[9] D. Fernandes Jr., W. L. A. Neves, J. C. A. Vasconcelos and M. V. Godoy, "Coupling Capacitor Voltage Transformer: Laboratory Test and digital Simulations," International Conference on Power System Transients (IPST'05) in Montreal, Canada, June 19-23, 2005, Paper No. IPST05 - 076.

[10] D. Fernandes Jr., W. L. A. Neves and J. C. A. Vasconcelos, "Coupling Capacitor Voltage Transformer Representation for Electromagnetic Transient Studies," International Conference on Power System Transients - IPST 2003 in New Orleans, USA. Paper No. IPST03 -142.

[11] Galvan, A.; Cooray, V. and "Analysis of lightning-induced voltages in a network of conductors using the ATP-EMTP program" 10th International Conference on (Conf. Publ. No. 445) Electromagnetic Compatibility, 1997. 1-3 Sept. 1997 pp.153 - 157.

[12] Ghassemi, F.; Gale, P.F.; Clegg, B.; Cumming, T. and Coutts, C.; "Method to measure CVT transfer function" IEEE Transactions on Power Delivery, Volume 17, Issue 4, Oct. 2002 pp.915 – 920.

[13] Graovac, M.; Iravani, R. Xiaolin Wang and McTaggart, R.D.; "Fast ferroresonance suppression of coupling capacitor voltage transformers" IEEE Transactions on Power Delivery, Volume 18, Issue 1, Jan 2003 pp.158 – 163.

[14] Ghassemi,F.;Gale,P.;Cumming,T.;Coutts,C.and "Harmonic voltage measurements using CVTs" IEEE Transactions on Power Delivery, Volume 20, Issue 1, Jan 2005 pp 443 – 449.

[15] Tziouvaras, D.A.; McLaren, P.; Alexander, G.; Dawson, D.; Esztergalyos, J.; Fromen, C.; Glinkowski, M.; Hasenwinkle, I.; Kezunovic, M.; Kojovic, L.; Kotheimer, B.; Kuffel, R.; Nordstrom, J. and Zocholl, S.; "Mathematical models for current, voltage, and coupling capacitor voltage transformers" IEEE Transactions on Power Delivery, Volume 15, Issue 1, Jan. 2000 pp.62 – 72.

[16] Bayadi, A.; Harid, N. and Zehar, K.; "Dynamic surge arrester protection performance on high voltage systems using EMTP" 39th International Universities Power Engineering Conference, 2004. UPEC 2004. Volume 1, 6-8 Sept. 2004 pp.118 – 122.

[17] Iravani, M.R.; Chaudhary, A.K.S.; Giesbrecht, W.J.; Hassan, I.E.; Keri, A.J.F.; Lee, K.C.; Martinez, J.A.; Morched, A.S.; Mork, B.A.; Parniani, M.; Sharshar, A.; Shirmohammadi, D.; Walling, R.A. and Woodford, D.A.; "Modeling and analysis guidelines for slow transients. III. The study of ferroresonance" IEEE Transactions on Power Delivery,Volume 15, Issue 1, Jan. 2000 pp.255 – 265.

[18] Mozaffari, S.; Sameti, M. and Soudack, A.C.; "Effect of initial conditions on chaotic ferroresonance in power transformers" IEE Proceedings-Generation, Transmission and Distribution, Volume 144, Issue 5, Sept. 1997 pp. 456 – 460.

[19] Chakravarthy, S.K. and Nayar, C.V.; "Ferroresonant oscillations in capacitor voltage transformers" IEE Proceedings Circuits, Devices and Systems, Volume 142, Issue 1, Feb. 1995 pp. 30 – 38.

[20] Sommerville, W.; Gover, J.; Sanchez, R. and Bou, J.; "Modeling of capacitive and electromagnetic field shielding effects in a CVT" Proceedings Electrical Insulation Conference and Electrical Manufacturing Expo, 2005. 23-26 Oct. 2005 pp.378 – 382.

[21] He, B.; Yiquan Li and Bo, Z.Q.; "An adaptive distance relay based on transient error estimation of CVT" IEEE Transactions on Power Delivery, Volume 21, Issue 4, Oct. 2006 pp. 1856 – 1861.

[22] Ghassemi, F.; Merron, J.; Cole, D. and Gale, P.; "Effect of CVTs on power system monitoring and fault recording" Eighth IEE International Conference on Developments in Power System Protection, 2004. Volume 2, 5-8 April 2004 pp.514 – 517.

[23] Loxton, A.E. and Britten, A.C.; "The measurement and assessment of corona power losses on 400 kV transmission lines" 6th Africon Conference in Africa, 2002. Volume 2, 2-4 Oct. 2002 pp.613 – 616.

PROFILES

ASSOCIATED PROF. DR SAAD MEKHILEF
He received the B. Eng. degree in Electrical Engineering from University of Setif in 1994, and Master of Engineering science and PhD from University of Malaya 1998 and 2003 respectively. He is currently a Associate Professor at Department of Electrical Engineering; University of Malaya. Dr Saad is the author and co-author of more than 90 publications in international journals and proceedings. He is actively involved in industrial consultancy, for major corporations in the power electronics projects. His research interests include industrial electronics, power conversion techniques, control of power converters, renewable energy and energy efficiency

MR. CHENG HOCK LIM
He was born in Malaysia on June 30, 1981. He graduated from Universiti Tenaga Nasional with a Bachelor Degree in Electrical and Electronic Engineering (Hons) in 2004. Currently, He is pursuing his Master of Electrical Energy and Power System in University Malaya, Malaysia.

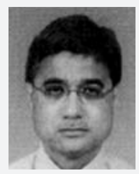

DR AB. HALIM ABU BAKAR
Dr Ab. Halim Abu Bakar was born in Malaysia on March 13, 1953. He graduated from Southampton University (England) with a B. Sc (Hons) in 1976, M.Eng and PhD from University Technology Malaysia in 1996 and 2003. His employment experience is with Tenaga Nasional Berhad (TNB) for the past 30 years. Among the posts that he had held were Chief Engineer Protection and General Manager (Asset Maintenance) Transmission Division. Presently he is with University of Malaya as a Senior Lecturer. He has presented papers in several conferences locally and abroad and involved in several conferences such as Vice-Chairman (Technical) CEPSI-1996, Committee Member CIGRE Symposium Malaysia 1999, Corresponding Member IEE 7th international Conference on Development in Power System Protection Amsterdam 2001, committee Member 3rd TNB technical Conference 2001 Malaysia and Special Reporter for CIGRE PARIS session 2004. He is responsible for establishing the RTDS in TNB for relay acceptance.

A CFD ANALYSIS ON THE EFFECT OF VORTEX FINDER AND CYLINDRICAL LENGTH ON CYCLONE HYDRODYNAMICS AND CENTRIFUGAL FORCES

(Date received: 4.2.2008)

Luqman Chuah A.[1], Jolius Gimbun[2], Thomas S. Y. Choong[1] and A. Fakhru'l-Razi[1]
[1]*Department of Chemical and Environmental Engineering, Faculty of Engineering,*
Universiti Putra Malaysia, 43400 UPM, Serdang, Selangor Darul Ehsan.
[2]*Faculty of Chemical and Natural Resources Engineering,*
University Collage of Engineering and Technology Malaysia,
KUKTEM, Locked Bag 12, 25000 Kuantan, Pahang Darul Makmur.
E-mail: chuah@eng.upm.edu.my/ tyc15@hotmail.com

ABSTRACT

The article presents a Computational Fluid Dynamics (CFD) calculation to predict and to evaluate the flow field and centrifugal forces of gas cyclones. The numerical solutions were carried out using commercial CFD code FLUENT 6.0. The problem of modelling highly swirling flow is overcame by means of an algebraic turbulence model, and all the features of the experimentally observed gas flow in a cyclone are shown to be computationally reproduced. It was found that CFD simulations predict excellently the axial and tangential velocity with an average deviation of ± 0.5 m/s from the presented experimental data. The physical mechanism for prolonged cyclone cylindrical body and vortex finder has also been successfully elucidated. Specifically, results obtained from the computer modelling exercise have demonstrated that CFD with RSM turbulence model is suitable for modelling a flow field and hydrodynamic of cyclone.

Keywords: *Centrifugal Force, CFD, Cyclones, Cylindrical Height, Hydrodynamics, Vortex Finder*

1.0 INTRODUCTION

Cyclones used in many technical applications [1], such as physical separation processes (especially dust from a gas stream) and chemical reactions (combustion of solid low calorific value fuels). In spite of the wide use and simple geometry, the real working principles of a cyclone chamber are far from being fully understood, mainly owing to the extreme complexity of the swirling turbulent flow field inside the device [2]. The gas stream enters the cyclone tangentially and force by its geometry into a vortex motion in the cylindrical section, spiralling downwards until the conical section is reached. In this part of the device, the centrifugal forces can be several times greater than gravity, contributing to particle separation. Then, the gas flow is deflected upwards and outflows from the exhaust duct (also called *vortex finder*), maintaining the swirling motion. The complexity of the flow pattern inside the chamber is due to the high turbulence level, strong anisotropy, three-dimensionality (3-D) and possible non stationary features typical of highly swirling motions, so that both experimental analysis and numerical simulations become notably difficult. Probably, this is the cause that basic cyclone design has evolved very little from the first applications.

Analytical solutions for the gas motion have been reported in the past [3, 4], but, due to the approximations introduced, their results are only valid in delineating the main features of the vortex flow. Numerical solutions have been also developed [5, 6], but they are strongly dependent on the turbulence model used and satisfactory agreement with experimental data has been achieved using the second-order Reynolds-stress model (RSM) as closure assumption for the turbulence modelling in a general purpose finite volume code [7, 8, 9]. Early experimental investigators of the cyclone chamber behaviour used Pitot tubes [10] and hot-wire anemometry [11]. They aimed first at determining the most efficient shape of a cyclone and then at understanding the turbulent flow structure, but the two techniques have several drawbacks and the reliability of their results cannot be guaranteed. Detailed measurements of the gas flow in a cyclone became possible only recently with the availability of Laser Doppler Velocimetry (LDV) and revealed a very complex structure with 3-D time dependent instabilities originated by the strongly swirling flow [12].

The present study was thus undertaken in an effort to carry out a modelling and simulation on the gas flow field within the whole body of a laboratory scale cyclone from the inlet chamber to the exhaust duct. In this study, the CFD calculations are carried out using commercial finite volume code FLUENT 6.0 while the centrifugal forces calculation are performed in the MS Excel spreadsheet. The CFD prediction is compared with the presented experimental data obtained from the literature. An attempt was also made to evaluate the flow field of cyclones with the different vortex finder length and cylindrical body height.

2.1 CFD

The numerical calculation was made with a fine numerical grid as shown in Figure 1. The numerical grid contains 38432 nodes to yield a reasonable prediction. The CFD simulation was performed with a Pentium IV 2.8 GHz HP workstation XW8000 with 512 cache-memory, 1 GB RAM-memory, and 110 GB hard-disc memory. The geometrical dimensions and configuration of these cyclones are given in Table 1 and Figure 2, respectively.

Table 1: Geometrical dimensions of cyclones studied

Geometry (cm)	*a*	*b*	*De*	*S*	*h*	*H*	*B*	*D*
Stairmand cyclone	9.5	3.8	6.4	9.5	28.5	76	7.25	19

The finite volume methods have been used to discretised the partial differential equations of the model using the SIMPLE method for pressure-velocity coupling and the Quick scheme to interpolate the variables on the surface of the control volume. The RSM turbulence model was used in this model due to the anisotropic nature of the turbulence in cyclones. Standard Fluent wall functions were applied and high order discretisation schemes were also used. A velocity inlet boundary was used to specify an air inflow of 7.6 m/s. The simulations were carried out with a zero underflow component. The underflow was therefore represented using a wall boundary. An outflow boundary condition was used to represent the cyclone overflow. A detailed description of the CFD modelling and simulation are presented in previous papers on the prediction of cyclone performance under various operating condition [8, 9].

Stairmand high efficiency cyclone of 0.1 m diameter as shown in Table 2 was evaluated for the study of vortex finder length and cylindrical height on cyclone hydrodynamics. The CFD surface mesh of all five different cyclones is shown in Figure 3.

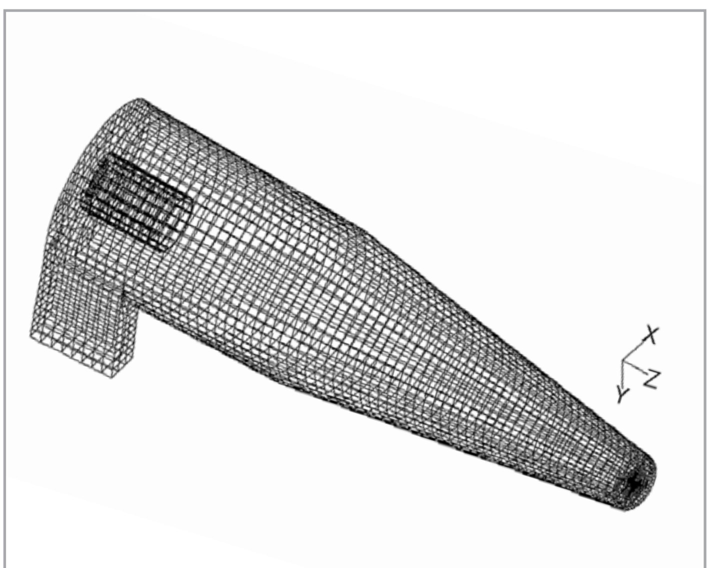

Figure 1: CFD surface mesh of Stairmand cyclone

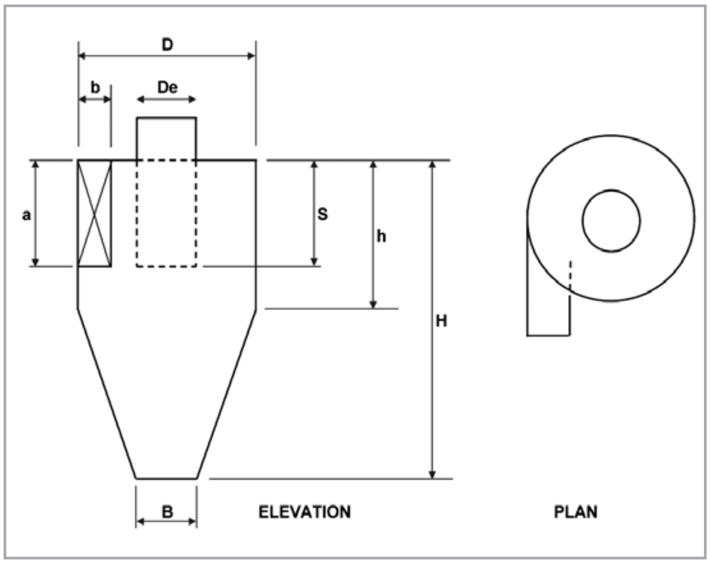

Figure 2: Tangential cyclone configuration

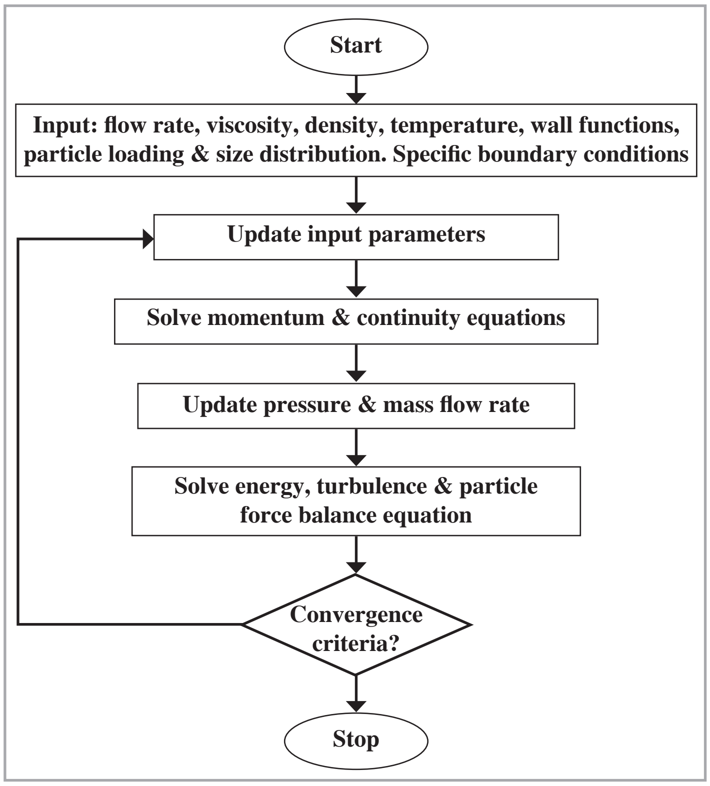

Figure 3: Overview of the segregated solution method

Table 2: Dimension of the tested cyclones

Cyclone no.	Cylindrical height (*h*)	Cyclone height (*H*)	Vortex finder (*S*)	Common for all cyclones
A	0.25	5	0.05	D = 0.1
B	0.2	4.5	0.05	a = 0.05
C	0.15	4	0.05	b = 0.02
D	0.15	4	0.15	D_e = 0.05
E	0.15	4	0.2	B = 0.0375

All measurement units are in m and cyclone C is a Stairmand high efficiency cyclone

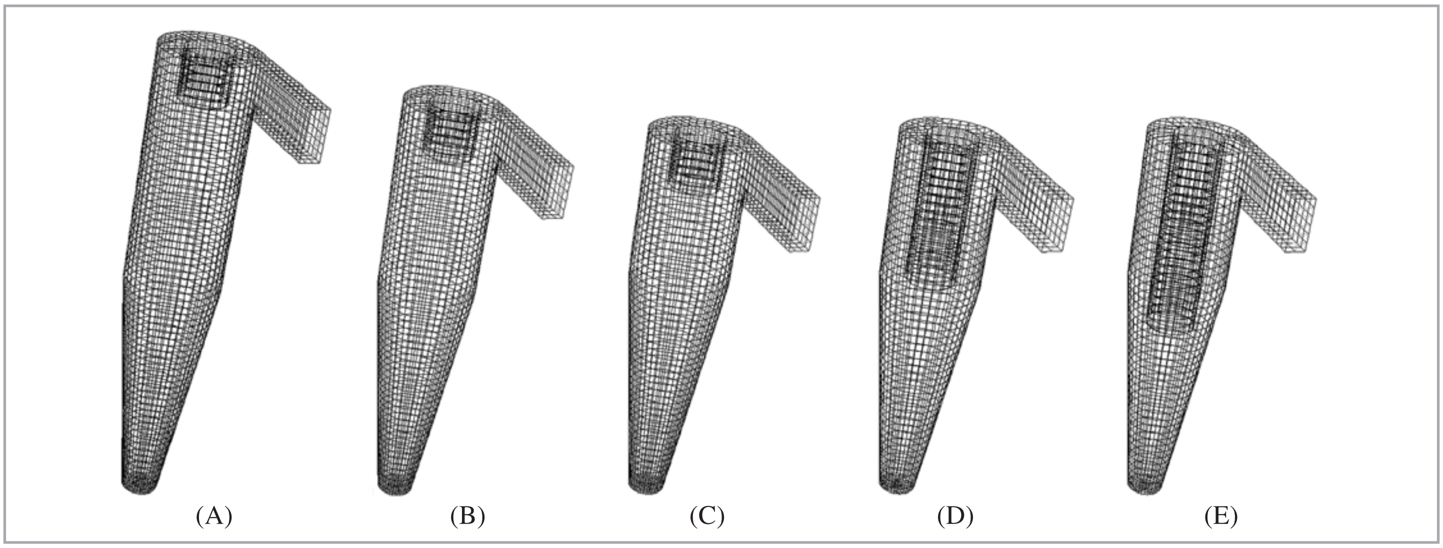

Figure 4: CFD surface mesh of the cyclone of different cylindrical height (A to C), and vortex finder length (C to E)

2.2 GOVERNING EQUATIONS

The governing equation for the turbulent, steady, isothermal and incompressible fluid flow in a cyclone is given by the Navier-Stokes equation as given below:

$$\rho\left(\frac{\partial u_i}{\partial t}\right) = 0 \text{ (continuity equation)} \quad (1)$$

$$\rho\left(\frac{\partial u_i}{\partial t}\right) = -\left(\frac{\partial P}{\partial x}\right) + \text{div(grad } u)$$
$$+ S_x \text{ (momentum equation)} \quad (2)$$

The trajectory of a particle is obtained by integrating the force balance on the particle. This force balance equates the particle inertia with the force acting on the particle, and is given by (for the *x*-direction in Cartesian coordinates) as:

$$\frac{du_p}{dt} = F_D\,(u - u_p) + g_x\left(\frac{\rho_p - \rho}{\rho_p}\right) + F_x \quad (3)$$

$$F_D = \frac{18\mu}{\rho_p d_p^2} \bullet \frac{C_D Re}{24} \quad (4)$$

Re is the relative Reynolds number, which is defined as:

$$Re = \frac{\rho d_p |u_p - u|}{\mu} \quad (5)$$

The values of C_D may be taken from standard sources.

2.3 Centrifugal Force

Centrifugal forces play an important role for particle separation in cyclone. Centrifugal force is usually shown as a pseudo force that is resulted from the body's inertia carrying it straight while some other force makes it move in a curved path. If the particle move in a circular path with radius *r* and velocity v_c along the path, then it has angular velocity,

$$\omega = V_r / r \quad (6)$$

and,

$$\textit{Centrifugal force, } F_c = \frac{mv_c^2}{r} = \omega w^2 r \quad (7)$$

For analysis of cyclone the centrifugal force is commonly expressed as a ratio of gravity force,

$$\frac{\textit{Centrifugal force}}{\textit{Gravity force}} = \frac{F_c}{F_g} = \frac{mv_c^2/r}{mg} = \frac{v_c^2/r}{g} \quad (3)$$

3.0 RESULT AND DISCUSSIONS

3.1 Prediction of cyclone hydrodynamics

Fraser *et al*. [14] have carried out a measurement on tangential and axial velocity of a standard Stairmand cyclone using a Laser Doppler Anemometry (LDA) system. LDA has been proven to be a useful tool to study the swirling flow pattern in centrifugal dedusting devices without having to insert probes, which may disturb the swirl [15]. Direct CFD plot of static pressure, Reynolds number and tangential velocity contour are shown in Figures 5. The low-pressure centre in Figure 5A can be responsible for the flow reversion and deviation of the axial velocity peak to the wall of the vortex finder pipe as shown in Figures 6 and 7. The strongest inward velocity found just under the vortex finder wall (Figure 5B) which was represented by a higher Reynolds number (as referred to Equation 5). Those findings agree with an earlier work of Peng *et al.* [14] on the similar cyclone type. The tangential velocity contours in Figure 4C also agree with the theory that tangential velocity must be zero on the axis of rotation. The comparison between LDA result and CFD simulation are shown in Figures 6 and 7. CFD with RSM turbulence model predict the cyclone axial and tangential velocity well with an average deviation of ±0.5 m/s from the Fraser's experiment. It can be concluded that CFD prediction has high accuracy in simulating the flow field in cyclone.

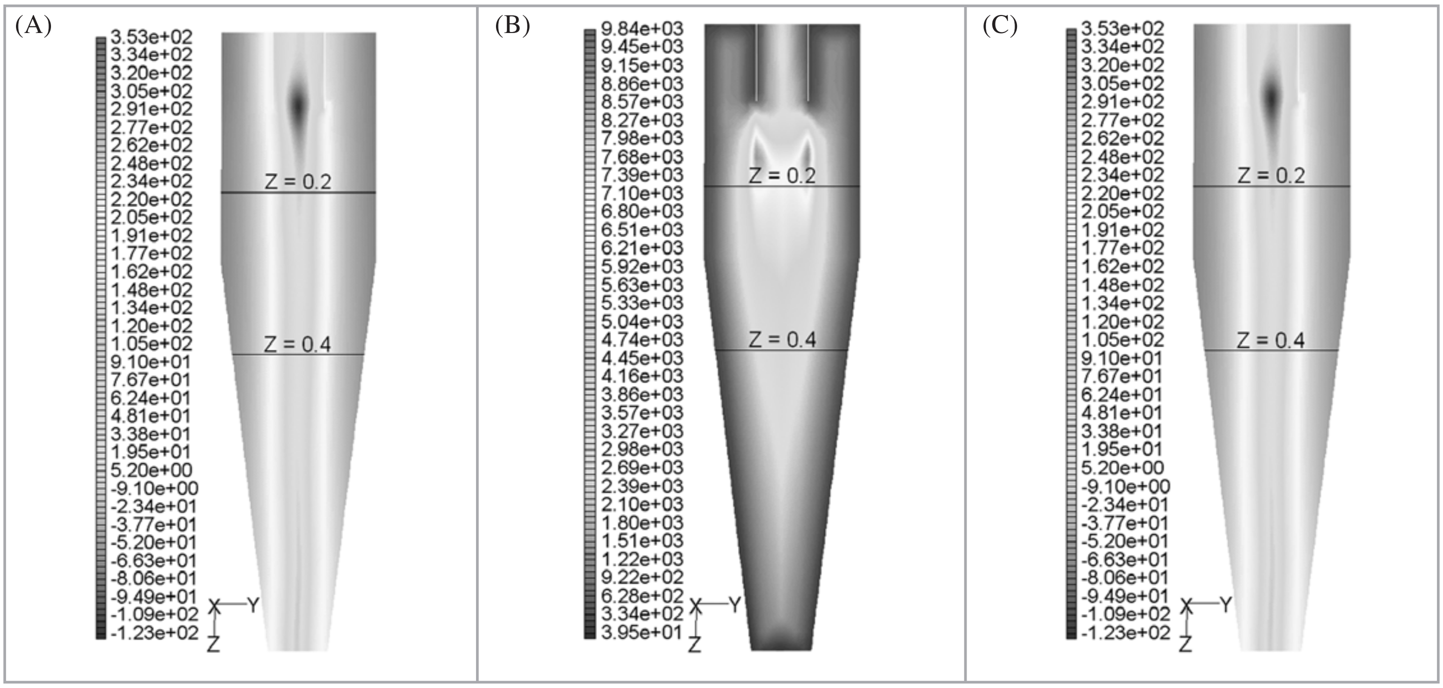

Figure 5: (A) Static pressure contour (*Pa*), (B) Reynolds number contour, (C) Tangential velocity contour (m/s)

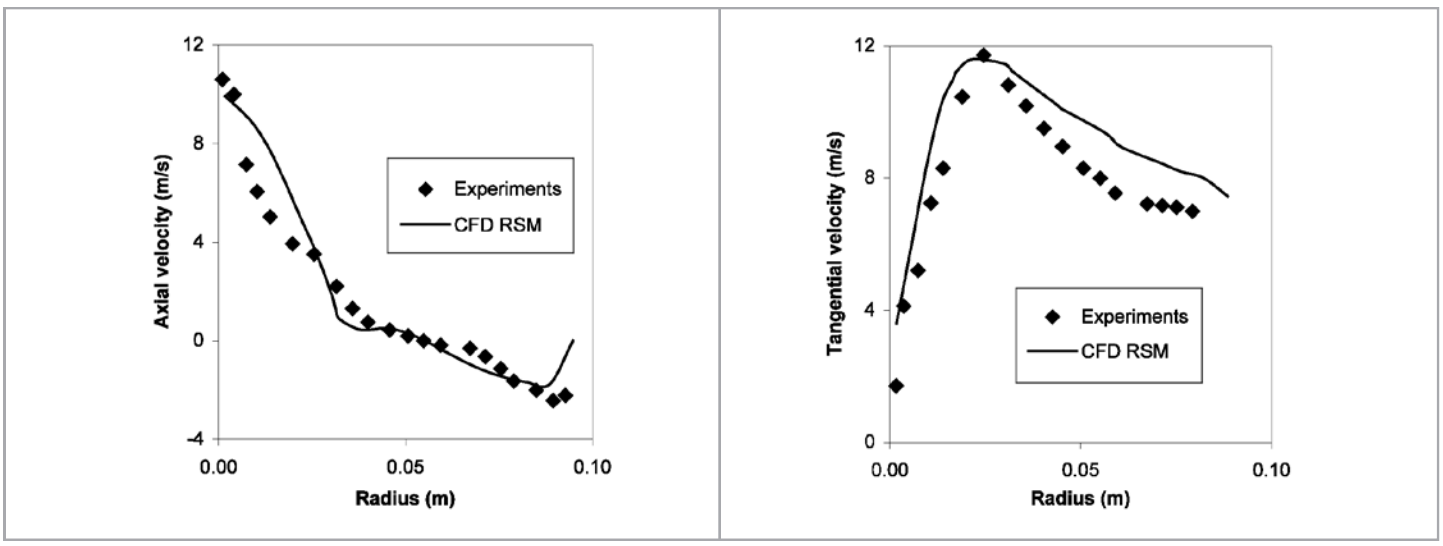

Figure 6: Axial and tangential velocity at Z = 0.2 m of Stairmand cyclone. Data point obtained from [14].

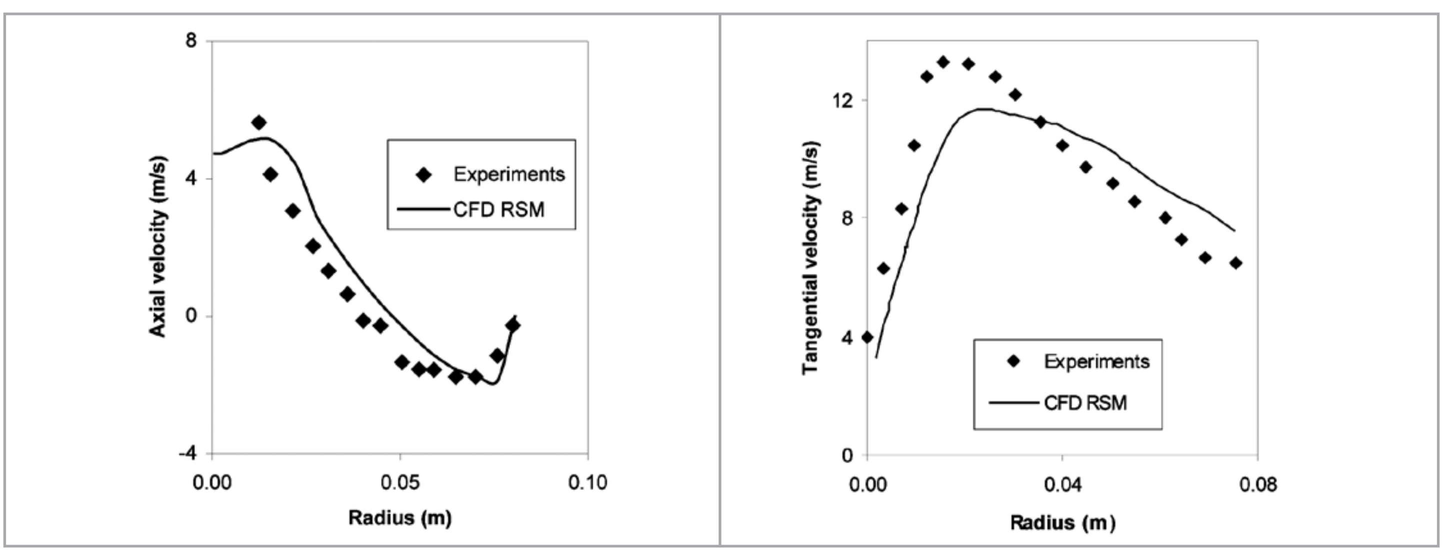

Figure 7: Axial and tangential velocity at Z = 0.4 m of Stairmand cyclone. Data point obtained from [13]

A ratio of centrifugal to gravity force analysis on various height of the cyclone has been carried out to evaluate the pattern of centrifugal force inside the cyclone body. The numerical calculations were performed via MS Excel spreadsheet using a tangential velocity obtained from CFD simulations. The comparison of the centrifugal force at two different height of Staimand cyclone is shown in Figure 8.

It was found that the resultant centrifugal force at various height of cyclone is not much different except at the tangential velocity peak. From Figures 6 and 7, the tangential velocity profiles for both heights (Z = 0.2m and Z = 0.4m) are similar, indicating the similar centrifugal force profiles exist along the radius. Figure 8 showed that the centrifugal force decreases with the increase of cyclone radius (Figure 7) and therefore led to a sharper separation as revealed by Coker [15]. Therefore, a cyclone with a smaller body diameter tends to have sharper separation efficiency.

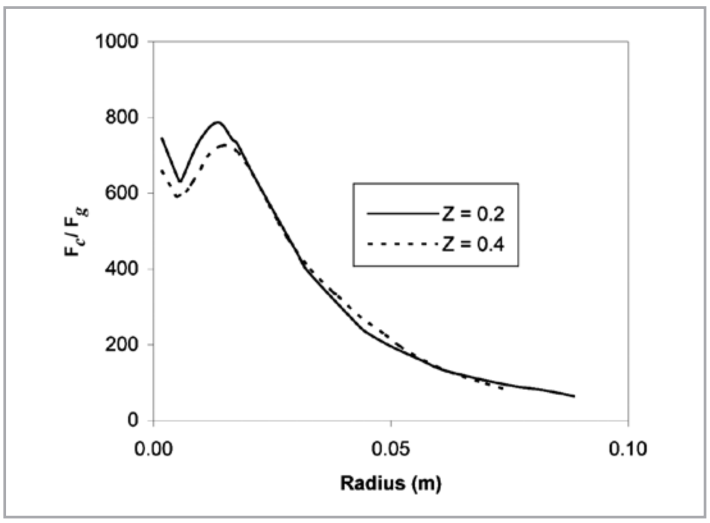

Figure 8: Calculated centrifugal to gravity force ratio on a different height of Stairmand cyclone

3.2 Evaluation on cylindrical height

Zhu and Lee [16] observed that cyclone collection efficiency decreases as the ratio *h/D* increases. The mechanism behind Zhu and Lee observation is further investigated in this work via CFD simulation using cyclones with different cylindrical height. The turbulent Reynolds number inside the three cyclones of different cylindrical height, *h*, is shown in Figure 9. It is found that the maximum turbulence occurs under the vortex finder. For cyclones (A) and (B), in the region below the vortex finder, the tangential gas flow in outer vortex collidies with gas flow in the inner vortex. This gives rise to chaotic flow at the boundary of the inner and outer vortex just below the vortex finder. This may reduce the tangential velocity inside the inner vortex just above the bottom of the vortex finder and may even cause flow short-circuting leading to flow in the reverse direction out of the inlet. This would not only lead to the loss of energy and increased pressure drop in cyclone, but adversely affect the cyclone separation efficiency.

As show in Figure 10a, the simulation result shows that a tangential velocity decreases as *h* increase (Figure 9). Since the collection efficiency of cyclone is directly related to the centrifugal force which is proportional to the tangential velocity, an increase in *h* will increase the collection efficiency. The comparison of the centrifugal force of the cyclone of a different cylindrical height is shown in Figure 10. The axial velocity was also found to increase with *h* (Figure 9). The higher axial velocity contributes to lower collection efficiency because of higher possibility of particle sucked through the vortex finder.

The comparison of the centrifugal force of the cyclone of a cylindrical height is shown in Figure 11. In a cyclone, the pressure drop decreases with increased wall friction coefficient, concentration of solid and also leght of apparatus. High peak tangential velocity causes larger centrifugal force in the inner region, which in turn leads to higher separation efficiency and high pressure drop. It can be clearly seen that centrifugal force field in cyclones (A) and (B), due to the low tangential force near vortex finder, is relatively lower along the axis as compared cyclone (C). The practical implication is that particles within the flow in cyclones (A) and (B) will only very briefly experience the centrifugal force and are more likely to escape than be captured. This low centrifugal force region will certainly hinder the separation performance of these cyclones.

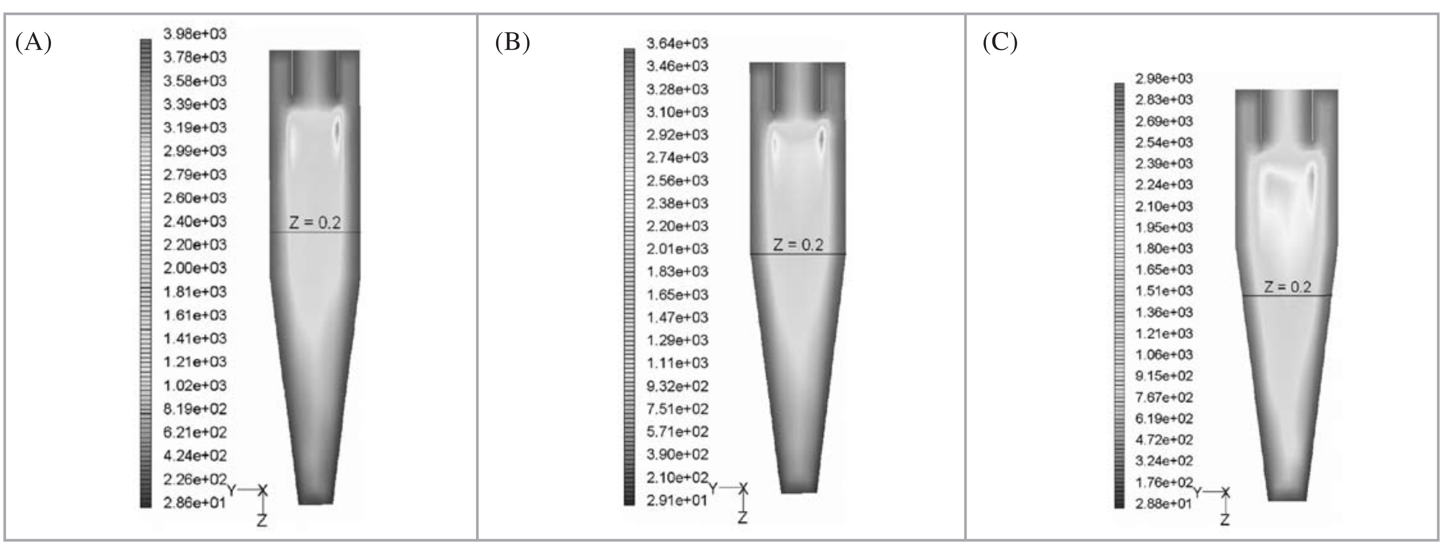

Figure 9: Turbulent Reynolds number of the cyclone of different cylindrical body height

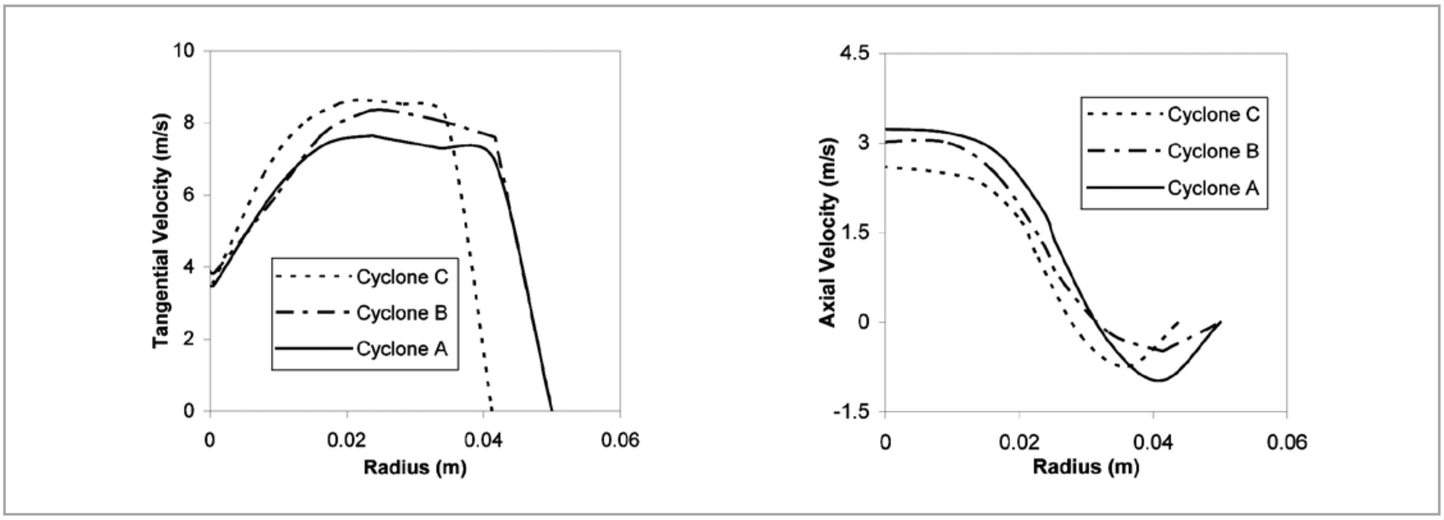

Figure 10: Tangential and axial velocity at Z = 0.2 m of cyclone of a different cylindrical body height

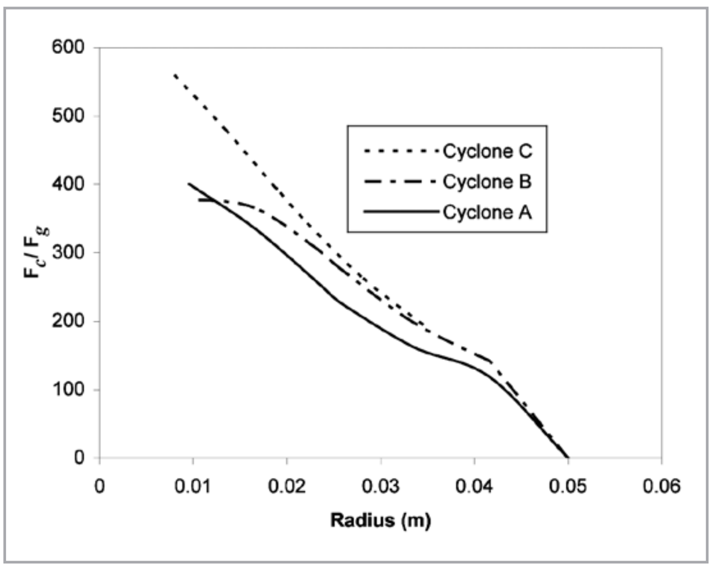

Figure 11: Centrifugal force at Z = 0.2 m of cyclone of a different cylindrical body height

3.3 EVALUATION ON VORTEX FINDER

The vortex finder size is an especially important dimension, which significantly affects the cyclone performance as its size plays a critical role in defining the flow field inside the cyclone, including the pattern of the outer and inner spiral flows. Kim and Lee [17] described how the ratio of the diameters of cyclone body (D) and the vortex finder (D_e) affected the collection efficiency and pressure drop of cyclones, and proposed an energy-effective cyclone design. Moore and Mcfarland [18] also tested six cyclones, with different vortex finders' diameter, and concluded that the variation in the vortex finder diameter under the constraint of a constant cyclone Reynolds number produced a change in the aerodynamic particle cut off diameter. Zhu and Lee [16] depicted the effects of the vortex finder length on the particle collection efficiency using seven different cyclones, and suggested that the difference between the cyclone cylinder height and vortex finder length played a significant role in the particle collection characteristics, and that the vortex finder length could be optimised. The turbulent Reynolds number inside the three cyclones of a different vortex finder length is shown in Figure 12. Cyclone (C) has a uniform turbulent intensity distribution under the vortex finder. However, for cyclones (D) and (E), the turbulence intensity is rather weak. For cyclone (D) and (E), longer vortex finder has led to re-entrained flow into the vortex finder, hence, increasing the axial velocity.

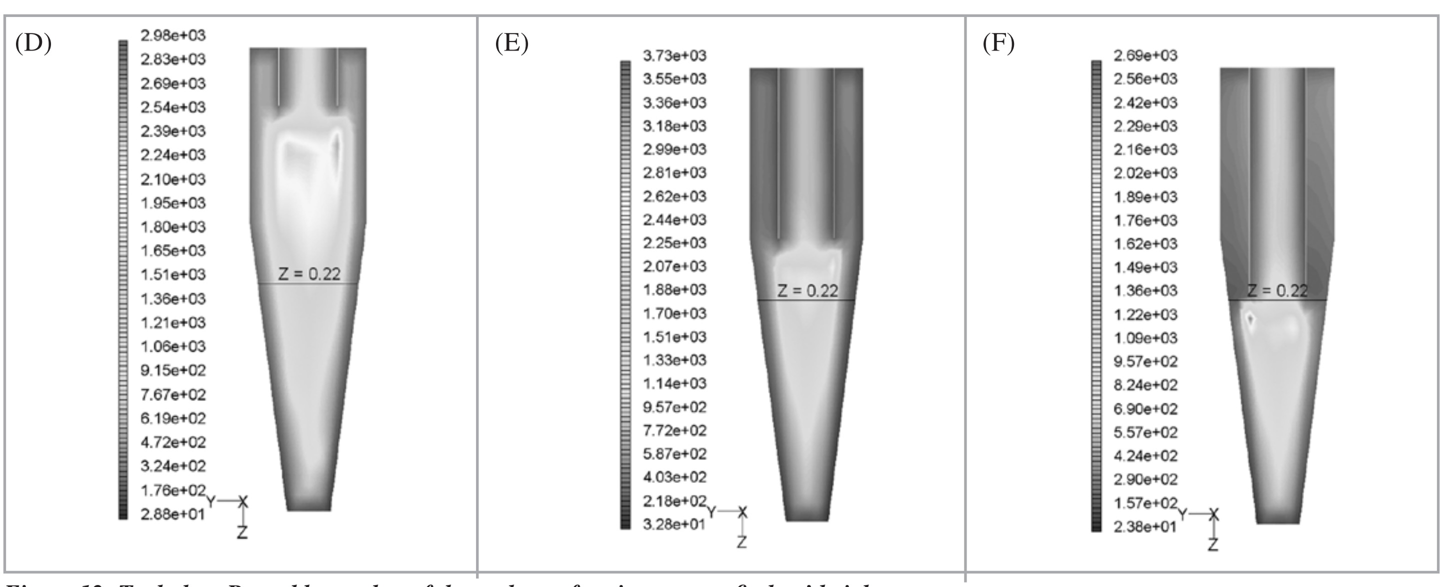

Figure 12: Turbulent Reynolds number of the cyclone of various vortex finders' height

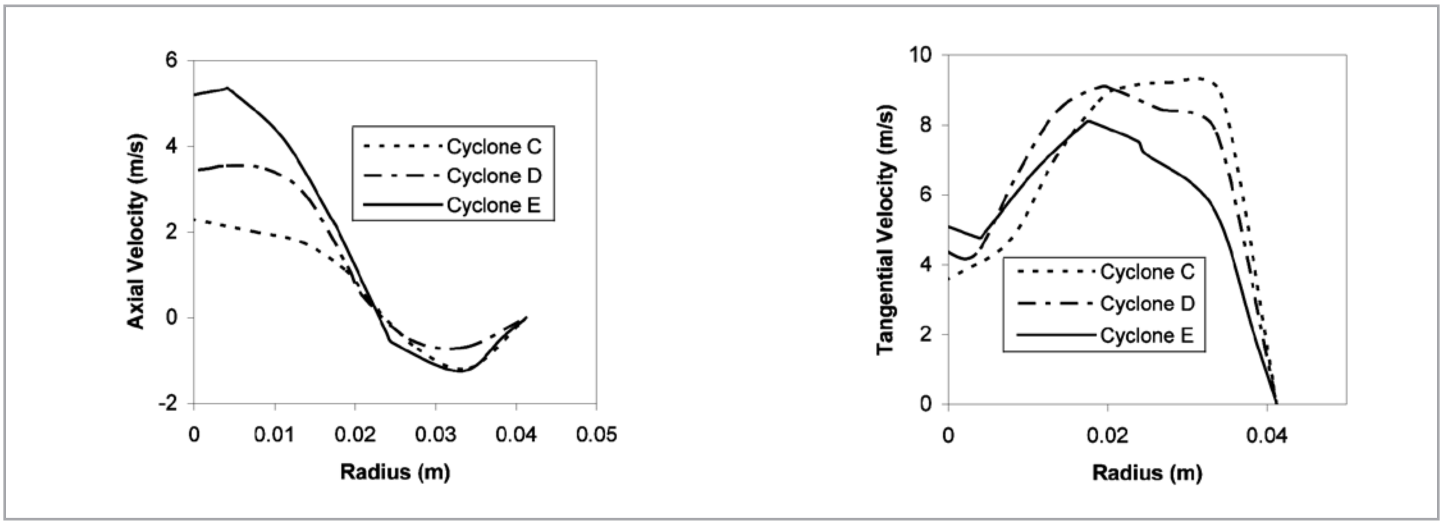

Figure 13: Axial and tangential velocity at Z = 0.22 m of cyclone with different vortex finder lengths

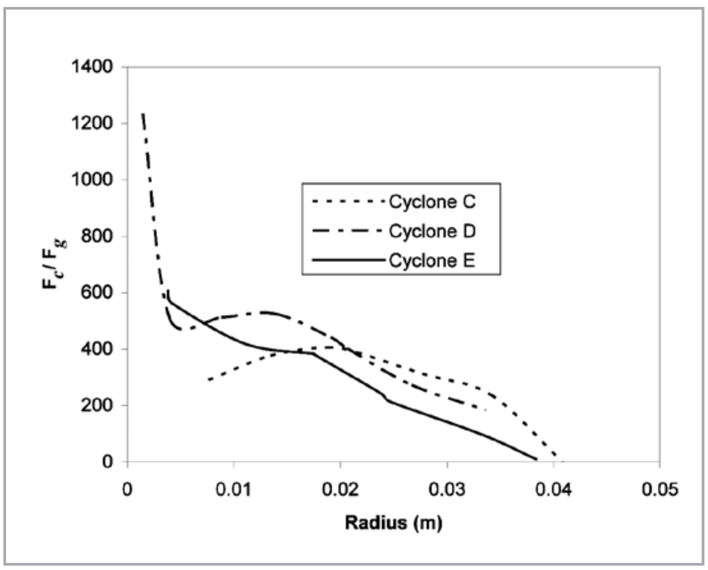

Figure 14: Centrifugal force at Z = 0.22 m of cyclone of a different vortex finder length

Prolonging the vortex finders, *S*, more than the cylindrical body, *h*, result in a lower tangential velocity in cyclone (Figure 13b). That could be an explanation why a cyclone with longer *S* has lower separation efficiency as the tangential velocity relates directly to the centrifugal forces. In other way a longer *S* causes a higher axial velocity (Figure 12) thus increases a possibility of particle sucked into the vortex finder. Figure 14 shows that cyclone having an *S/h* of 1.0 has a higher resultant centrifugal force which will theoretically lead to higher separation efficiency.

4.0 CONCLUSIONS

The CFD code FLUENT 6.1 with the RSM turbulence model, predicts very well the flow field of cyclones and can be used in cyclone design for any dimensions. CFD with RSM turbulence model predict the cyclone axial and tangential velocity well with an average deviation of ±0.5 m/s from the Fraser's experiment. The calculated centrifugal force using a tangential velocity obtained from CFD simulation has successfully demonstrated its relationship with the cyclone radius. The physical mechanism when the cyclone cylindrical body and vortex finder are prolonged also has successfully elucidated. It was found that the tangential velocity and centrifugal force decreases as the cylinder height and vortex finder are lengthened. Results obtained from the computer modelling exercise have demonstrated that CFD and is a reliable method of modelling the cyclones. This method of analysis is almost certainly less expensive than experiment, and represents a cost-effective route for design optimisation. ■

NOMENCLATURE

d_p	Particle diameter
F_c	Centrifugal force
F_D	Drag force per unit particle mass
F_g	Gravity force
m	Mass
P	Fluid pressure
r	Radius
S_x	Source term
u_i	Fluctuating velocities components (i = 1, 2, 3 ....)
u_p	Fluid phase velocity
v_c	Tangential velocity
ω	Angular velocity
ρ	Fluid density
ρ_p	density of the particle
μ	molecular viscosity of fluid
C_D	Drag coefficient
$\partial/\partial t$	Stokesian derivative with respect to time *t*
$\partial/\partial x$	Stokesian derivative with respect to position at *x*-axis

REFERENCES

[1] A. K. Gupta, D. G. Lilley and N. Syred, *Swirl Flows*, Abacus Press, Tunbridge Wells, 1984.

[2] G. Solero and A. Coghe, Experimental fluid dynamic characterisation of a cyclone chamber, *Experimental Thermal and Fluid Science*, 27 (2002) pp. 87-96.

[3] C. C. Hwang, H. Q. Shen, G. Zhu and M. M. Khonsary, On the main flow pattern in hydrocyclones, *J. Fluids Eng*., 115 (1983) pp. 21–25.

[4] L. X. Zhou and S. L. Soo, Gas–solid flow and collection of solids in a cyclone separator, *Powder Technol*., 63 (1990) pp. 45–53.

[5] F. Boysan, W. H. Ayers and J. Swithenbank, A fundamental mathematical modelling approach to cyclone design, *Trans. IChemE*, 60 (1982) pp. 222–230.

[6] S. Nieh and J. Zhang, Simulation of the strongly swirling aerodynamic field in a vortex combustor, *J. Fluids Eng*., 114 (1992) pp. 367–374.

[7] E. D. Cristea, A. Coghe, G. Solero, P. Conti, 3-D numerical computation and validation of high solid loading flow inside a gas cyclone separator, in *Proceedings of the 1998 ASME Fluids Engineering Summer Meeting*, Washington, DC, 1998.

[8] J. Gimbun, T. G. Chuah, A. Fakhru'l-Razi and Thomas S. Y. Choong, The influence of temperature and inlet velocity on cyclone pressure drop: a CFD study, *Chem. Eng. Process*., 44 (2005) pp. 7-12.

[9] J. Gimbun, Thomas S. Y. Choong, T. G. Chuah, A. Fakhru'l-Razi, A CFD study on the prediction of cyclone collection efficiency, *Int. Journal of Computational Engineering Science*, (2004) (in press).

[10] A. J. Linden, Investigations into cyclone dust collectors, *Proc. Inst. Mech. Eng*., 130 (1949) pp. 233–251.

[11] B. P. Ustimenko and M.A. Bukhman, Turbulent flow structure in a cyclone chamber, *Teploenergetika*, 15 (1968) 64–67.

[12] T. O'Doherty, R. Jaryczewski, C. J. Bates, N. Syred, Velocity characteristics of cyclone combustors, Vol. 1: Laser Anemometry, ASME, 1991.

[13] G. E. Klinzing R.D. Marcus, F. Rizk and Leung, *Pneumatic Conveying of Solid,* 2nd ed., Chapman and Hall, new York, 1997.

[14] S. M. Fraser, A. M. Abdel Rasek and M. Z. Abdullah, (1997) Computational and experimental investigation in a cyclone dust separator, *Proc. Instn. Mech. Engrs*., 211 (Part E) (1997) pp. 247-257.

[15] W. Peng, A. C. Hoffmann, P. J. A. J. Boot, A. Udding, H. W. A. Dries, A. Ekker and J. Kater, Flow pattern in reverse-flow centrifugal separators, *Powder Technol*., 127 (2002) pp. 212-222.

[16] A. K. Coker, Understand cyclone design, *Chem. Eng. Progr*., 28 (1993) pp. 51–55.

[17] Y. Zhu and K. W. Lee, Experimental study on small cyclones operating at high flowrates, *J. Aerosol Sci*., 30 (1999) pp. 1303–1315.

[18] J. C. Kim and K. W. Lee (1990) Experimental study of particle collection by small cyclones, *Aerosol Science and Technology*, 12 (1990) pp. 1003–1015.

[19] M. E. Moore and A. R. Mcfarland, (1993) Performance modeling single-inlet aerosol sampling cyclone, *Environmental Science and Technology*, 27 (1993) pp. 1842–1848.

RHEOLOGICAL PROPERTIES OF SS316L MIM FEEDSTOCK PREPARED WITH DIFFERENT PARTICLE SIZES AND POWDER LOADINGS

(Date received: 10.7.2008)

Sri Yulis M. Amin[1], Khairur Rijal Jamaludin[2,3], and Norhamidi Muhamad[2]

[1]Department of Mechanical and Manufacturing Engineering,
Universiti Tun Hussein Onn Malaysia, 86400 UTHM, Batu Pahat, Johor Darul Takzim
[2]Precision Process Research Group, Department of Mechanical and Materials Engineering,
National University of Malaysia, 43600 UUM, Bangi, Selangor Darul Ehsan
[3]Department of Mechanical Engineering, College of Science and Technology,
Universiti Teknologi Malaysia, International Campus, 54100 UTM, Kuala Lumpur
Email: [1]yulis@uthm.edu.my, [2, 3]khairurrijal@gmail.com./ khairur@citycampus.utm.my

ABSTRACT

Rheological study has been performed experimentally to evaluate the influence of different particle sizes and powder loadings to the rheological properties of SS316L MIM feedstock. The effects of different particle size, powder loading, shear rate and temperature has been investigated using capillary rheometer. The effect of shear rate to the feedstock viscosity was evaluated and result demonstrated that the feedstocks are pseudo-plastic. Their viscosity also shows strong dependence on the shear rate. The activation energy of each feedstock indicates the sensitivity to temperature and shear stress. The moldability index of the feedstock is also significant. The results indicate that the high powder loading feedstock at 64% volumes demonstrate the best rheological properties. The feedstock achieved desirable injection molding characteristics, such as homogeneous, stable, flow behavior index, $n < 1$, moderate activation energy (E) and high moldability index (α).

Keywords: *Metal Injection Molding (MIM), Particle Size, Powder Loading, Rheological Properties*

1.0 INTRODUCTION

Metal Injection Molding (MIM) is a manufacturing process capable of producing high-performance and complex shaped metal parts at low cost [1, 2]. In general, MIM is the process of mixing fine metal powders with plastic binder to form a feedstock, injection molding of the green part, extracting the binder, and finally sintering. The major advantages of this process includes high sintered density, more intricate shape, better mechanical properties, and better surface finish compared to the traditional powder metallurgy compacts [3]. Recent interest had been directed at particular MIM components with high added value, including sport equipments, eyeglasses, wristwatches, jewellery, and *etc*. [2].

The molding stage is the critical step for fabricating compact parts without cracking or distortions. This step requires specific rheological behavior of the feedstock such as flow behavior index, $n < 1$ and moderate amount of activation energy, E. Non-homogeneous melt flow and powder-binder separation during the injection molding process may defects the compacts, resulting in cracking and warpage during debinding and sintering, and ultimately poor physical and mechanical properties of the final parts [2]. Rheological analysis can be made to quantify the stability of the feedstock for achieving a successful manufacturing process [4, 5, 6].

The most important rheological property in MIM is viscosity, which relates a shear stress to shear rate. It is known that, a molded part would obtain its desired shape without any physical defects when the viscosity is controlled within a narrow range [7]. High melt viscosity has been identified as a reason for the molding difficulty [4, 5]. The melt viscosity is influenced by the particle size distribution, particle shape and the density of the powder, and it can be reduced by adding additives such as lubricants and plasticisers [8]. It is known that feedstock viscosity with low temperature sensitivity and low sensitivity to shear thinning behavior is desired [7]. Thus, parameters such as flow behavior indexes, n; activation energy, E: and moldability index, α; are important in the rheological investigations.

Most experiments that investigate the rheological properties of the MIM feedstocks are focusing on the best rheological properties. Huang *et. al*. [3] investigates on the effects of shear rate, solid volume fraction (powder loading) and melt temperature on the rheological behavior of the Fe/Ni MIM feedstocks, prepared by readily available polymer binder systems. He concluded that the binder system which had stable relationships in both the shear-rate dependence and temperature-dependence of the viscosity would be selected as a binder for the feedstock. Furthermore, Karatas *et. al*. [4] studied the rheological properties of the ceramic feedstocks, using polyethylene (PE) and three waxes (carnauba, bees wax and paraffin) with steatite powder. The experiment concluded that the formulation proposed has met the specific requirement and suitable to be injection molded. The flow behavior index (n) parameters have been determined to be less than 1, indicated a pseudo-plastic behavior.

For evaluating the influence of TiC addition on the rheological behavior and stability of SS316L MIM feedstock, Khakbiz *et. al*. [7] performed a rheological study using a capillary rheometer. They concluded that the rheological behavior of the feedstocks is highly depends on the blend composition. The addition of TiC particles to the stainless steel powder enhances the feedstock viscosity at relatively low shear rates, *i.e* < 500s-1. Furthermore, the feedstock instability increases, particularly at higher powder loading. By increasing shear rate and temperature, the viscosity decreases and the instability of the feedstock has improved. Krauss *et. al*. [6] conducted an experiment using capillary rheometer to analyse the rheological behavior of alumina powder feedstock containing polyethylene glycol (PEG), polyvinylbutyral (PVB) and stearic acid (SA) at different powder loadings. Some of the feedstocks showed a pseudo-plastic behavior ($n < 0$) and the viscosity displayed strong dependence to the shear rate. The results indicate that the low powder loading feedstock exhibits a best rheological behavior. Meanwhile, an experiment performed by Faiz Ahmad [9] to study the flow properties of composite mixes comprised of aluminum powder and glass fibers compounded into a plastic binder. The optimum powder loading was determined and the viscosity of the composite mixture decreased with the increase of shear-rate. The optimum level of fiber content would reduce the relative viscosity of the composite mixture. Composite mixture with longer fibers results in high viscosity. This present paper evaluates the effect of powder loadings and particle sizes to the rheological behavior and moldability of SS316L feedstock. This involves an investigation to the influence of temperature and shear rate to the viscosity of the MIM feedstocks.

2.0 EXPERIMENTAL PROCEDURES

2.1 Starting Materials

The metal powder used in the study is a gas atomised SS316L powder (ANVAL, Sweden). The characteristic of the powder is as shown in Table 1, while Table 2 shows the chemical composition of the powder.

Table 1: Characteristics of metal powder used in this study

Powder	Stainless steel, SS 316L
Manufacturer	ANVAL, Sweden
Particle shape	Spherical
D_{50}	11.225 µm (fine) and 19.606 µm (coarse)
Pycnometer density	7930 kg/m^3

Table 2: Chemical composition of the metal powder

C	Si	Mn	P	S
0.027	0.44	1.39	0.026	0.01

Cr	Ni	Mo	Fe
16.7	10.4	2.09	balanced

The binder system composed of polyethylene glycol, PEG as the major component (73%), polymethyl methacrylate, PMMA as backbone polymer (25%), and stearic acid as surfactant (2%). The surfactant acts as lubricant that enhances the dispersion of powder in the binder during mixing, and also enhances the powder loading and green strength [8] without sacrificing the flow properties of the mixtures.

2.2 Compounding

In order to study the effect of powder loading and particle size to the rheological behavior of the MIM feedstocks, the formulations of coarse and fine powder feedstock with powder loading of 62 and 64% volume is prepared. The remaining volume fraction is binder, consists of 73% weight of polyethylene glycol (PEG) and 25% weight of polymethyl methacrylate (PMMA). About 2% weight of stearic acid (SA) is used as a surfactant.

Table 3: Formulation of feedstocks

Powder Loading (% Volume)	Powder particle	Abbreviation
62	Fine	F62_16
62	Coarse	F62_31
64	Fine	F64_16
64	Coarse	F64_31

Table 3 illustrates the composition of the feedstock used in this study. The PMMA powder was dissolved with acetone for 15 minutes at 1 *gm*. of PMMA for each 4 *ml* acetone. The feedstock was prepared with Z-blade type mixer, having a rotation frequency of 25 *rpm*. The components of the feedstock were added simultaneously at room temperature for 30 minutes. The mixer temperature was set at 70^{o}C and the mixing continued until 1 hour. After mixing, the dough is removed from the mixer and cooled to 60^{o}C, before the dough is subsequently fed into a strong crusher in order to produce homogenised granules.

2.3 Rheological Properties Measurement

The test was conducted using a CFT-500D Shimadzu capillary rheometer as shown in Figure 1. L/D=10 die was attached underneath the extruder barrel. The test was conducted at constant capillary temperature of 125^{o}C and the load applied to the tester ranges from 30-60 *kgf*.

The barrel was filled with the feedstock and pressed lightly using a piston before it left in the barrel for 10 to 15 minutes to attain a thermal equilibrium. The pressure drop across the die was recorded for calculating the shear stress at the die wall. The flow rate through the capillary was calculated using a relation provided by the Japanese Industrial Standard, JIS K7210 [10]:

Figure 1: CFT-500D Shimadzu capillary rheometer

$$Q = 0.4/t \text{ (cm}^3\text{/s)} \quad (1)$$

Where, t is the time for the piston to travel from 3*mm* point to 7*mm* point in the barrel. The shear rate $\hat{\gamma}$ was calculated using Equation (2):

$$\hat{\gamma} = 32/\pi D^3 * 10^3 \ (s^{-1}) \quad (2)$$

Where, D is the capillary diameter, 1*mm*. The flow behavior index is determined by the Power law equation as shown in equation (3):

$$\eta = K \hat{\gamma}^{\,n-1} \quad (3)$$

Where, η is the viscosity, K is the constant. While, the Arrhenius's equation is applied to determine the activation energy, E as shown in Equation (4):

$$\eta = \eta_o \exp (E/RT) \quad (4)$$

Where η_o is the viscosity at reference temperature, R is the gas constant and T is the melt temperature. According to equation (4), ln η vs. 1/T at certain shear rate is obtained. The graphs show tendency to fit into straight lines. The slopes of the graph indicate that the temperature seems to be dependent to the viscosity, or the activation energy, E. Large values of the activation energy indicate high sensitivity of viscosity to temperature.

The moldability index (α) of the binder formulations and PIM feedstock is calculated using Equation (5) proposed by Weir *et al*. [4, 5]:

$$\propto = 10^9 \text{ (n)}/\eta_o \ (E/R) \quad (5)$$

Where, η_o is the apparent viscosity at the reference shear rate at 100, 10 000 and 100 000 s^{-1}.

3.0 RESULTS AND DISCUSSION

3.1 Flow Behavior Index, *n* (Shear Sensitivity)

Figure 2 shows the viscosity of the feedstock as a function of shear rate at 125°C. The melt exhibit a shear thinning or pseudo-plastic behavior. The viscosity of a pseudo-plastic substance decreases as the shear rate increases (shear thinning). This could be due to particle orientation and ordering with flow as well as breakage of particle agglomerates released together with the binder [2].

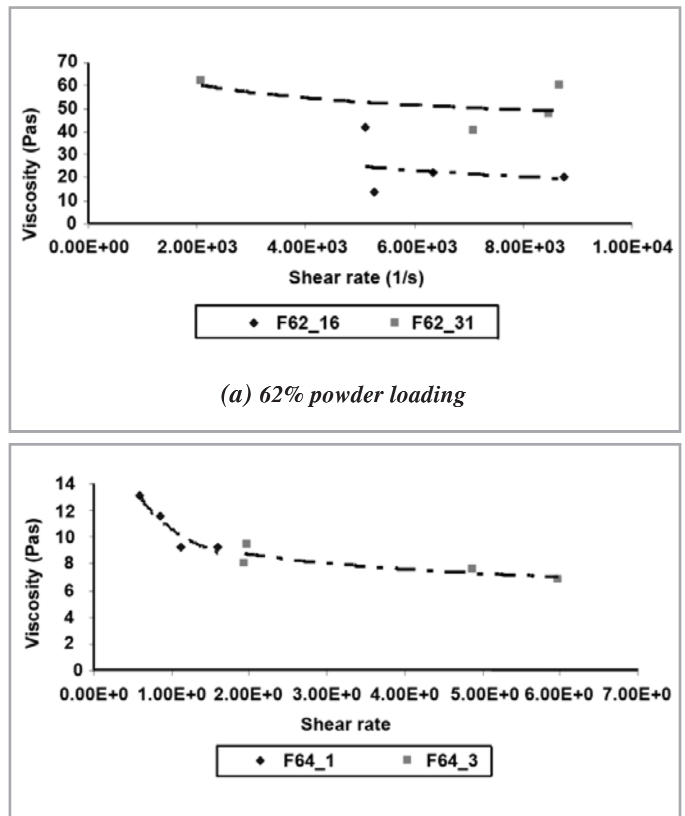

(a) 62% powder loading

(b) *64% powder loading*

Figure 2: Viscosity of MIM feedstock as a function of shear rate at temperature of 125°C. (a) 62% powder loading and (b) 64% powder loading

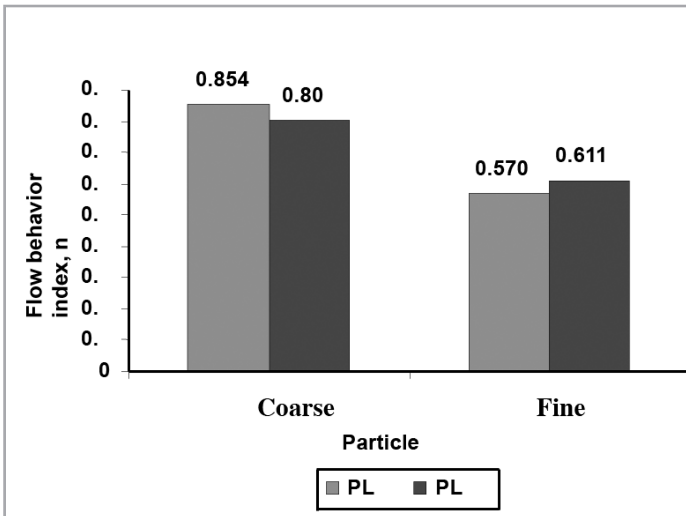

Figure 3: The flow behavior index of feedstock at 125°C as a function of particle size at different powder loading

Figure 3 shows the flow behavior index, *n* of the feedstock at 125°C. Most feedstock exhibit a shear thinning or pseudo-plastic behavior, as the flow behavior index, *n* is smaller than 1. The lower the value of the flow behavior index, the more viscosity dependence to the shear rate [7]. However, some molding defects such as jetting is associated with low flow behavior index. Jetting is undesirable since it causes severe defects, including weld lines and other imperfections in the final molded part [6]. For coarse particle feedstock, the flow behavior index decreases as the powder loading increases; this is in contrast to the fine powder feedstock. This means that the viscosity is more sensitive to shear rate particularly for the coarse powder feedstock. Feedstock F62_16 has the lowest value of flow behavior index compared to other feedstock, indicates that the feedstock is much dependence to the shear rate and demonstrates the best pseudo-plastic behavior. But this is undesirable because lower the flow behavior index is leading to the slip flow phenomena, which cause molding defects. Thus F62_31 is considered as the best feedstock in term of flow behavior index.

3.2 Activation Energy, *E* (Temperature Sensitivity)

Another important characteristic of MIM feedstock is temperature-dependence to the viscosity. Pure binder has a viscosity that usually varies exponentially with absolute temperature *T* [2]. Therefore, the effect of temperature on the viscosity of the feedstock was evaluated.

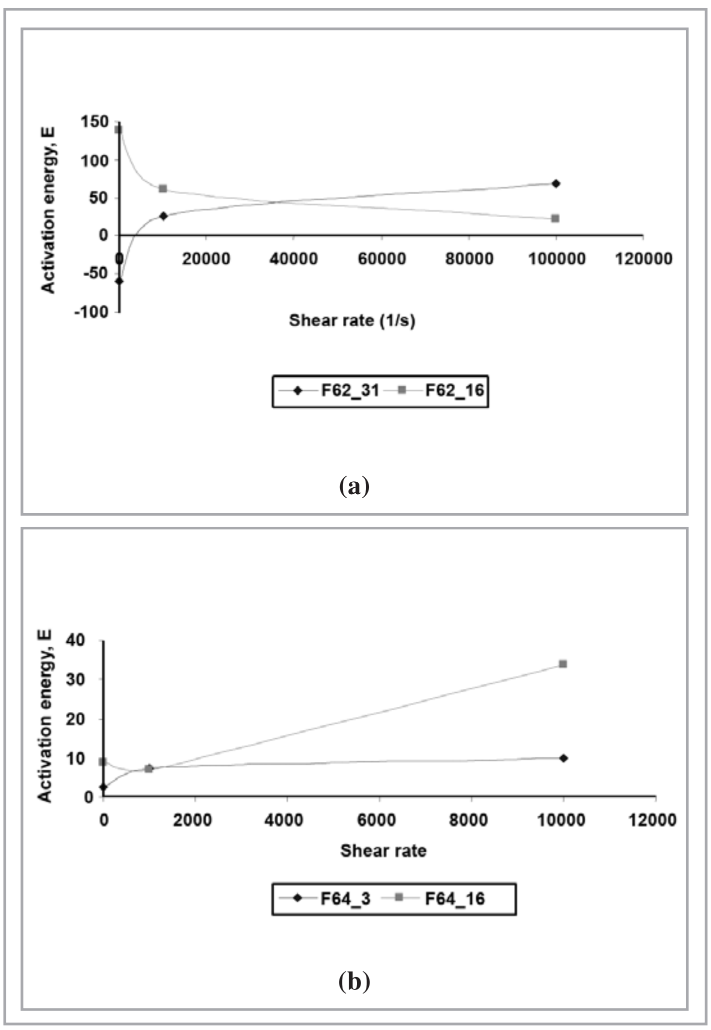

Figure 4: Activation energy of PIM feedstock as a function of shear rate at different powder loadings of (a) 62% and (b) 64%

The activation energy as a function of shear rate is shown in Figure 4. The activation energy of the coarse powder feedstock is proportional to the shear rate. Furthermore, at higher powder loading, the activation energy was found to be high, particularly at high shear rates. High value of flow activation energy indicates a strong temperature-dependence of the feedstock to the viscosity. Therefore, any small fluctuation of temperature during molding results in a sudden viscosity change, resulting defects in the molded parts, such as cracking and distortion due to the stress concentration [7]. In addition, feedstock with high temperature sensitivity is also sensitive to pressure [2]. As pressure increases, the melt is becoming more viscous. But in contrast the fine powder feedstock demonstrates the inverse proportional of the activation energy to the shear rate, particularly at low shear rates. The small value of the activation energy result less temperature sensitive, thus it minimizes stress concentration, cracks and distortion on the molded parts. Figure 4 exhibits the flow activation energy is high at high powder loading. The occurrence of a powder-binder separation phenomenon during a rheological testing is the possible reason for the increase of the activation energy.

3.3 Moldability Index, α

The feedstock moldability index is shown in Table 4. The index has been calculated using Equation (5).

Table 4: Moldability index, α obtained in this study

Feedstock	Moldability index, α
64_31	-5.07E+03
62_31	-6.41E+04
64_16	-4.28E+03
62_16	-4.97E+03

Table 4 demonstrates that the moldability index is for the coarse and fine powder feedstock decreases as the powder loading increases. This result is in good agreement with Khakbiz [7], that the higher powder loading led to the high moldability index. In the absence of problems such as jetting or high residual stresses, the higher value of the moldability index is desirable since feedstock with low flow behavior index are prone to powder-binder separation. As shown in Table 4, the F64_16 exhibits the highest value of the moldability index and thus is the best feedstock to be injection molded.

4.0 CONCLUSIONS

The rheological behavior of the feedstocks composed of 316L stainless steel has been investigated. The results revealed the pseudo-plastic or a shear-thinning behavior of the feedstock. Clearly, the fine the particle size, the lower the flow behavior index and thus indicates greater pseudo-plastic behavior of the feedstock. The high sensitivity of shear thinning is undesirable because it leads to the slip flow phenomenon, causes a molding defects. Coarse powder and fine powder feedstock at low and high powder loading respectively is more temperature-dependence to the viscosity (higher value of activation energy). This indicates less temperature tolerance during injection molding since any small fluctuation of temperature during molding results in a sudden viscosity change. Meanwhile, the value of the moldability index, α decrease as the powder loading increased, and is same for both particle sizes. High value of the moldability index is desirable since feedstock with low value of flow behavior index prone to powder-binder separation. A feedstock with a good homogeneity, high stability, a high flow behavior index, low activation energy and high moldability index were found to have optimum injection molding characteristics. Thus, 64% volume is identified as the best powder loading for the injection molding. ■

REFERENCES

[1] German, R. M. Powder Injection Molding, Metal Powder Industries Federation, Princeton, N.J., 1990

[2] German, R.M., and Bose, A., Injection Molding of Metal and Ceramic, Metal Powder Industries Federation, Princeton, N.J, 1997

[3] Huang, B., Liang, S., and Qu, X., "The rheology of metal injection molding", Journal of Materials Processing Technology, Vol. 137, pp. 132-137, 2003.

[4] Karatas, C., Kocer, A., Unal, H.I., and Saritas, S., "Rheological properties of feedstocks prepared with steatite powder and polyethylene-based thermoplastic binders", Journal of Materials Processing Technology, Vol 152, pp. 77-83, 2004.

[5] Iriany, Rheology properties study on the feedstock contains palm stearin for metal injection molding, Doctor of Philosophy Thesis, National University of Malaysia, 2002.

[6] Krauss, V. A., Pires, E. N., Klein, A. N., and Fredel, M. C., "Rheological properties of alumina injection feedstocks", Materials Research, Vol. 8, Num. 2, pp. 187-189, 2005.

[7] Khakbiz, M., Simchi, A., and Bagheri, R., "Analysis of the rheological behavior and stability of 316L stainless steel- TiC powder injection molding feedstock", Materials Science and Engineering A, Vol. 407, pp. 105-113, 2005.

[8] Mohd Afian Omar, "The influence of stearic acid on the properties of injection moulding of stainless steel powder", Journal of Technology, Vol. 10, Num. 2, pp. 37-45, 2001.

[9] Faiz Ahmad, "Rheology of metal composity mixes for powder injection molding", International Journal of Powder Metallurgy, Vol. 41, Num. 6, pp 43-48, 2005.

[10] Shimadzu. Shimadzu flowtester CFT-500D: Instruction manual. Kyoto: Shimadzu Corp.

PROFILES

SRI YULIS M. AMIN
Department of Mechanics,
Faculty of Mechanical and Manufacturing Engineering,
Universiti Tun Hussein Onn Malaysia,
86400 Batu Pahat, Johor

ENGR. KHAIRUR RIJAL JAMALUDIN
Department of Mechanical Engineering,
College of Science and Technology,
Universiti Teknologi Malaysia,
Int Campus, Jalan Semarak,
54100 Kuala Lumpur

ASSOC. PROF. DR NORHAMIDI MUHAMAD
Department of Mechanics and Materials Engineering,
Faculty of Engineering and Architecture,
Universiti Kebangsaan Malaysia,
43600 Bangi, Selangor